Vol. 68 • No. 2
February 2025

Microwave Journal

horizon house®
Founded in 1958
mwjournal.com

MILLER MMIC

Advancing RF MMIC Design Through Human-AI collaboration and competition

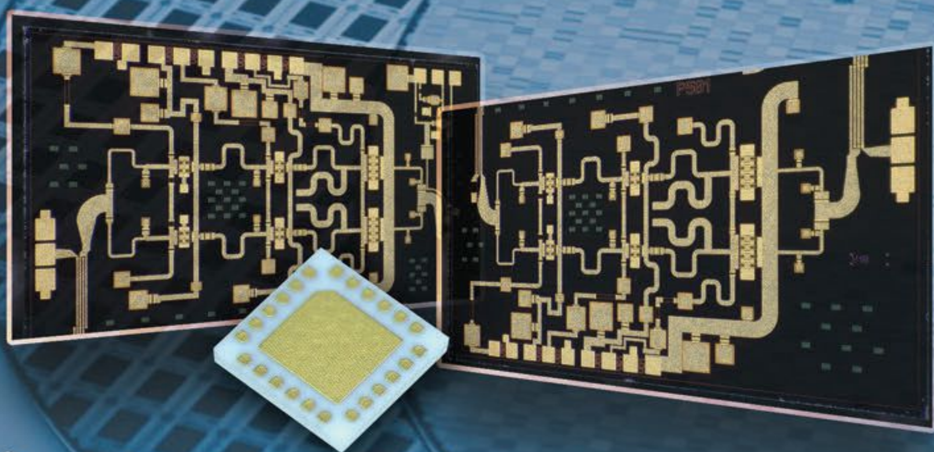

Miller MMIC is a global provider of RF semiconductor solutions with expertise in GaAs and GaN processes. We offer a diverse range of products tailored to various wireless applications. Our product lineup encompasses a wide array of offerings, including Low Noise Amplifiers, Distributed Amplifiers, Power Amplifiers, Driver Amplifiers, RF Switches, RF PIN Diode Switches, and numerous other voltage- and digitally-controllable RF components.

RapidRF MILLER MMIC RapidRF AI Platform for RF MMIC Design

RF Distributed Low Noise Amplifiers

PN	Freq Low (GHz)	Freq High (GHz)	Gain (dB)	NF(dB)	P1dB (dBm)	Voltage (VDC)	Current (mA)	Package
MMW001T	DC	20.0	17~19	1~3.5	23 @ 10GHz	8.0	145	die
MMW4FP	DC	50.00	16.00	4.00	24.00	10	200	die
MMW507	0.20	22.0	14.0	4 - 6	28.0	10.0	350	die
MMW508	DC	30.0	14.0	2.5dB @ 15GHz	24.5	10.0	200	die
MMW509	30KHz	45.0	15.0		20.0	6.0	190	die
MMW510	DC	45.0	11.0	4.5	15.5	6.0	100	die
MMW510F	DC	30.00	20.00	2.50	22.00			die
MMW511	0.04	65.0	10.0	9.0	18.0	8.0	250	die
MMW512	DC	65.0	10.0	5.0	14.5	4.5	85	die
MMW5FN	DC	67.00	14.00	2.00	19.00	4.5	81	die
MMW5FP	DC	67.00	14.00	4.00	21.00	8	140	die
MMW011	DC	12.0	14.0		30.5	12.0	350	die

Low Noise Amplifiers

PN	Freq Low (GHz)	Freq High (GHz)	Gain (dB)	NF(dB)	P1dB (dBm)	Voltage (VDC)	Current (mA)	Package
MML040	6.0	18.0	24.0	1.5	14.0	5.0	35	die
MML058	1.0	18.0	15.0	1.7	17.0	5.0	35	die
MML063	18.0	40.0	11.0	2.9	15.0	5.0	52	die
MML080	0.8	18.0	16.5/15.5	1.9/1.7	18/17.5	5.0	65/40	die
MML081	2.0	18.0	25/23	1.0/1.0	16/9.5	5.0	37/24	die
MML083	0.1	20.0	23.0	1.6	11.0	5.0	58	die

RF Driver Amplifier

PN	Freq Low (GHz)	Freq High (GHz)	Gain (dB)	NF(dB)	P1dB (dBm)	Voltage (VDC)	Current (mA)	Package
MM3006	2.0	20.0	19.5	2.5	22.0	7.0	130	die
MM3014	6.0	20.0	15.0	-	19.5	5.0	107	die
MM3017T	17.0	43.0	25.0		22.0	5.0	140	die
MM3031T	20.0	43.0	20.0		24.0	5.0	480	die
MM3051	17.0	24.0	25.0	-	25.0	5.0	220	die
MM3058	18.0	40.0	20/19.5	2.5/2.3	16/14	5/4	69/52	die
MM3059	18.0	40.0	16/16	2.5/2.3	16/15	5/4	67/50	die

GaAs Medium Power Amplifier

PN	Freq Low (GHz)	Freq High (GHz)	Gain (dB)	P1dB (dBm)	Psat (dBm)	Voltage (VDC)	Current (mA)	Package
MMP107	17.0	21.0	19.0	30.0	30.0	6.0	400	die
MMP108	18.0	28.0	14.0	31.5	31.0	6.0	650	die
MMP111	26.0	34.0	25.5	33.5	33.5	6.0	1300	die
MMP112	2.0	6.0	20.0	31.5	32.0	8.0	365	die
MMP501	20.0	44.0	15.0	27 -- 32	29 - 34	5.0	1200	die
MMP502	18.0	47.0	14.0	28.0	30.0	5.0	1500	die

PN: MMW5FP

RF GaAs MMIC DC-67GHz

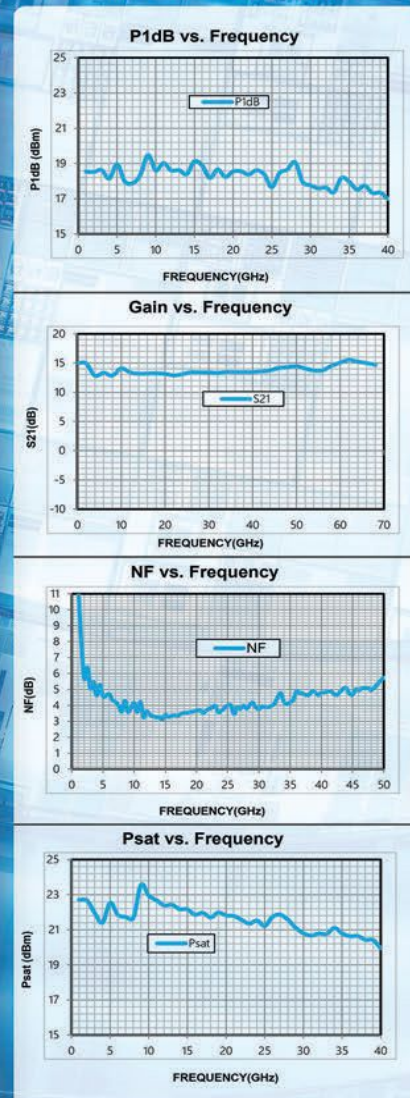

CALL US 1-833-2MILLER(264-5537)

WWW.MILLERMMIC.COM

RapidRF

sales@millermmic.com
support@millermmic.com

DC TO 86 GHz

Filter Technologies

For Every Application

Selection and Solutions

- 1500+ in-stock models
- Low pass, high pass, band pass, band stop, diplexers and triplexers
- In-house design and manufacturing capability
- Fast, affordable custom capabilities

LEARN MORE

Cavity

- Passbands to 43.5 GHz
- Stopbands to 57 GHz
- Bandwidths as narrow as 1%
- 100+ dB rejection

Ceramic Resonator

- Fractional bandwidths from 0.5 to 40%
- Excellent power handling, up to 20W
- High Q in miniature SMT package

Lumped L-C

- Wide catalog selection
- Several package options including aqueous washable
- Variety of filter topologies

LTCC

- Tiny size, as small as 0202
- Industry's widest selection of mmWave LTCC filters
- Proprietary designs with stopband rejection up to 100 dB

Microstrip

- Connectorized designs with 4 to 40% fractional bandwidth
- Power handling up to 10W
- Flat group delay

MMIC Reflectionless

- Patented topology absorbs and internally terminates stopband signals
- Perfect for pairing with amplifiers, mixers, multipliers, ADC/DACs & more
- Cascadable with other filter technologies

Rectangular Waveguide

- WR-12, WR-15 and WR-28 interfaces
- Passbands up to 87 GHz
- High stopband rejection, 40 dB

Suspended Substrate

- Ultra-wide passbands up to 26 GHz
- Wide stopbands up to 40 GHz
- High Q

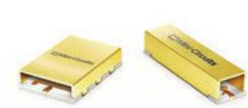

Thin Film on Alumina

- Passbands from DC to 40 GHz
- High rejection with wide passband
- Miniature SMT package

Mini-Circuits®


Signal & Spectrum Analyzer · 10 Hz – 30 GHz


RF-LAMBDA
THE LEADER OF RF BROADBAND SOLUTIONS
BROADBAND SSPA / EMC BENCHTOP
SOLID STATE POWER AMPLIFIER
0.1-22GHZ
ULTRA BROADBAND SSPA
RFLUPA01M22GA
4W 0.1-22GHZ
RFLUPA0218GB
20W 1-19GHZ
300W 6-18GHZ SOLID STATE BROADBAND
400W 8-11GHZ
SOLID STATE BROADBAND
0.1-6GHZ VHZ,
UHF, L, S, C BAND
RFLUPA02G06GC
100W 2-6GHZ
RFLUPA0706GD
30W 0.7-6GHZ
MADE IN USA
6-18GHZ C, X, KU BAND
RFLUPA08G11GA
50W 8-11GHZ
RFLUPA0618GD
60W 6-18GHZ
RFLUPA06G12GB
25W 6-12GHZ
18-50GHZ K, KA, V BAND
RFLUPA18G47GC
2W 18-47GHZ
RFLUPA27G34GB
15W 27-34GHZ
RFLUPA47G53GA2
10W 47-53GHZ
RFLUPA27G34GB
30W 18-40GHZ
BENCHTOP RF MICROWAVE SYSTEM POWER AMPLIFIER
RAMP00G06GA- 30W 0.01-6GHZ
RAMP39G48GA- 4W 39-48GHZ
RAMP01G22GA- 8W 1-22GHZ
RAMP27G34GA- 8W 27-34GHZ
www.rflambda.com
sales@rflambda.com
1-888-976-8880
1-972-767-5998
San Diego, CA, US
Carrollton, TX, US
Ottawa, ONT, Canada
Frankfurt, Germany

Microwave Journal

CONTENTS

February 2025
Vol. 68 • No. 2
Satellite & Radio Communications
mwjournal.com

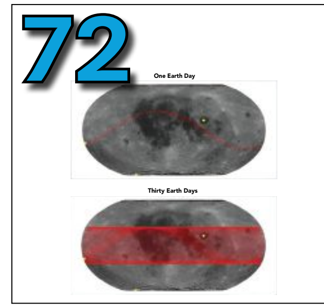

Cover Feature

Perspective

Special Reports

Technical Features

ACCESS NOW!
digital.microwavejournal.com

eXclusive Digital Content ›››

68 YEARS OF PUBLISHING EXCELLENCE

Has Amplifier Performance or Delivery Stalled Your Program?

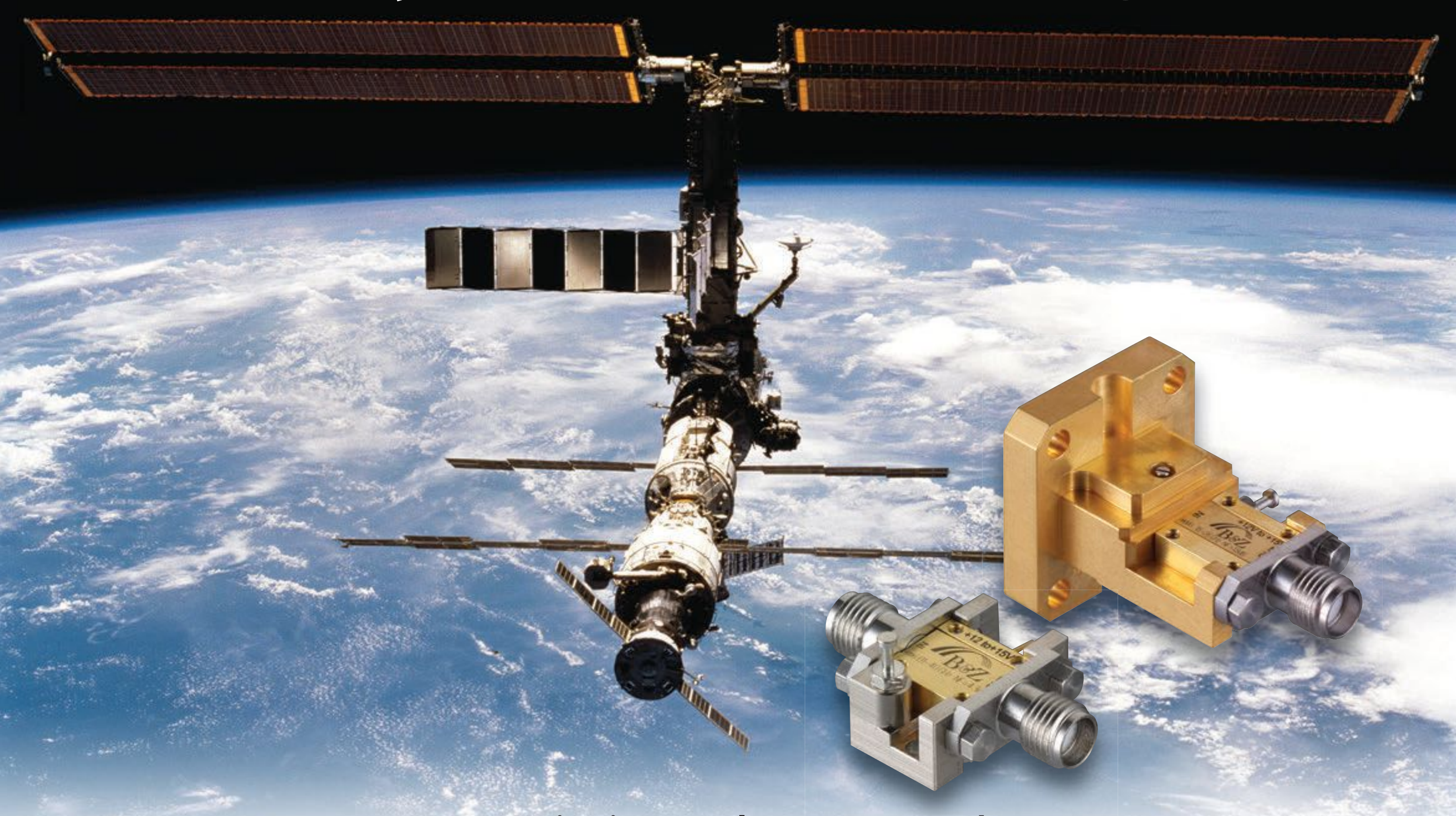

Noise Figure In Select Frequency Bands

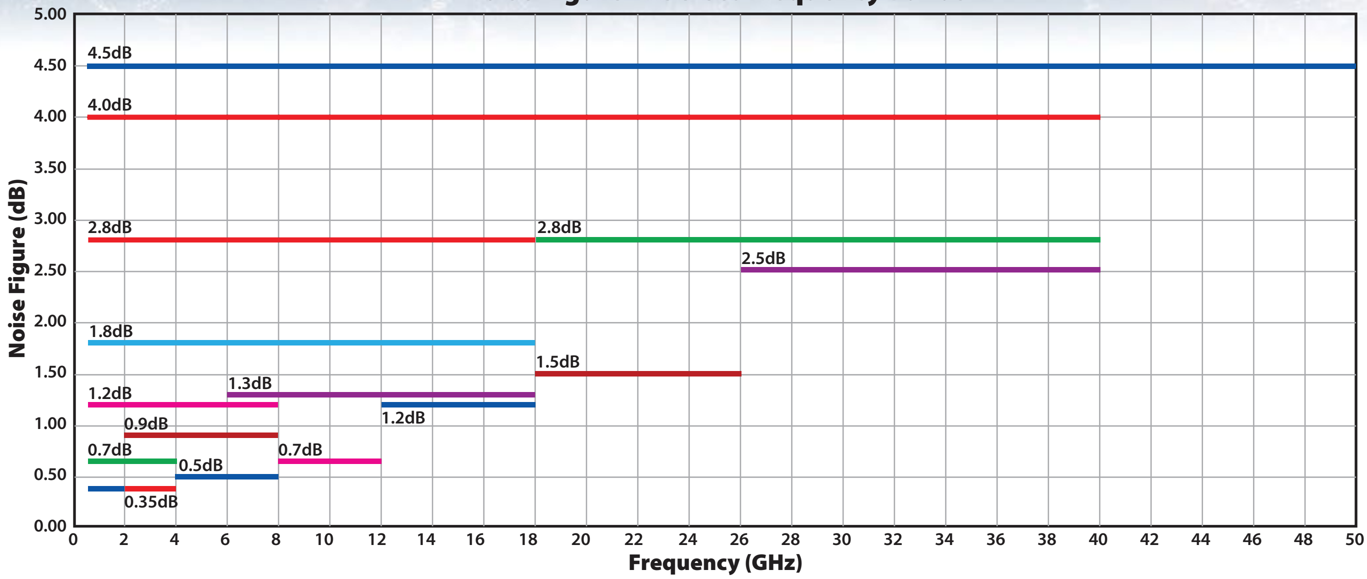

B&Z TECHNOLOGIES

Innovating to Excel

www.bnztech.com

Microwave Journal

CONTENTS

mwjournal.com

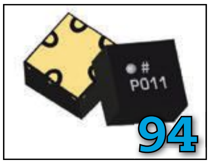

Product Features

Tech Brief

Departments

Microwave Journal (USPS 396-250) (ISSN 0192-6225) is published monthly by Horizon House Publications Inc., 685 Canton St., Norwood, MA 02062. Periodicals postage paid at Norwood, MA 02062 and additional mailing offices.

POSTMASTER: Send address corrections to Microwave Journal, PO Box 1028, Lowell, MA 01853 or e-mail mwj@e-circ.net.com. Subscription information: (978) 671-0446. This journal is issued without charge upon written request to qualified persons working in the RF & microwave industry. Other subscriptions are: domestic, $130.00 per year, two-year subscriptions, $200.00; foreign, $225.00 per year, two-year subscriptions, $400.00; back issues (if available) and single copies, $20.00 domestic and $30.00 foreign. Claims for missing issues must be filed within 90 days of date of issue for complimentary replacement.

Posted under Canadian international publications mail agreement #PM40612608

EXECUTIVE EDITORIAL OFFICE

685 Canton Street, Norwood, MA 02062
Tel: (781) 769-9750
FAX: (781) 769-5037
e-mail: mwj@mwjournal.com

EUROPEAN EDITORIAL OFFICE

16 Sussex Street, London SW1V 4RW, England
Tel: Editorial: +44 207 596 8730 Sales: +44 207 596 8740
FAX: +44 207 596 8749

SUBSCRIPTION SERVICES

Send subscription inquiries and address changes to:
Tel: (978) 671-0446
e-mail: mwj@e-circ.net

www.mwjournal.com

Printed in the USA

Microwave Journal ONLINE .COM

LEARNING CENTER

Access webinars on-demand from the archived webinars and events page at www.mwjournal.com/events

Catch *Frequency Matters*, the industry update from *Microwave Journal*, microwavejournal.com/FrequencyMatters

WHITE PAPERS

Look for additional content from:

ALTAIR

Anritsu
Advancing beyond

Extended Reality (XR) Spreading in Business Field

FEATURED eBooks

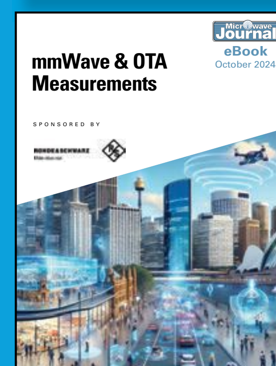

mwjournal.com/ebooks

Join Us Online

Follow us @Pathindle @MWJEric @MWJEditor

Join us at the RF and Microwave Community

Become a fan at facebook.com/microwavejournal

Visit us @ mwjournal.com

Microwave Journal podcasts include the RF/microwave update series, Frequency Matters, plus interviews with industry experts and executives.

https://podcasts.microwavejournal.com

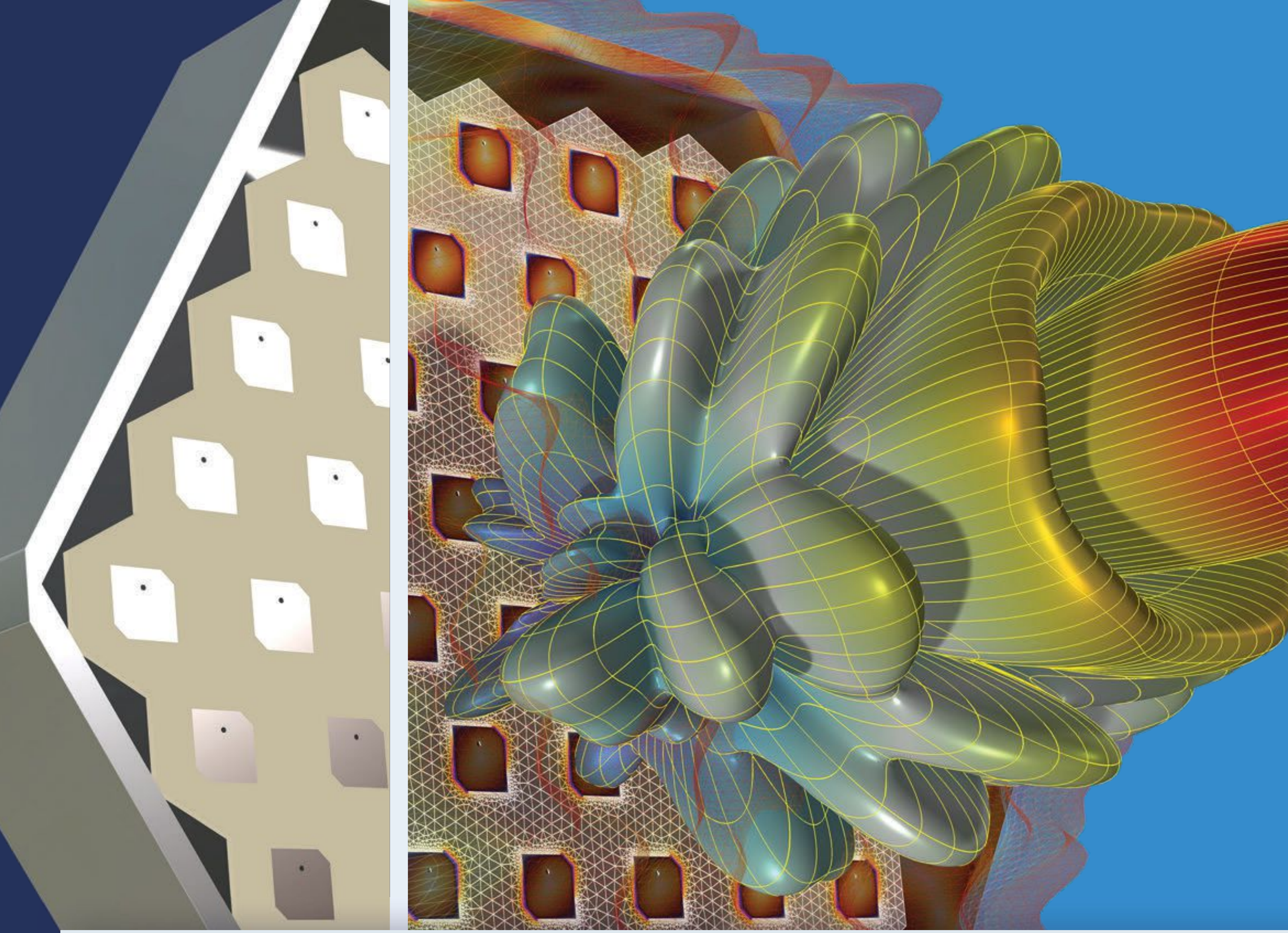

DC TO 50 GHz

MMIC Amplifiers

300+ Models Designed in House

Options for Every Requirement

CATV (75Ω)

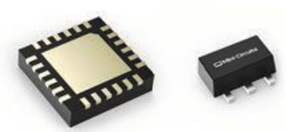

Supporting DOCSIS® 3.1 and 4.0 requirements

Dual Matched

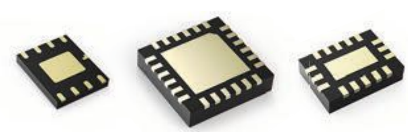

Save space in balanced and push-pull configurations

Hi-Rel

Rugged ceramic package meets MIL requirements for harsh operating conditions

High Linearity

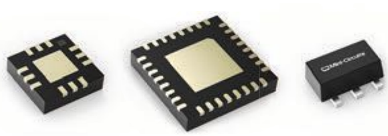

High dynamic range over wide bandwidths up to 45 GHz

Low Noise

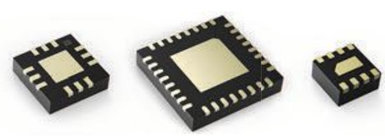

NF as low as 0.38 dB for sensitive receiver applications

Low Additive Phase Noise

As low as -173 dBc/Hz @ 10 kHz offset

RF Transistors

<1 dB NF with footprints as small as 1.18 x 1.42mm

Variable Gain

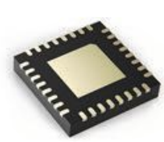

Up to 31.5 dB digital gain control

Wideband Gain Blocks

Flat gain for broadband and multi-band use

STAY CONNECTED TO COMING EVENTS

MARK YOUR CALENDAR

FEBRUARY

19-21
iWAT
Cocoa Beach, Fla.
https://attend.ieee.org/iwat-2025

MARCH

1-8
IEEE Aerospace Conference
Big Sky, Mont.
www.aeroconf.org

3-6
MWC
Barcelona, Spain
www.mwcbarcelona.com

10-13
Satellite 2025
Washington, DC
www.satshow.com

15-20
IPC APEX EXPO 2025
Anaheim, Calif.
www.ipcapexexpo.org

25-27
EMV
Stuttgart, Germany
https://emv.mesago.com/events/en.html

30-4/4
EuCAP 2025
Stockholm, Sweden
www.eucap2025.org

APRIL

8-9
IEEE Texas Symposium
Waco, Texas
https://texassymposium.org

14-15
WAMICON
Cocoa Beach, Fla.
www.ieeewamicon.org

MAY

19-22
CS Mantech
New Orleans, La.
https://csmantech.org/

Register online at signalintegrityjournal.com

ONLINE PANEL SERIES

3/14
Using AI in the Design of Electronic Systems

Call for Papers Deadlines

3/11 EuMW

3/30 IEEE RFID-TA

FOR DETAILS VISIT MWJOURNAL.COM/EVENTS

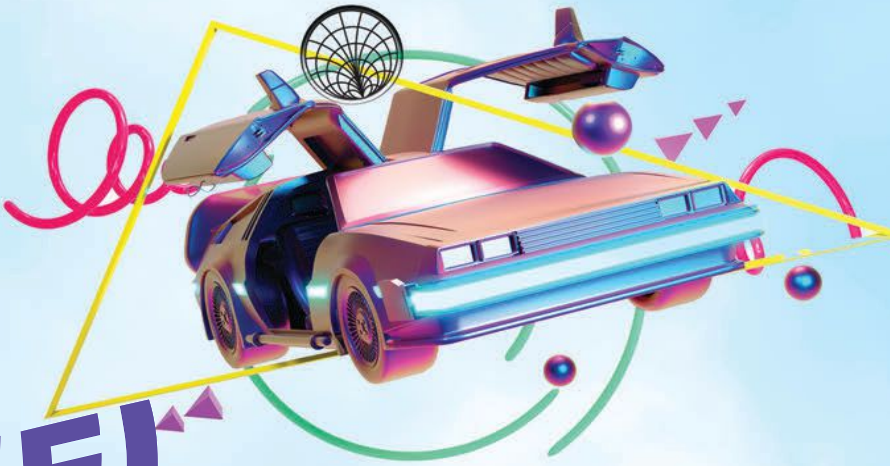

Stefano Maurri, Stefano Selleri
University of Florence, Florence, Italy

Mr. Spock, We Need to Print a Circuit!

Star Trek is one of the most successful Sci-Fi series ever. It began with Star Trek (1966 to 1969), the first iconic series, followed by Star Trek Next Generation (1987 to 1994) and several other series and full-length movies. The special effects, especially in the first series, were somewhat naïve. Despite the premise, the futuristic look is very recognizable as being in the 1960s and 1980s. However, if you have keen eyes and are looking at Season 1, Episode 12[1] of Star Trek: The Next Generation, titled "Datalore," you will find some nice eye candy for microwave engineers.*

*The episode aired on January 18, 1988, in the U.S.[2] In the context of the show, the episode takes place at a stardate, the fictional time measurement scale used by the Star Trek franchise, of 41242.4 on planet Omicron Theta. This is the home planet of the android, Data, the second-officer of the USS Enterprise. An exploration team from the Enterprise finds a lab that they learn is the one where Dr. Noonien Soong indeed built Data. In the panoramic view of the lab, the Quintel Q2001 mask aligner, shown in **Figure 1**, appears here, playing the role of a far-future fantastic item.*

Indeed, Quintel Corporation was founded in 1978 to provide an alternate source for OEM-level product support for the Canon, Kasper and Cobilt brands of contact mask aligners. In 1986, Quintel introduced its own line of mask alignment exposure systems to serve the microelectronic industry better, so the Quintel Q2001 shown on Star Trek: The Next Generation is one of the first they produced. In 2005, Quintel was then acquired by Neutronix, a company dating back to 1989, that still operates in the mask alignment segment as NxQ.

*As a personal note from the authors, the RF Microwave and Electromagnetics lab at the University of Florence used an even older version of a Quintel Q2001. This piece of equipment, shown in **Figure 2**, had an electromechanical timer and a slightly different eyepiece from the one seen in the Star Trek: The Next Generation episode. It was purchased second-hand in 1992 and is now considered an industrial archaeology item. The photo in Figure 2 was taken some time ago when the mask aligner was still in use. So, maybe the one in the Star Trek: The Next Generation series was indeed the futuristic version!*

Fig. 1 The Quintel Q2001 mask aligner featured as a "futuristic device" from Star Trek: The Next Generation.

Fig. 2 The Quintel Q2001 mask aligner at the University of Florence.

References

1. www.imdb.com/it/title/tt0708698/?ref_=ttep_ep12
2. en.wikipedia.org/wiki/Datalore

[*]Or episode 13. The first episode "Encounter at Farpoint," was split into two parts, so "Datalore" is the 12th title but the 13th to be aired.


Meet us at SATSHOW 2025
Washington, D.C. | March 10-13, 2025 | Meeting Suite #3
Always Connected
Qorvo brings innovation and scale to SATCOM applications. Our system level support and broad portfolio of products are connecting the world through space.
Visit qorvo.com/go/satcom to see our complete portfolio for SATCOM.
© 01-2025 Qorvo US, Inc. | QORVO is a trademark of Qorvo US, Inc.

COVER FEATURE
INVITED PAPER

The Art, Science and Magic of Invisibility: Designing Transparent Antennas

Baha Badran
Taoglas, San Diego, Calif.

Imagine a world where antennas vanish, seamlessly blending into their surroundings. Transparent antennas are turning this concept into a reality. This article examines the technical complexities and approaches involved in designing and manufacturing transparent antennas for high volume production, highlighting the interplay between RF design principles, material science, physics, mechanical engineering and advanced manufacturing processes. There are numerous applications for transparent antennas, from automotive sunroofs to electric vehicle (EV) charging display screens and more to be discovered. By unraveling the art, science and magic behind this invisible technology, this article aims to inspire further advancements, paving the way for a future of covert connectivity.

WHAT IS A TRANSPARENT ANTENNA?

Transparent antennas are made from transparent conductive films and are designed to be virtually invisible to the human eye. These ultra-low-profile, flexible antennas are placed on transparent, nonmetal surfaces, such as glass, plastic or other clear materials, allowing light to pass through without obstructing visibility. Their transparency enables concealed antenna placement and allows them to be placed on various surfaces, which would previously have been undesirable or unusable for other antenna types. Typical applications include glass surfaces such as windows, screens and sunroofs of automotive and commercial transportation, EV charging and parking bays, digital signage and display screens and point-of-sale kiosks.

Taoglas now offers six different Taoglas Invisible Antenna™ products in its portfolio. The TFX series can be used standalone or in a custom combination to enhance cellular, Wi-Fi and GNSS antenna installations. Each antenna comes with a pre-adhered adhesive for ease of installation and has an enclosed carrier terminated with a FAKRA or an SMA connector. ***Figure 1*** shows the TFX62.A, a 5G/4G cellular antenna with coverage from 600 MHz to 6 GHz.

Taoglas has also worked on multiple custom antenna designs based on this patented transparent technology. One custom solution created an 8-in-1 combination antenna, integrating cellular, Wi-Fi, GNSS and other antenna technologies into a single transparent film. In this particular use case, the edges of the transparent film were rounded to fit the unique requirements of the application and to offer a covert appearance.

DESIGN & DEVELOPMENT CONSIDERATIONS

Taoglas first began development of transparent antennas in 2020 and commercially introduced the first

▲ Fig. 1 **TFX62.A, a transparent 5G/4G cellular antenna.**


The only
QPL Certified
MECHANICAL
SWITCH
House!
Quick Turn
RF FILTER
Prototypes
are in our DNA!
Huge Library
of PASSIVES
with Best in Show
HIGH POWER
COUPLER
offering!
RUGGED & RELIABLE
AGILE & ADAPTIVE
HIGH POWER & VARIETY
RLC
RF MECHANICAL SWITCHES,
RF FILTERS & RF PASSIVES
AS9100 CERTIFIED, MADE IN USA
High Performance Precision Microwave Components
Serving the world-wide aerospace & defense community since 1959
Robust Catalog Portfolio - no hassle, quick turn, custom solutions our specialty
RLC Electronics | 83 Radio Circle, Mt. Kisco, NY 10549 | 914-241-1334 | sales@rlcelectronics.com | www.rlcelectronics.com

three products in the Taoglas Invisible Antenna series in February 2023 with support for cellular (TFX62.A), Wi-Fi (TFX257.A) and GNSS (TFX125.A). The motivation was to design a solution that was as transparent as possible, building upon the company's technical knowledge in different antenna types, including flexible printed circuit board (PCB) antennas. Flexible antennas are attached via a "peel and stick" process and can be bent, folded or stretched to conform to various shapes and surfaces. This flexibility enables the integration of antennas into unconventional locations, such as the curved edges of a smartphone or the interior of a vehicle. However, these flexible antennas are typically black and would be highly visible on a transparent surface, such as glass.

The core challenge in designing transparent antennas lies in reconciling two seemingly contradictory properties: conductivity and transparency. Conductive materials, essential for efficient antenna performance, typically absorb or reflect light, making them opaque. The more transparent the material, the less conductive it is, which can degrade antenna performance. Transparency is measured in visible light transmission (VLT), which is the percentage of visible light that passes through the material as opposed to being reflected or absorbed. Finding the right balance between performance and transparency is crucial.

Taoglas has observed several responses to translating an antenna design from copper to a transparent material. Whether or not a resonance shift occurs is dependent on the design of the antenna. More often than not, a resonance shift is not seen and the impedance response is fairly similar. However, a drop in performance for both antenna efficiency and peak gain can be expected. The designs are also reflected fairly accurately in simulation models, as shown in ***Figure 2***.

Taoglas regularly provides custom antenna solutions to customers. These antennas are designed to optimize RF performance for a specific environment. These projects often involve combining and integrating several

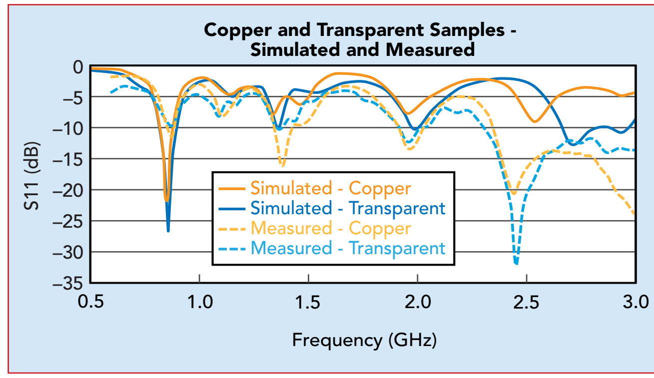

Fig. 2 **Simulated and measured results for copper and transparent material.**

different technologies. Taoglas is thus ideally suited to identify technical challenges, propose and evaluate potential solutions and provide expert opinions to ensure technical challenges are overcome.

Several types of materials can be used for transparent antennas. Each presents a different compromise between RF performance and transparency. One of the materials is a metal mesh conductive film that exhibits properties that make it an excellent choice for antenna applications when considering sheet resistance, VLT, power, color and haze.

Transparent films are not solid metals, making it difficult to solder cables directly. For high volume production, a reliable, repeatable and easy-to-manufacture connection method is needed. The design has to ensure that the antenna remained invisible, even with the necessary cables and connections. An electromechanical connection method is most often required to ensure an optimal RF connection is in place. This method is also the friendliest from production and assembly points of view.

Another challenge with transparent films is the difficulty of creating a multi-layer stacked film with a physical electrical connection between these layers. This

structure is similar to using via holes in PCBs. This poses a considerable challenge for RF engineers and the ability to create controlled impedance transmission lines such as on-ground coplanar waveguides (CPWG).

Finally, there are mounting and adhesion considerations. The double-sided adhesive must be clear enough to maintain invisibility and provide strong adhesion for the expected product lifetime. For instance, considering the potential placement of the transparent antenna on a car window, the adhesive cannot yellow from the sun's UV rays or lose strength from excessive heat.

MATERIAL AND CONNECTION METHOD

After experimenting with different materials, a sub-mm metal mesh conductive film was selected for its performance, reliability and transparency. The material for the housing or carrier is ABS/PC and the material for the antenna is PET. Taoglas Invisible Antenna products feature a VLT of greater than 74 percent TCF. Compare this to the automotive industry's standards, which require a VLT of 70 percent for the front windshield. The material is also heat-resistant and UV-protected. The antennas can operate from -40°C to 85°C and can withstand a non-condensing 65°C, 95 percent relative humidity environment.

To connect to the cables, a solution was developed that involved a mechanical connection method using clips to create a consistent RF connection. This was achieved by feeding the antenna from the edge and using an invisible tail to act as a cable. ***Figure 3*** shows the unique PCB adapter board with a FAKRA connector solution.

ENSURING OPTIMAL RF PERFORMANCE AND INTEGRATION CONSIDERATIONS

While covert, it is important to remember that transparent antennas are still antennas. Ground plane considerations are relevant and each antenna should be placed at least 20 mm from metal to maintain performance. Like other antennas, key performance metrics for transparent antennas include antenna efficiency, impedance matching, gain, radiation patterns and bandwidth coverage. ***Figure 4*** shows the TFX62.A antenna total efficiency versus frequency when mounted on a 4 mm plastic substrate.

Taoglas has added to its Taoglas Invisible Antenna

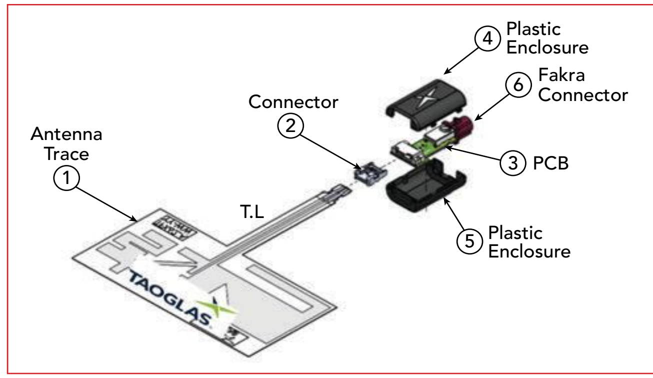

▲ Fig. 3 **The unique PCB adapter board with FAKRA connector solution.**

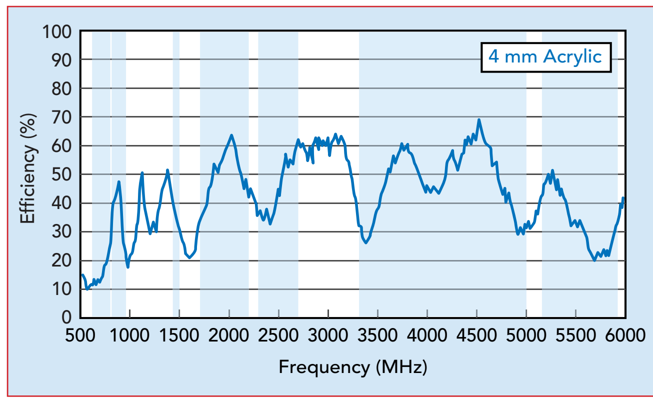

▲ Fig. 4 **TFX62 antenna efficiency versus frequency.**

MILLER MMIC

AI Powered RFIC Design Platform

RapidRF

Revolutionizing RFIC Design with AI-Driven Innovation.
Our AI driven design platform is redefining the future of the RFIC design industry. We automate the design of RFICs for the next generation of wireless communication, accelerating innovation for a smarter future.

AI-Driven Design Automation – Multiplying Engineers Productivity

- Technology Independent: GaAs, GaN, and Silicon proven
- Fast and reliable: more than 100x faster than an experienced design engineer
- AI-Driven Layout Optimization: cutting down costs, maximizing performance

Reference Design Done by Experienced Engineer

≈10 Days/Design

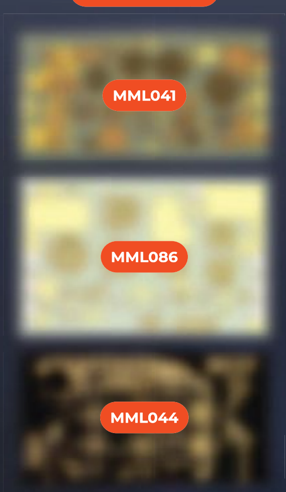

AI MMIC Design Process

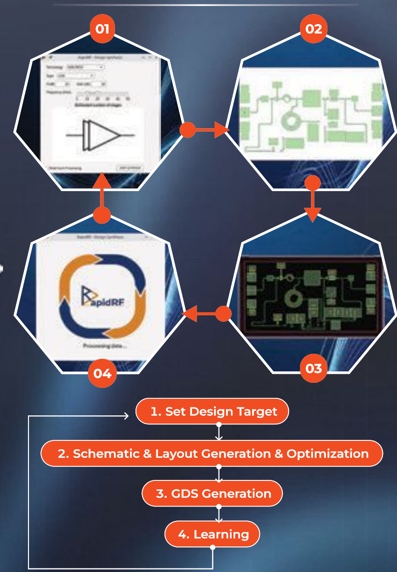

Design Done by RapidRF AI Platform

≈5 Hours/Design

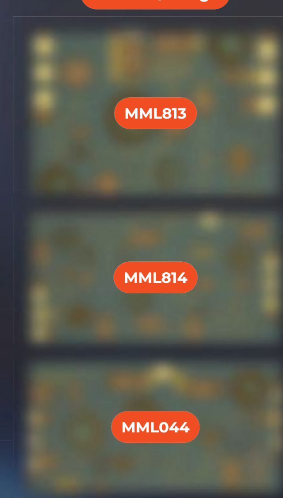

Performance Comparisons: RapidRF AI vs Human Engineer Designs

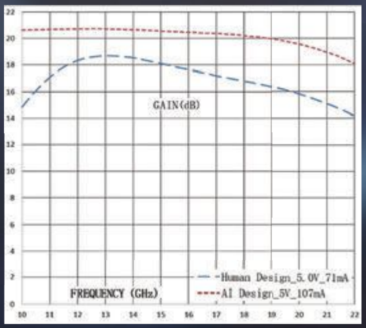

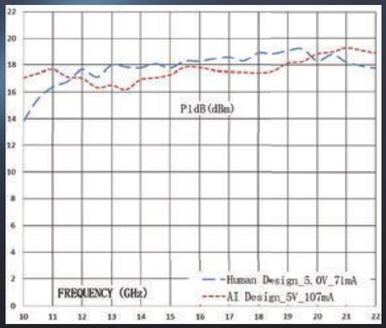

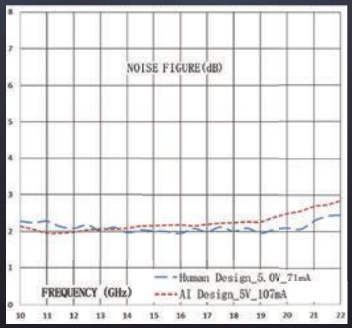

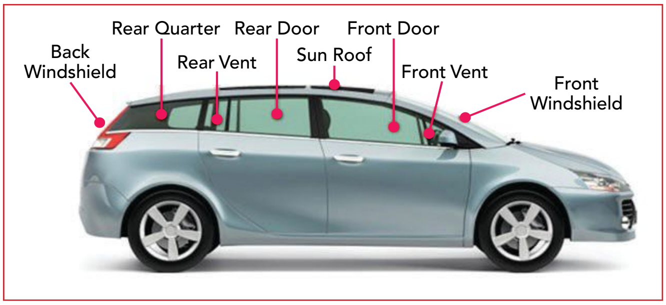

Fig. 5 **Glass placement options on a vehicle.**[1]

portfolio with SMA connector options. These include the TFX62.C for cellular applications, the TFX125.B for GNSS applications and the TFX257.B for Wi-Fi applications. Modular design allows for customizable MIMO configurations. The antennas can be placed orthogonally to each other to maximize coverage and throughput while minimizing coupling.

APPLICATION EXAMPLES

While transparent antennas cannot match the performance of solid conductive materials like copper, they offer unique benefits. For instance, placing a cellular transparent antenna on a window provides the closest possible access to external signals, improving signal strength, coverage and data rates. In automotive applications, covertly installed transparent antennas can be placed on automotive glass in the front/rear windshield, sunroof and/or side window locations. These antennas can serve as replacements for large external antennas. Transparent antennas can enhance vehicle-to-vehicle (V2V) and vehicle-to-infrastructure (V2I) communication, enabling advanced driver-assistance systems and autonomous driving features. When used in place of external antennas, they provide cost savings and simplify the installation process, as no drilling is required and instead use a "peel and stick" adhesive. ***Figure 5*** shows some of the areas where covert transparent antennas could be installed.

One potential application is the use of transparent antennas on vehicle glass to enable satellite communication in cars. This would provide reliable connectivity in remote areas where cellular networks are unavailable. Both established and new satellite operators are exploring how to approach the emerging satellite IoT market. Traditionally relying on proprietary protocols, satellite operators are now exploring the advantages of leveraging existing wireless IoT technologies, such as LoRaWAN, NB-IoT, LTE-M and 5G NR Low Power. Integrating these technologies can create seamless transitions from terrestrial to satellite networks, which are known as non-terrestrial networks (NTN).

This advancement of NTN brings new commercial opportunities for satellite providers, module and chipset manufacturers, along with antenna providers. The automotive industry has proposed n256 and n255 as the industry standard bands for the 5G NB-IoT and 5G NR standards. This is in line with the 3GPP Rel-17. ***Table 1*** highlights the frequencies and regional use of these NTN bands.

It is interesting to note that band n23 is listed here for the North American region. North America represents a large market for several applications. Bands n23 should be

TABLE 1

NTN BAND DESIGNATIONS AND REGIONS

NTN Satellite Band	Uplink (MHz)	Downlink (MHz)	Region
n255 (FDD)	1626.5 to 1660.5	1525 to 1559	Global
n256 (FDD)	1980 to 2010	2170 to 2200	Europe
n23 (FDD)	2000 to 2020	2180 to 2200	North America

covered in any antenna design to ensure the solution can operate in North America. Bands n23 and n256 are similar in terms of start and stop frequency for each channel. Designing for a combined n23/n256 solution would not increase the complexity of the design or the R&D development time required. Designing for a combined n23/n256 band provides more commercial opportunities.

Most of the NTN technologies currently in development are focused on IoT applications. The large latency and low throughput associated with GEO satellites currently limit the range of potential applications. As more LEO satellites come online, the potential exists for low latency, high-throughput applications in this segment.

A link budget is required to determine whether specified antenna parameters, such as antenna gain, will result in a functional system. The link budget considers the entire RF path and calculates the received power at a receiver. If the power received is higher than the receiver sensitivity, the received signals can be decoded. Additionally, link budgets can be used to calculate the bit error rates (BER) of wireless technologies, such as NB-IoT. This is done by calculating the Energy Spectral Density or SNR $\left(\frac{E_b}{N_0}\right)$ and estimating the system noise. ***Figure 6*** shows the SNR versus BER for some representative modulation schemes.

Taoglas has undertaken a research project in collaboration with the European Space Agency. This project involves designing an array of antennas to increase gain and enable beamforming and beam steering to provide high performance connectivity. Typical satcom antennas for LEO constellations are passive, omnidirectional and have a peak gain of approximately 3 dBi. Transparent antennas are typically planar and thus inherently omnidirectional, with a low peak gain. To increase the link margin in the link budget, this gain could be increased by adding additional satcom antennas, thus creating a distributed antenna system (DAS). Signals from satcom satellites are circularly polarized, while the transparent antennas are linear.

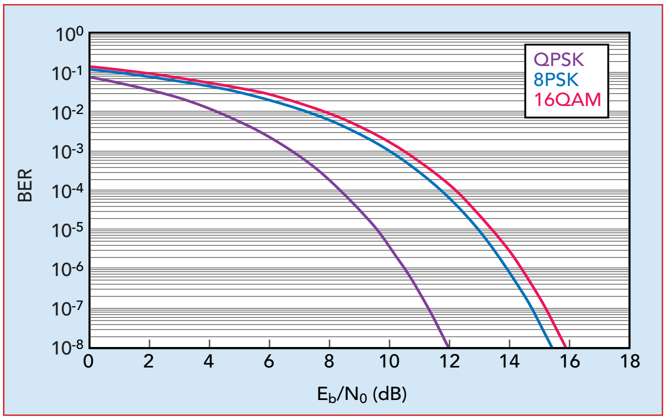

Fig. 6 **BER for various modulation schemes.**

A DAS is a network of antennas spaced within a particular area and connected to a common source. It was initially envisioned to replace a single high-power an-

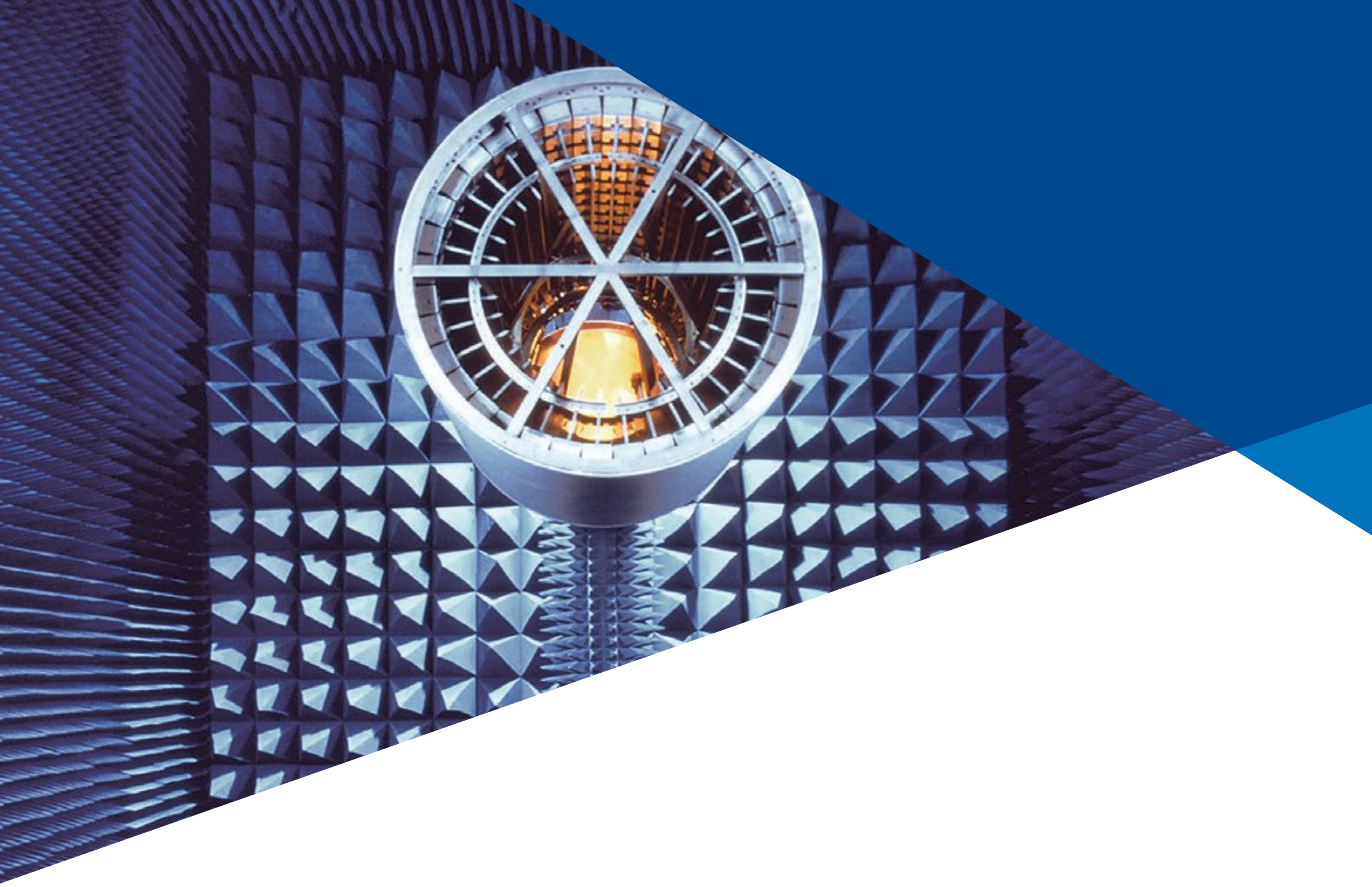

tenna with several low-power antennas. This allowed for improved reliability and less total power required due to the more localized coverage area. Generally, DAS is intended to provide coverage to several areas independently, such as in a building. Typical use cases for DAS are to deliver cellular, Wi-Fi or emergency service coverage, indoors or outdoors, to hotels, subways, airports, hospitals, businesses or roadway tunnels.[2]

Vehicle-DAS (vDAS) involves locating antennas around the vehicle to increase the effectiveness of the DAS. Typically, several antenna technologies exist in modern vehicles. These include GNSS for navigation and timing, 5G MIMO arrays, vehicle-to-everything antennas, AM/FM/DAB antennas and Bluetooth/Wi-Fi antennas for connecting devices.

The compatibility of transparent antennas with a DAS depends on their physical integration into the system, their transparency requirements and the overall RF technical specifications. Since there is a trade-off between RF performance and transparency, an antenna with the required RF performance may not be transparent enough. Increasing the number of antennas in the DAS while increasing the transparency may alleviate this problem. Theoretically, transparent antennas should be able to be integrated into a DAS just like any other antenna, provided they have an appropriate connector. Feasibility studies into this application are ongoing.

Other applications include smart buildings and industrial applications. In these applications, transparent antennas can be attached to the windows of homes, offices and shopping malls, offering connectivity without compromising aesthetics. Antenna placement on windows with cable connections to routers hidden in the walls can improve a building's aesthetic and ensure a seamless connection. Devices like EV chargers and parking meters can benefit from the on-screen placement of transparent antennas, where traditional external antennas would be visible and intrusive.

THE FUTURE OF ANTENNAS IS CLEAR

Antennas are often overlooked, yet they are the unsung heroes that enable seamless communication. Traditional antennas can be bulky and disrupt the aesthetic appeal of many devices or require complex installations, such as permanently drilling into a vehicle's roof. Transparent antennas represent a significant breakthrough and offer a unique alternative. As this technology continues to advance and evolve, there will undoubtedly be more applications for transparent antennas, shaping the future of covert connectivity. ■

References

1. "Auto Glass," AutomotiveConcepts.com, Web: http://www.automotiveconceptsmd.com/files/automotiveconcepts/wp-content/uploads/Auto-Glass-21093.jpg.
2. "What is a Distributed Antenna System (DAS)?," L-Com, Web: https://www.l-com.com/frequently-asked-questions/what-is-a-distributed-antenna-system-das?srsltid=AfmBOopR6yr95Lth16Bw4EQ8cVtyYmQTwjz29mqLWZ_eRy6RAtz33bwg.

RF-LAMBDA

MADE IN USA

THE LEADER OF RF BROADBAND SOLUTIONS

EMC Broadband RF Power Amplifier

High Power Solid State

HUNDREDS IN STOCK

FAST SHIPPING

FREQUENCY UP TO 90GHZ

POWER UP TO 2KW CW

REMC06G18GG

6-18GHZ 300W

- AUTOMATIC BUILT IN SELF CALIBRATION AND BIAS ADJUSTMENT.
- OVER TEMPERATURE, CURRENT, INPUT POWER PROTECTION.
- VSWR MEASUREMENT AND OPEN CIRCUIT PROTECTION.
- USER FRIENDLY CONTROL INTERFACE.
- REMOTE ETHERNET CONTROL AND FIRMWARE UPDATE.
- HIGH POWER EFFICIENCY AND LIGHTWEIGHT.

RAMP42G47GA 42-47GHZ 8W

RAMP18G40GB-U 18-40G 20W

RAMP05M80GC 0.5-80GHZ

REMC02G06GE 2-6GHZ 500W

REMC08G11GE 8-11GHZ 400W

RF Amplifiers and Sub-Assemblies for Every Application

Delivery from Stock to 2 Weeks ARO from the catalog or built to your specifications!

- Competitive Pricing & Fast Delivery
- Military Reliability & Qualification
- Various Options: Temperature Compensation, Input Limiter Protection, Detectors/TTL & More
- Unconditionally Stable (100% tested)

ISO 9001:2000 and AS9100B CERTIFIED

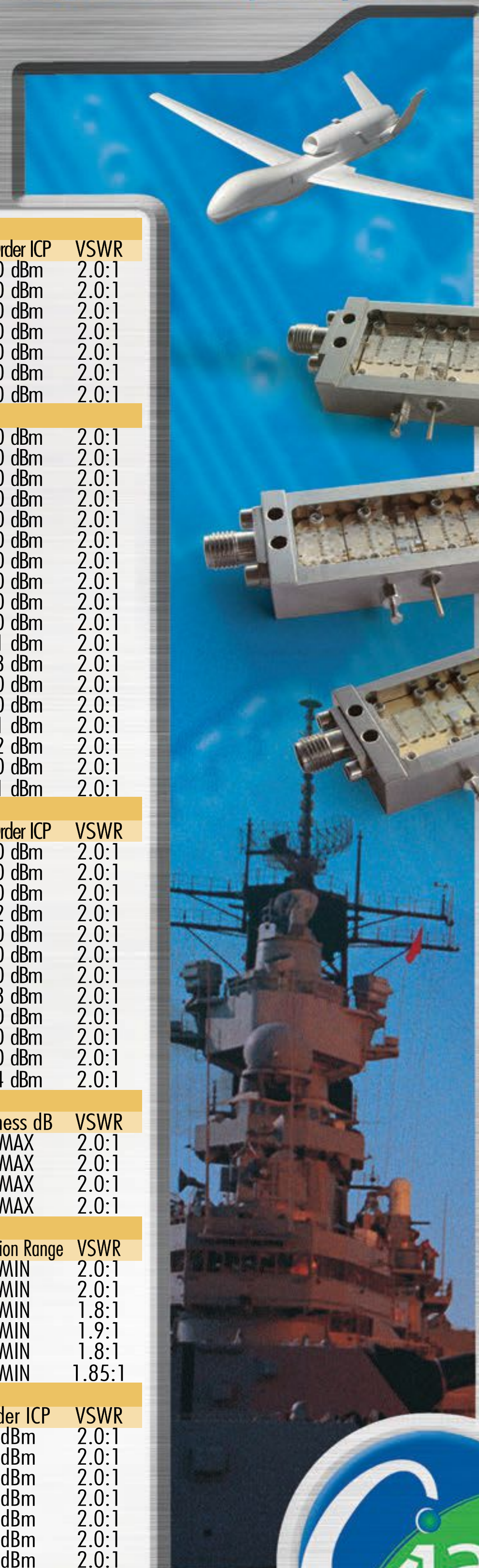

OCTAVE BAND LOW NOISE AMPLIFIERS

Model No.	Freq (GHz)	Gain (dB) MIN	Noise Figure (dB)	Power-out @ P1-dB	3rd Order ICP	VSWR
CA01-2110	0.5-1.0	28	1.0 MAX, 0.7 TYP	+10 MIN	+20 dBm	2.0:1
CA12-2110	1.0-2.0	30	1.0 MAX, 0.7 TYP	+10 MIN	+20 dBm	2.0:1
CA24-2111	2.0-4.0	29	1.1 MAX, 0.95 TYP	+10 MIN	+20 dBm	2.0:1
CA48-2111	4.0-8.0	29	1.3 MAX, 1.0 TYP	+10 MIN	+20 dBm	2.0:1
CA812-3111	8.0-12.0	27	1.6 MAX, 1.4 TYP	+10 MIN	+20 dBm	2.0:1
CA1218-4111	12.0-18.0	25	1.9 MAX, 1.7 TYP	+10 MIN	+20 dBm	2.0:1
CA1826-2110	18.0-26.5	32	3.0 MAX, 2.5 TYP	+10 MIN	+20 dBm	2.0:1

NARROW BAND LOW NOISE AND MEDIUM POWER AMPLIFIERS

Model No.	Freq (GHz)	Gain (dB) MIN	Noise Figure (dB)	Power-out @ P1-dB	3rd Order ICP	VSWR
CA01-2111	0.4 - 0.5	28	0.6 MAX, 0.4 TYP	+10 MIN	+20 dBm	2.0:1
CA01-2113	0.8 - 1.0	28	0.6 MAX, 0.4 TYP	+10 MIN	+20 dBm	2.0:1
CA12-3117	1.2 - 1.6	25	0.6 MAX, 0.4 TYP	+10 MIN	+20 dBm	2.0:1
CA23-3111	2.2 - 2.4	30	0.6 MAX, 0.45 TYP	+10 MIN	+20 dBm	2.0:1
CA23-3116	2.7 - 2.9	29	0.7 MAX, 0.5 TYP	+10 MIN	+20 dBm	2.0:1
CA34-2110	3.7 - 4.2	28	1.0 MAX, 0.5 TYP	+10 MIN	+20 dBm	2.0:1
CA56-3110	5.4 - 5.9	40	1.0 MAX, 0.5 TYP	+10 MIN	+20 dBm	2.0:1
CA78-4110	7.25 - 7.75	32	1.2 MAX, 1.0 TYP	+10 MIN	+20 dBm	2.0:1
CA910-3110	9.0 - 10.6	25	1.4 MAX, 1.2 TYP	+10 MIN	+20 dBm	2.0:1
CA1315-3110	13.75 - 15.4	25	1.6 MAX, 1.4 TYP	+10 MIN	+20 dBm	2.0:1
CA12-3114	1.35 - 1.85	30	4.0 MAX, 3.0 TYP	+33 MIN	+41 dBm	2.0:1
CA34-6116	3.1 - 3.5	40	4.5 MAX, 3.5 TYP	+35 MIN	+43 dBm	2.0:1
CA56-5114	5.9 - 6.4	30	5.0 MAX, 4.0 TYP	+30 MIN	+40 dBm	2.0:1
CA812-6115	8.0 - 12.0	30	4.5 MAX, 3.5 TYP	+30 MIN	+40 dBm	2.0:1
CA812-6116	8.0 - 12.0	30	5.0 MAX, 4.0 TYP	+33 MIN	+41 dBm	2.0:1
CA1213-7110	12.2 - 13.25	28	6.0 MAX, 5.5 TYP	+33 MIN	+42 dBm	2.0:1
CA1415-7110	14.0 - 15.0	30	5.0 MAX, 4.0 TYP	+30 MIN	+40 dBm	2.0:1
CA1722-4110	17.0 - 22.0	25	3.5 MAX, 2.8 TYP	+21 MIN	+31 dBm	2.0:1

ULTRA-BROADBAND & MULTI-OCTAVE BAND AMPLIFIERS

Model No.	Freq (GHz)	Gain (dB) MIN	Noise Figure (dB)	Power-out @ P1-dB	3rd Order ICP	VSWR
CA0102-3111	0.1-2.0	28	1.6 Max, 1.2 TYP	+10 MIN	+20 dBm	2.0:1
CA0106-3111	0.1-6.0	28	1.9 Max, 1.5 TYP	+10 MIN	+20 dBm	2.0:1
CA0108-3110	0.1-8.0	26	2.2 Max, 1.8 TYP	+10 MIN	+20 dBm	2.0:1
CA0108-4112	0.1-8.0	32	3.0 MAX, 1.8 TYP	+22 MIN	+32 dBm	2.0:1
CA02-3112	0.5-2.0	36	4.5 MAX, 2.5 TYP	+30 MIN	+40 dBm	2.0:1
CA26-3110	2.0-6.0	26	2.0 MAX, 1.5 TYP	+10 MIN	+20 dBm	2.0:1
CA26-4114	2.0-6.0	22	5.0 MAX, 3.5 TYP	+30 MIN	+40 dBm	2.0:1
CA618-4112	6.0-18.0	25	5.0 MAX, 3.5 TYP	+23 MIN	+33 dBm	2.0:1
CA618-6114	6.0-18.0	35	5.0 MAX, 3.5 TYP	+30 MIN	+40 dBm	2.0:1
CA218-4116	2.0-18.0	30	3.5 MAX, 2.8 TYP	+10 MIN	+20 dBm	2.0:1
CA218-4110	2.0-18.0	30	5.0 MAX, 3.5 TYP	+20 MIN	+30 dBm	2.0:1
CA218-4112	2.0-18.0	29	5.0 MAX, 3.5 TYP	+24 MIN	+34 dBm	2.0:1

LIMITING AMPLIFIERS

Model No.	Freq (GHz)	Input Dynamic Range	Output Power Range Psat	Power Flatness dB	VSWR
CLA24-4001	2.0 - 4.0	-28 to +10 dBm	+7 to +11 dBm	+/- 1.5 MAX	2.0:1
CLA26-8001	2.0 - 6.0	-50 to +20 dBm	+14 to +18 dBm	+/- 1.5 MAX	2.0:1
CLA712-5001	7.0 - 12.4	-21 to +10 dBm	+14 to +19 dBm	+/- 1.5 MAX	2.0:1
CLA618-1201	6.0 - 18.0	-50 to +20 dBm	+14 to +19 dBm	+/- 1.5 MAX	2.0:1

AMPLIFIERS WITH INTEGRATED GAIN ATTENUATION

Model No.	Freq (GHz)	Gain (dB) MIN	Noise Figure (dB)	Power-out @ P1-dB	Gain Attenuation Range	VSWR
CA001-2511A	0.025-0.150	21	5.0 MAX, 3.5 TYP	+12 MIN	30 dB MIN	2.0:1
CA05-3110A	0.5-5.5	23	2.5 MAX, 1.5 TYP	+18 MIN	20 dB MIN	2.0:1
CA56-3110A	5.85-6.425	28	2.5 MAX, 1.5 TYP	+16 MIN	22 dB MIN	1.8:1
CA612-4110A	6.0-12.0	24	2.5 MAX, 1.5 TYP	+12 MIN	15 dB MIN	1.9:1
CA1315-4110A	13.75-15.4	25	2.2 MAX, 1.6 TYP	+16 MIN	20 dB MIN	1.8:1
CA1518-4110A	15.0-18.0	30	3.0 MAX, 2.0 TYP	+18 MIN	20 dB MIN	1.85:1

LOW FREQUENCY AMPLIFIERS

Model No.	Freq (GHz)	Gain (dB) MIN	Noise Figure dB	Power-out @ P1-dB	3rd Order ICP	VSWR
CA001-2110	0.01-0.10	18	4.0 MAX, 2.2 TYP	+10 MIN	+20 dBm	2.0:1
CA001-2211	0.04-0.15	24	3.5 MAX, 2.2 TYP	+13 MIN	+23 dBm	2.0:1
CA001-2215	0.04-0.15	23	4.0 MAX, 2.2 TYP	+23 MIN	+33 dBm	2.0:1
CA001-3113	0.01-1.0	28	4.0 MAX, 2.8 TYP	+17 MIN	+27 dBm	2.0:1
CA002-3114	0.01-2.0	27	4.0 MAX, 2.8 TYP	+20 MIN	+30 dBm	2.0:1
CA003-3116	0.01-3.0	18	4.0 MAX, 2.8 TYP	+25 MIN	+35 dBm	2.0:1
CA004-3112	0.01-4.0	32	4.0 MAX, 2.8 TYP	+15 MIN	+25 dBm	2.0:1

CIAO Wireless can easily modify any of its standard models to meet your "exact" requirements at the Catalog Pricing.

Visit our web site at www.ciaowireless.com for our complete product offering.

Ciao wireless

Ciao Wireless, Inc. 4000 Via Pescador, Camarillo, CA 93012

Tel (805) 389-3224 Fax (805) 389-3629 sales@ciaowireless.com

DARPA Exploring Ways to Assess Ethics for Autonomous Weapons

The Autonomy Standards and Ideals with Military Operational Values (ASIMOV) program aims to develop benchmarks to objectively and quantitatively measure the ethical difficulty of future autonomy use cases and readiness of autonomous systems to perform in those use cases within the context of military operational values. DARPA has awarded seven contracts to an array of research performers, each exploring a different approach to addressing this challenge.

ASIMOV is attempting to tackle one of the chief concerns of its namesake, author Isaac Asimov: the ability of autonomous systems to follow human ethical norms. Asimov was a writer (and scientist) deeply concerned with exploring the unintended consequences of technology. He is famous for the "Three Laws of Robotics," introduced in 1942, which outline a simple, foundational ethic for robots. Much of his fiction explores the limitations and edge cases which effectively "break" the intentions of those laws, often with disastrous consequences for humans.

> Striving to create the ethical autonomy common language.

The challenges and opportunities Asimov predicted in his writing remain poignant today. The rapid development and impending ubiquity of autonomy and AI technologies across both civilian and military applications require a robust and quantitative framework to measure and evaluate not only the technical but, perhaps more importantly, the ethical ability of autonomous systems to follow human expectations. ASIMOV is tackling this challenge through the development and virtual demonstration of quantitative autonomy benchmarks.

"We don't know if what we're trying to do is even possible, but we know evaluating the ability of autonomous weapons systems to comply with human ethical norms is a conversation we have to have — the sooner, the better," says program manager Dr. T. J. Klausutis. "What we're doing is wildly aspirational. Through ASIMOV, DARPA intends to lead the national conversation around the ethics of autonomous weapons systems."

The ASIMOV program is striving to create the ethical autonomy common language to enable the developmental testing/operational testing (DT/OT) community to meaningfully evaluate the ethical difficulty of specific military scenarios and the ability of autonomous systems to perform ethically within those scenarios.

The seven performers on contract for ASIMOV are exploring multiple theoretical frameworks, as well as quantifiability and safety and assurance. The performers are CoVar, LLC; Kitware, Inc.; Lockheed Martin; RTX Technology Research Center; SAAB, Inc.; Systems & Technology Research, LLC; and the University of New South Wales.

ASIMOV performers are developing prototype generative modeling environments to rapidly explore scenario iterations and variability across a spectrum of increasing ethical difficulties. ASIMOV aims to build the foundation for defining the benchmark with, which future autonomous systems may be evaluated.

ASIMOV is designed to help inform a national and global conversation. The work being done will be public and the tools that will eventually be developed are intended to be open to the world for testing and utilization.

Lockheed Martin and MDA Demonstrate Capability for Defending Guam with Successful Flight Test

In December, Lockheed Martin and the Missile Defense Agency (MDA), in support of U.S. Indo-Pacific Command and the Department of Defense (DOD), successfully completed Flight Experiment Mission (FEM)-02. Completion of FEM-02 demonstrates significant regional capability with a live exo-atmospheric intercept of a medium-range ballistic missile (MRBM) target using the Aegis Guam System (AGS) from the island of Guam.

"In partnership with the MDA, Lockheed Martin went from contract award to intercept flight test in less than two years. This rapid integration of capabilities to demonstrate the defense of Guam was enabled by leveraging proven systems and Lockheed Martin's systems engineering, production and test excellence," said Paul Lemmo, vice president and general manager of Integrated Warfare Systems & Sensors at Lockheed Martin. "Lockheed Martin is fully committed to providing 21st Century Security solutions for Guam."

AGS, integrated with the AN/TPY-6 Radar, Vertical Launching System (VLS) and Standard Missile, could aid with pacing the Indo-Pacific threats and expanding joint all-domain operations for Guam and the region.

The FEM-02 test took place from Andersen AFB in Guam and demonstrated the defense of Guam against an air-launched MRBM. AGS was successful in acquiring and tracking the target using the AN/TPY-6 radar, planning and conducting the missile engagement using the Aegis system, launching the interceptor from the VLS on Guam and intercepting the target

FEM-02_TPY-6 (Source: MDA)

over the broad ocean area.

This test provided DOD a better understanding of the missile defense system's ability to counter threats in a realistic environment and the preliminary analysis indicates a significant step forward in the MDA's efforts to protect the U.S. and its allies from emerging missile threats.

Revolutionary UK-Built Atomic Clock Will Make Military Operations More Secure Through Quantum Technology

Military personnel will use groundbreaking quantum technology to conduct more secure and precise operations, thanks to a new high-tech atomic clock developed at the top-secret Defence Science and Technology Laboratory (Dstl). The quantum clock will be a leap forward in improving intelligence, surveillance and reconnaissance by decreasing reliance on GPS technology, which can be disrupted and blocked by adversaries.

The clock's precision is so refined that it will lose less than one second over billions of years, allowing scientists to measure time at an unprecedented scale. It is the first device of its kind to be built in the U.K. and will be deployable on military operations in the next five years.

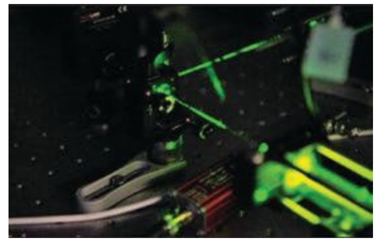

Atomic Clock (Source: Ministry of Defence (U.K.))

The applications of quantum clocks extend beyond precision timekeeping. Further improvement to GPS accuracy could transform global navigation systems, aiding in everything from satellite communication to aircraft navigation.

Further research will see the technology decrease in size to allow mass manufacturing and miniaturization, unlocking a wide range of applications such as use by military vehicles and aircraft.

Improved clocks, such as this atomic device, will allow the Ministry of Defence to further support current and future capabilities.

The trial involved key partners, including Infleqtion (U.K.), Aquark Technologies, HCD Research and Imperial College London, as well as in-house technology developed at Dstl's quantum laboratory. These prototype frequency standards were tested in collaboration with the Royal Navy's Office of the Chief Technical Officer and the Army Futures team at the BattleLab.


Reactel, Inc.
Reacting First to All Your Filter Needs.
Filter Solutions For Mission Critical Applications
High Performance, Rugged Packaging, Small Size and Weight
Great things can come in small packages. Reactel filters are ideally suited for the demanding environments that unmanned vehicles encounter.
Many manufacturers rely on Reactel to provide units which are:
High performance - Lightweight - Low profile
Contact a Reactel engineer with your filter or multiplexer requirements. We can create a unit which will be the perfect fit for your applications.
REACTEL, INC.
RF & Microwave Filters - Multiplexers - Multifunction Assemblies
REACTEL, INC.
REACTEL, INC.
REACTEL, INC.
8031 Cessna Avenue • Gaithersburg, Maryland 20879 • (301) 519-3660 • reactel@reactel.com • reactel.com
Intertek
RoHS
RoHS Compliant 2002/95/EC
in
MADE IN MD
Since 1979

CommercialMarket

Cliff Drubin, Associate Technical Editor

Over 480 Orbital Launches and 43,000 Active Satellites Expected by 2032

The space industry is transforming rapidly as new reusable rockets and low Earth orbit (LEO) mega-constellations (1,000+ satellites) enter the commercial space market. These LEO systems are quickly becoming the mainstay satellite option for their ability to support low latency and high throughput network applications and extend terrestrial network coverage. As of 2024, there are over 14,000 satellites in orbit, with more than 10,400 actively functioning. Of these active satellites, over 93 percent are in LEO. The rise of mega-constellations from the U.S., China and Europe have become significant drivers in the expansion of satellite connectivity for the global telecommunications sector, which, according to a new report from ABI Research, will culminate in an annual orbital launch cadence of over 480 launches to support over 43,000 active satellites in orbit by 2032.

SpaceX and its Starlink network have deployed roughly 7,000 satellites in LEO. It is the largest mega-constellation, followed by Eutelsat Oneweb and emerging LEO operators such as Amazon Project Kuiper and Telesat Lightspeed. China is on the rise as a new space tech superpower, with the announcement and launch of several LEO mega-constellations by Shanghai Spacecom Satellite Technology/Spacesail (14,000 satellites), Shanghai Lanjian Hongqing Technology (10,000 satellites) and China Satellite Network Group Ltd. (Guowang to 13,000 satellites).

"The market is seeing an increased focus on deployments in LEO particularly for communications and emerging markets. While satellites with communication payloads will continue to be dominant in satellite networks up to 2032 (at 88 percent of the market), Earth observation satellites, signals intelligence and technology and training satellites are expected to grow significantly throughout the forecast period at an average compound annual growth rate of 15 percent. This will be driven by demand for greater Earth and space situational awareness and synergies with AI, machine learning and machine vision. Therefore, we anticipate that satellite design will continue to support more edge computing, software-defined and regenerative architectures as customers seek a total space solution that can handle more diverse and complex applications," said Andrew Cavalier, space tech senior analyst at ABI Research.

5G Americas Publishes Comprehensive Insights on AI's Role in Cellular Networks

A new 5G Americas white paper titled "Artificial Intelligence in Cellular Networks" has been released. This document dives into the transformative potential of AI/machine learning across telecommunications networks, emphasizing its pivotal role in advancing efficiency, scalability and innovation across the evolving 5G landscape.

"AI is transforming cellular networks by enabling dynamic, agile decision-making and adaptive operations to address the growing complexity of 5G systems while laying the foundation for beyond 5G and 6G technologies," said Dr. Christina Chaccour, emerging network tech and AI manager at Ericsson and co-leader of the working group.

The white paper is the first in a series of 5G Americas white papers focused specifically on AI in the wireless cellular industry. It highlights critical developments and opportunities for AI integration, focusing on enhancing network reliability, optimizing resource utilization and fostering innovation. As networks transition from 5G Advanced to beyond 5G and 6G, AI is poised to underpin next-generation services and infrastructure.

Key Insights from the white paper:

- Layered Analysis: AI enhances network performance at every layer, from optimizing signal quality and spectral efficiency in the physical layer (L1) to enabling advanced mobility management and dynamic resource allocation in data link (L2) and network (L3) layers. Use cases like beamforming optimization and cross-layer processes, such as life cycle management, are driving transformative efficiencies.
- Cross-Layer Processes: AI facilitate send-to-end network optimization, including intent-driven networking and lifecycle management, ensuring a cohesive and efficient telecommunications ecosystem.
- RAN Innovations: AI enhances Radio Access Networks (RAN), including applications in Open RAN architectures that leverage RAN intelligent controllers for network programmability and resource optimization.
- Generative AI in Telecom: The white paper highlights how generative AI is redefining telecommunications by enabling innovations such as intent prediction, synthetic data generation and dynamic customer interaction. Advanced use cases include OSS/BSS automation, troubleshooting and semantic communication for more efficient data transmission.
- Responsible AI: The paper underscores the importance of trustworthy practices, emphasizing transparency, explainability and privacy in AI deployment. It advocates for robust monitoring systems, bias mitigation and ethical design principles to ensure AI-driven networks maintain public trust and operational reliability.

As the telecom industry gears up for the challenges of 6G, "Artificial Intelligence in Cellular Networks" provides a roadmap for integrating AI into telecom infrastructure. It offers actionable insights for operators, manufacturers and technologists to navigate the evolv-

For More Information Visit mwjournal.com for more commercial market news.

ing landscape of cellular networks.

Over 100 M Wi-Fi HaLow Devices to Arrive on the Market by 2029

According to global technology intelligence firm ABI Research, Wi-Fi HaLow technology, the sub-1 GHz extension of Wi-Fi, is poised to transform the IoT market with its adoption expected to surge from several million Wi-Fi HaLow-enabled devices in 2024 to over 100 million by 2029. This dramatic growth is driven by its ability to address key connectivity challenges in various industries including smart home automation, smart building management, connected agriculture, industrial IoT and beyond.

"Wi-Fi HaLow offers robust, long-range connectivity with low power consumption, making it an ideal solution for whole home, building, facility or neighborhood level IoT applications requiring reliable, scalable wireless deployments. By operating in the sub-1 GHz spectrum, Wi-Fi HaLow provides enhanced signal penetration, enabling operation of beyond 1 km in certain configurations, and up to 10x longer range compared to 2.4 GHz Wi-Fi. Meanwhile, it can support thousands of devices from a single access point, reducing deployment complexity and total cost of ownership (TCO) compared to other IoT technologies," explained Andrew Zignani, senior research director at ABI Research.

> Offers robust, long-range connectivity with low power consumption.

There are several other additional benefits driving Wi-Fi HaLow's adoption. With support for multiple channel bandwidths, Wi-Fi HaLow can enable both large-scale sensor networks with more limited throughput requirements in addition to indoor and outdoor video surveillance applications, which require significantly higher data rates of up to tens of Mbps. With low power consumption, devices can operate for months or years without frequent battery replacements, essential for smart homes and industrial applications. Additionally, by leveraging unlicensed spectrum like conventional Wi-Fi, it reduces TCO through the avoidance of additional subscription, network operation or traffic charges, which can be cost prohibitive in deployments of thousands of client devices. By supporting IP natively, Wi-Fi HaLow can reduce any potential network architecture, setup and device management challenges. Finally, Wi-Fi HaLow can help reduce the burden on congested Wi-Fi frequency bands, enhancing network performance.

Around the **Circuit**

Barbara Walsh, Multimedia Staff Editor

COLLABORATIONS

Quantic Wenzel, a business of **Quantic Electronics** and an industry leader in mission-critical frequency control and timing solutions, has partnered with the **Australian Research Council (ARC) Centre of Excellence for Engineered Quantum Systems** to explore the effects of cosmic rays on quartz crystal oscillators. Research will take place at Australia's deep-underground Cryogenic Experimental Laboratory for Low-background Australian Research (CELLAR) in Victoria's Stawell Underground Physics Laboratory, an ideal environment to examine how cosmic rays influence quartz crystal oscillator phase noise and performance. Funded by the ARC's LIEF scheme, CELLAR's unique setup shields experiments from cosmic radiation, enabling conditions to study noise limitations in quartz crystal oscillators.

Soitec, a leader in the design and manufacture of innovative semiconductor materials, announced the continuation of its research collaboration with the **Microsystems Technology Laboratories (MTL)** of the **Massachusetts Institute of Technology (MIT)**, further solidifying its presence in the North American semiconductor sector. This initiative aims to diversify technological collaborations and anticipate the future needs of the industry. In the U.S., Soitec is intensifying its efforts amidst favorable industrial and regulatory dynamics supporting semiconductor development. In this respect, MIT plays a key role through its MTL, in which Soitec is now a member of the Industrial Advisory Board, which actively contributes to defining strategic research directions in microelectronics.

As part of its ongoing initiative to provide innovative systems solutions for industrial and smart home energy management, **NXP Semiconductors** announced that its continued strategic collaboration with **geo** (Green Energy Options Ltd.), the leading provider of residential energy management solutions, enabled the launch of geo's SeeZero home energy management system (HEMS), a revolutionary Matter™-certified HEMS and one of the first HEMS designed to support true mass market deployment. This collaboration leverages geo's deep experience in energy management and NXP's intelligent system solutions for Matter, which integrate the key building blocks of both software and hardware for connectivity, processing and security, allowing the companies to pioneer this solution.

SynaXG, a leading provider of AI-RAN solutions, announced its membership in the **AI-RAN Alliance**, a collaborative initiative aimed at integrating AI into cellular technology to advance radio access network (RAN) technology and mobile networks. The alliance's mission is to enhance mobile network efficiency, reduce power consumption, and retrofit existing infrastructure, unlocking new economic opportunities for telecommunications companies with AI, facilitated by 5G and 6G networks. In joining the alliance, SynaXG will collaborate with founding members Arm, DeepSig Inc., Telefonaktiebolaget LM Ericsson, Microsoft, Nokia, Northeastern University, NVIDIA, Samsung Electronics, SoftBank, T-Mobile USA and the University of Tokyo, as well as other alliance members.

CONTRACTS

Raytheon, an **RTX** business, has been awarded a $590 million follow-on production contract from the **U.S. Navy** for the Next Generation Jammer Mid-Band (NGJ-MB) system. NGJ-MB is a cooperative development and production program with the Royal Australian Air Force (RAAF). The contract includes delivery of shipsets, support equipment, spares and non-recurring engineering support. The U.S. Navy and RAAF will employ NGJ-MB on the EA-18G GROWLER® to target advanced radar threats, communications, data links and non-traditional RF threats. The system reduces adversary targeting ranges, disrupts adversary kill chains and supports kinetic weapons to target. NGJ-MB allows naval crews to operate effectively at extended ranges and attack multiple targets simultaneously with advanced techniques.

Anduril has been awarded a $200 million, five-year indefinite delivery/indefinite quantity contract by the **U.S. Marine Corps** to develop and deliver a counter-unmanned aerial system (C-UAS) engagement system (CES) for the **Marine Air Defense Integrated System (MADIS)**. The MADIS CES Program of Record will provide cutting-edge, expeditionary C-UAS capabilities to protect the Marine Air Ground Task Force from evolving air threats. The MADIS CES is part of a block upgrade program for the Marine Corps' major expeditionary counter-drone system, designed to enhance lethality and ensure Marines are equipped with the latest C-UAS technology to defend against rapidly evolving threats.

The U.S. Defense Advanced Research Projects Agency (DARPA) has awarded **BAE Systems' FAST Labs™** research and development organization a $12 million contract as part of the High Operational Temperature Sensors program. Many critical defense and industrial systems, such as hypersonic aircraft and missiles, automotive, jet engine turbine and oil-and-gas systems, operate in extreme temperature conditions. Current sensors have limited performance as they cannot operate in temperatures higher than 225°C. Their capability is limited by the materials that comprise the sensors themselves, the accompanying circuitry (e.g., silicon-based transistor technology) and packaging.

Forsway, provider of cost-efficient hybrid satellite terrestrial solutions and equipment for broadband connectivity, secured a major development funding contract from the **European Space Agency** with support from the

Around the **Circuit**

Swedish National Space Agency. In the new project, Xtend 5G, Forsway will build a next-generation 5G NTN two-way/hybrid satellite connectivity system enabling the combined use of satellite and ground infrastructure to provide seamless connectivity anywhere, regardless of network. Xtend 5G will provide European government, defense, emergency services and critical infrastructure sectors with seamless connectivity anywhere, anytime, in an open or closed network and with full system control.

PEOPLE

▲ *Dr. Baaziz Achour*

Qualcomm Incorporated announced the appointment of **Dr. Baaziz Achour** to the role of chief technology officer (CTO), Qualcomm Technologies, Inc., and the retirement of Dr. James Thompson, both effective February 3, 2025. Dr. Achour first joined Qualcomm as a systems engineer in 1993. Over the course of his tenure with Qualcomm, Dr. Achour has held several leadership roles within the engineering organization, most recently as deputy CTO since 2023, and has been essential in contributing to nearly every generation of wireless technology. He was a key part of the leadership team that enabled the accelerated launch of 5G and will lead the evolution of cellular to 6G.

▲ *Greg Evans*

▲ *Ross Berntson*

Indium Corporation® announced the advancement of two executives to top posts in the corporation. Former CEO **Greg Evans** now serves as executive chair of the board of directors. **Ross Berntson** has been appointed CEO and continues as president. As executive chair, Evans provides guidance to the organization, facilitating a constructive and collaborative agenda that supports the CEO's leadership. As president and CEO, Berntson is responsible for the overall strategic direction and key decision-making that impacts the company's future.

▲ *Alan Mayer*

Global electronic test and measurement equipment specialist **Electro Rent** has appointed **Alan Mayer** as its chief revenue officer to spearhead the company's growth plans. Mayer joins Electro Rent with extensive global customer experience across multiple segments and verticals in technology companies, from startups to the Global 500, in both corporate and public sectors. Mayer brings 22 years of experience at Dell, where he led sales, services and customer success teams to champion the evolving needs of customers across the business.


There's nothing *Artificial* about our Intelligence.
See what we've been up to!
MARCH 10-13
SATELLITE 2025
BOOTH 1313
Since 1961, Greenray Industries has been a preferred provider of precision, high performance reference sources to many of the world's leading military, defense and industrial manufacturers.
With a range of critical design innovations that enhance product performance and reliability, our quartz crystal oscillators help engineers realize their unique frequency control solutions.
On the ground, in the air – and beyond.
GREENRAY
LEO, MEO & Deep Space ✦ Radar ✦ SATCOM ✦ Telemetry ✦ Airborne & Mobile Communications ✦ 5G & Stratum3 ✦ GPS

INVITED PAPER

Tower Opportunities and Key Questions for the 6G Evolution

Ed Knapp
American Tower Corporation, Boston, Mass.

As 5G networks are still rolling out around the world, the telecommunications industry is already looking toward the future. 5G brought improvements in connectivity with faster download speeds, lower latency and enhanced network reliability. With 6G, these capabilities will be even greater and meet the ever-growing demand for connectivity, which now stands at a 25 percent compound annual growth rate, effectively doubling every three years.

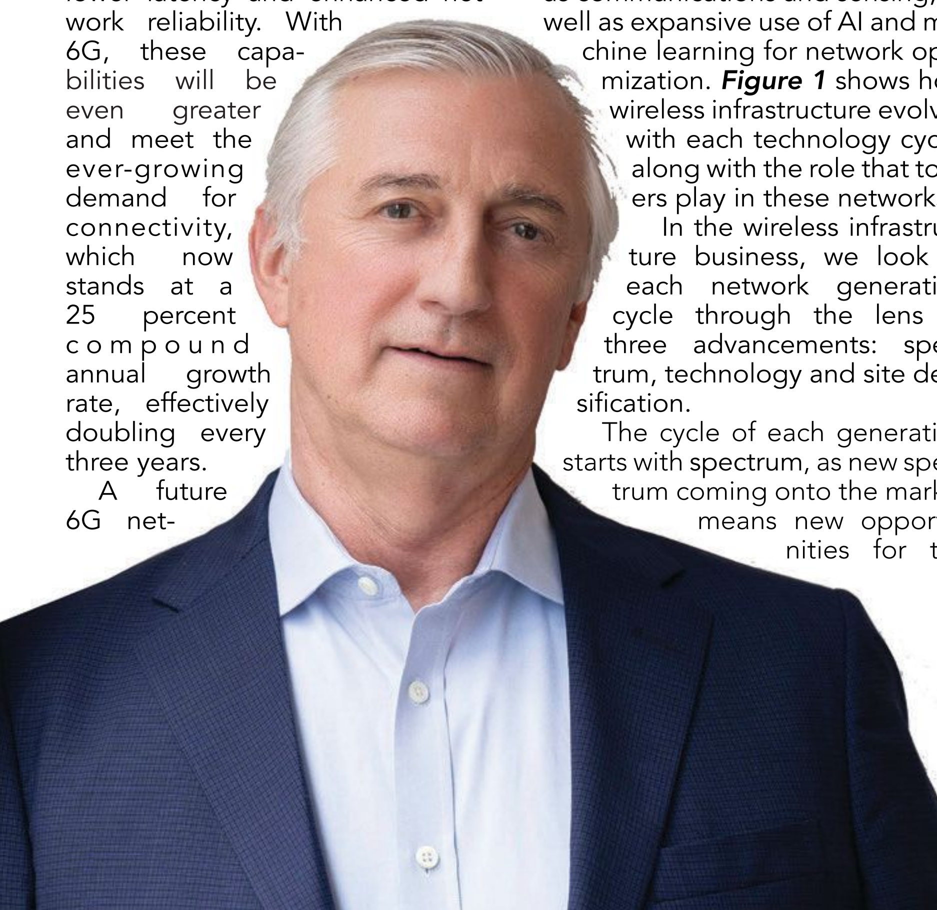

A future 6G network operating in sub-THz bands should be able to provide download speeds that allow upwards of 1 Tbps, which is about 100x faster than 5G. The enhanced capabilities of 6G will enable seamless integration of various technologies, such as communications and sensing, as well as expansive use of AI and machine learning for network optimization. ***Figure 1*** shows how wireless infrastructure evolves with each technology cycle, along with the role that towers play in these networks.

In the wireless infrastructure business, we look at each network generation cycle through the lens of three advancements: spectrum, technology and site densification.

The cycle of each generation starts with spectrum, as new spectrum coming onto the market means new opportunities for the tower business. High-powered, dedicated spectrum is the key and with future 6G frequencies in the 7 to 15 GHz and sub-THz bands, opportunities for new RF platforms will open up opportunities for innovative technology, radio development and testing services to optimize radio placement.

Spectrum is expensive, so once these new radios are deployed, how do we get more bits per second per hertz over their lifecycle? Increasing efficiency and lowering the cost per bit is where the technology roadmap comes into play. Many cellular technology companies and start-ups create technologies that become site upgrades. For a tower company, our customers are continuously adding to and upgrading existing radios, enabling more capacity at both the site and system level.

Finally, densifying the infrastructure is an important component of increasing capacity at the end of a generation cycle.

To see how the role of towers has evolved in the wireless ecosystem, we can look back to 4G. As an early innovator in the tower space, American Tower purchased and deployed new towers, enabling a cost-efficient, neutral-host model in which the towers could

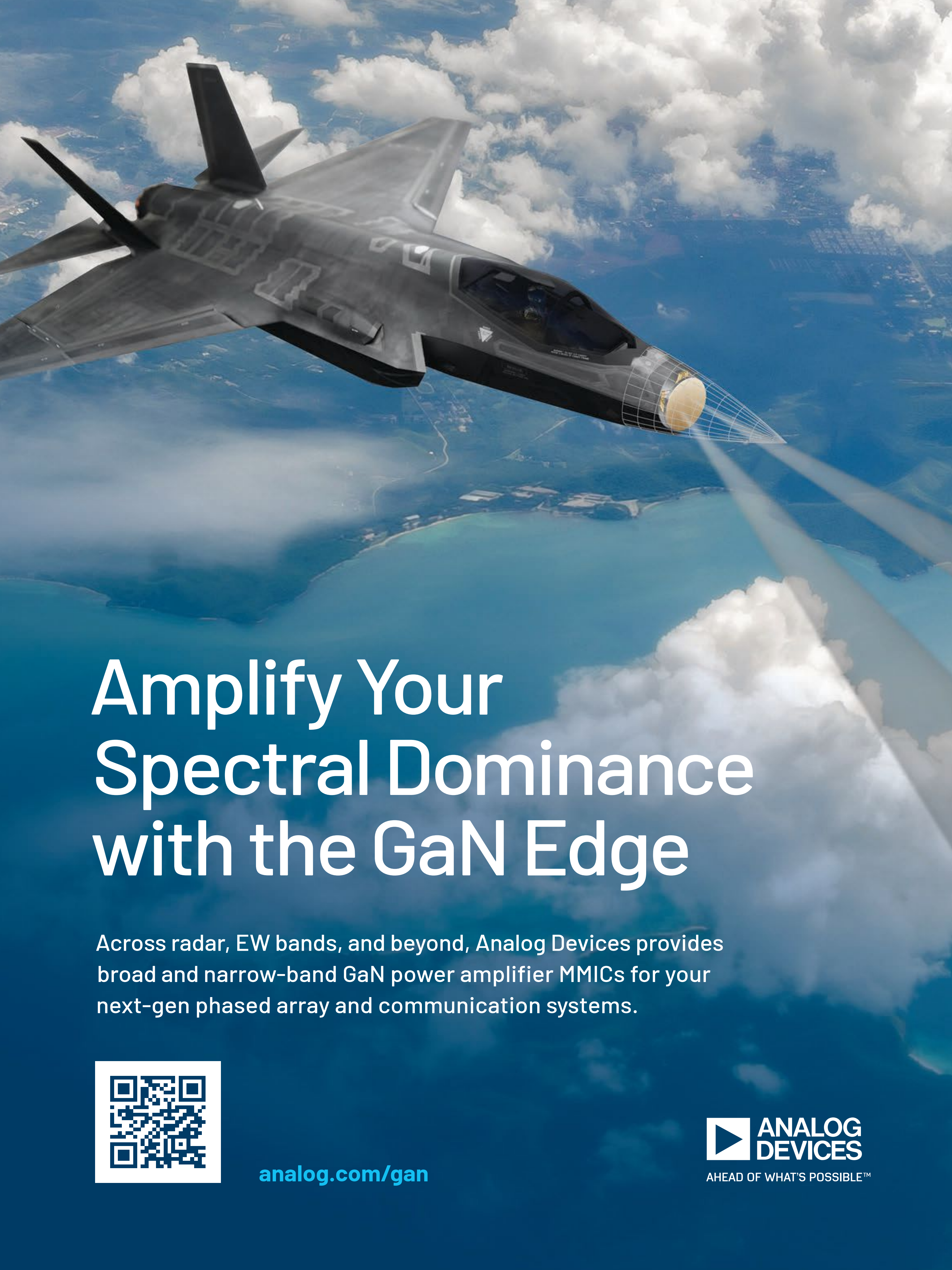
Amplify Your Spectral Dominance with the GaN Edge
Across radar, EW bands, and beyond, Analog Devices provides broad and narrow-band GaN power amplifier MMICs for your next-gen phased array and communication systems.
analog.com/gan
ANALOG DEVICES
AHEAD OF WHAT'S POSSIBLE™

MWJPerspective

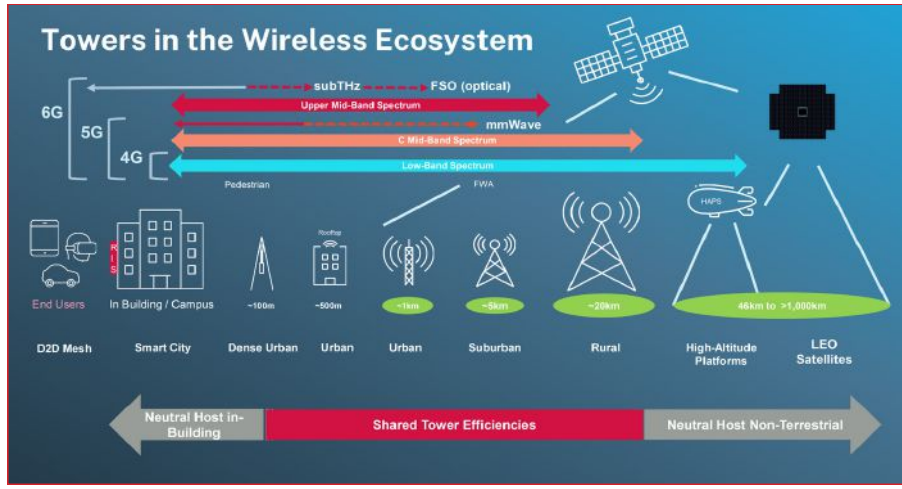

Fig. 1 Wireless infrastructure evolution.

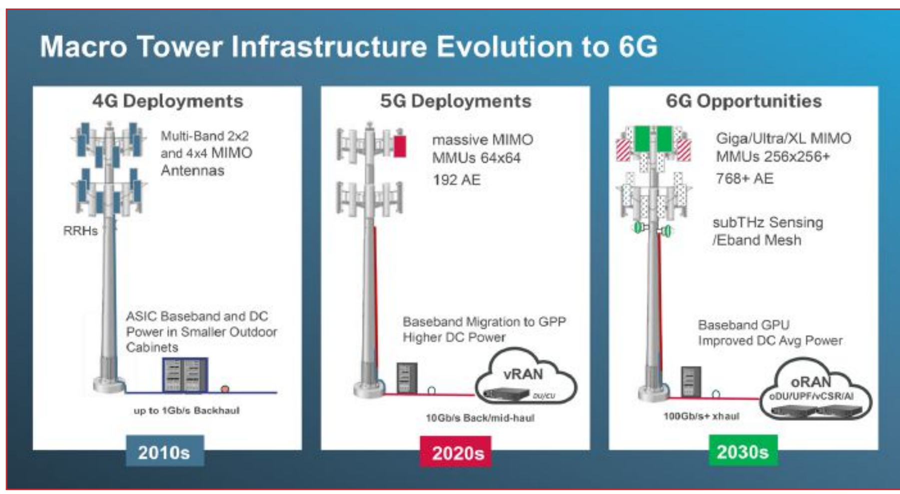

Fig. 2 Evolution of macro tower sites to 6G.

be shared by customers. The early low-band spectrum, below 2 GHz, made pedestrian and mobility services in urban, suburban and rural areas accessible. Mobile phones were less of a luxury as we moved to 4G and smartphones began to emerge. The introduction of 5G technology, coupled with massive MIMO, allowed the use of new mobile spectrum at 3 GHz mid-band and 28 GHz mmWave. Services were quickly extended to fixed wireless access (FWA) and future 5G standards will expand coverage using non-terrestrial networks such as high-altitude platforms and LEO satellites. Some of these capabilities still have a way to go before reaching the global marketplace, but we will soon see them become fully realized.

We might ask, what type of infrastructure, as shown in Figure 1, will we need in the future to maximize the availability of spectrum and device electronics for higher frequencies such as 3GPP's frequency range 2 (FR2) (24 to 71 GHz) and 6G FR3 (7 to 24 GHz) and even subTHz? How can we leverage 6G on existing towers for the mainstream rollout of population coverage and potentially integrated backhaul? One may also consider the local area potential of device-to-device or V2X sidelink in connection with reconfigurable intelligent surfaces. These can expand access to data-driven intelligent IoT services in cities. How do all these radio technologies play together cost-effectively and how do we enable future wireless infrastructure that will be even more resilient and more reliable?

Infrastructure investments are important to do most economically and we can see how critical these investments are when we look at the infrastructure evolution over

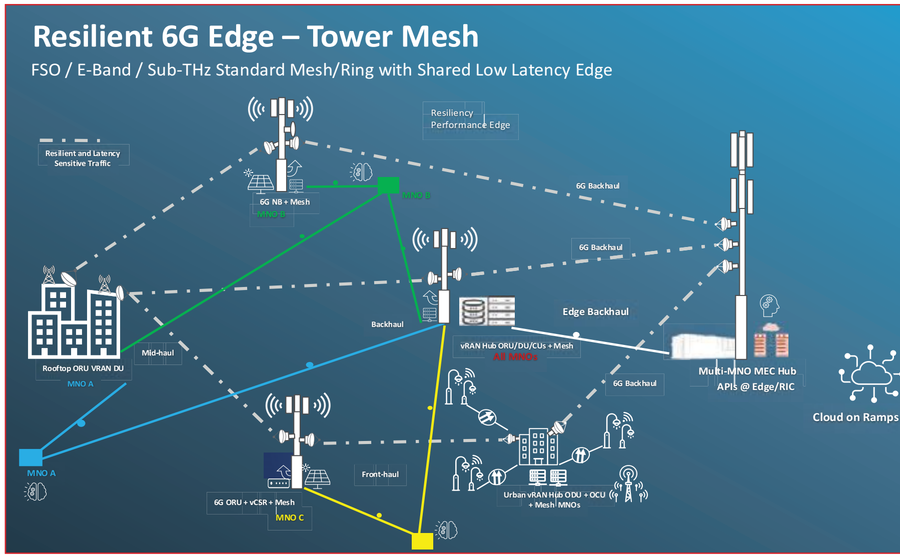

Fig. 3 **Resilient edge networks.**

time, as shown in ***Figure 2***. With 4G deployments, we introduced OFDMA with two- and four-layer, single-user MIMO and fiber-fed remote tower-top radio heads. Decades ago, placing active radios at the top of towers was difficult, but now, it is a common practice. We replaced shelters hosting baseband equipment and radios with outdoor cabinets. In parallel, the backhaul started to improve with the use of more and more fiber. With 5G, cellular operators moved to support massive MIMO with active beamforming in the mid-band spectrum to leverage the large existing base of 4G macro towers. Smaller cells were required with the early availability of mmWave, but this technology was limited to providing better access in places like stadiums, some FWA and other limited hotspot environments to enhance the user experience.

6G networks, when deployed using 3GPP Release 21 in 2029 and beyond, will require new radios operating on the same infrastructure with even higher mid-band and potentially sub-THz frequencies. It will drive another round of tower investment for new radio antennas, power amplifiers, filters and digital front-end radio processing. Infrastructure improvements to support legacy bands with 6G will require antenna upgrades and more advanced transceivers, together with support for open radio interfaces. Also, the architecture and functional splits between the tower, the base of the tower and the network will depend on the trend to standardize AI models for single-ended or end-to-end (device-to-network) and potentially new waveforms like orthogonal time frequency space modulation.

The range of capabilities we can enable on existing towers is critical to the 6G operator economics. Can we get 80 percent or more of the coverage from these higher mid-band frequencies to augment and extend what we do today with 5G at mid-band? Fixed wireless is increasingly a big part of the success of 5G, so how can we improve these services with 6G? Finally, one can envision existing towers with sub-THz radios for backhaul, FWA and sensing. Short, high bandwidth links open up the possibility to leverage our increasingly denser networks to enable a tower-to-tower mesh, as shown in ***Figure 3***. Can the higher FR2 bands and beyond provide reliable links with larger bandwidths, bringing us new capabilities to allow sensing of the environment around a tower for detection and control of drones and other mobile platforms? Does wireless connectivity as an overlay to fiber backhaul networks improve overall resiliency for mission-critical applications?

In the wireless access world that exists today, operators take all the customer traffic from their specific sites and route the data to their

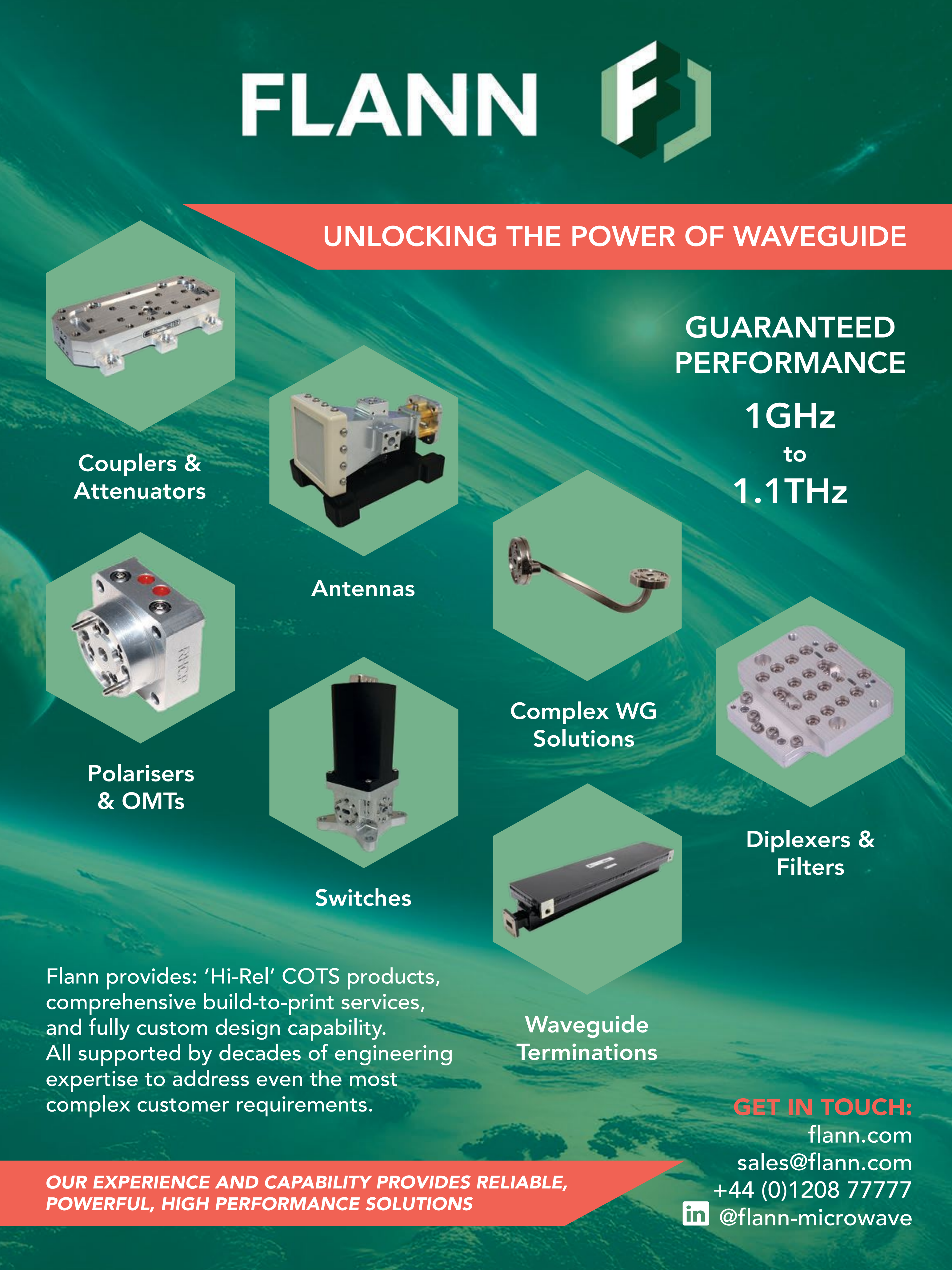
FLANN
UNLOCKING THE POWER OF WAVEGUIDE
GUARANTEED PERFORMANCE
1GHz
to
1.1THz
Couplers & Attenuators
Antennas
Complex WG Solutions
Polarisers & OMTs
Diplexers & Filters
Switches
Waveguide Terminations
Flann provides: 'Hi-Rel' COTS products, comprehensive build-to-print services, and fully custom design capability. All supported by decades of engineering expertise to address even the most complex customer requirements.
GET IN TOUCH:
flann.com
sales@flann.com
+44 (0)1208 77777
@flann-microwave
OUR EXPERIENCE AND CAPABILITY PROVIDES RELIABLE, POWERFUL, HIGH PERFORMANCE SOLUTIONS

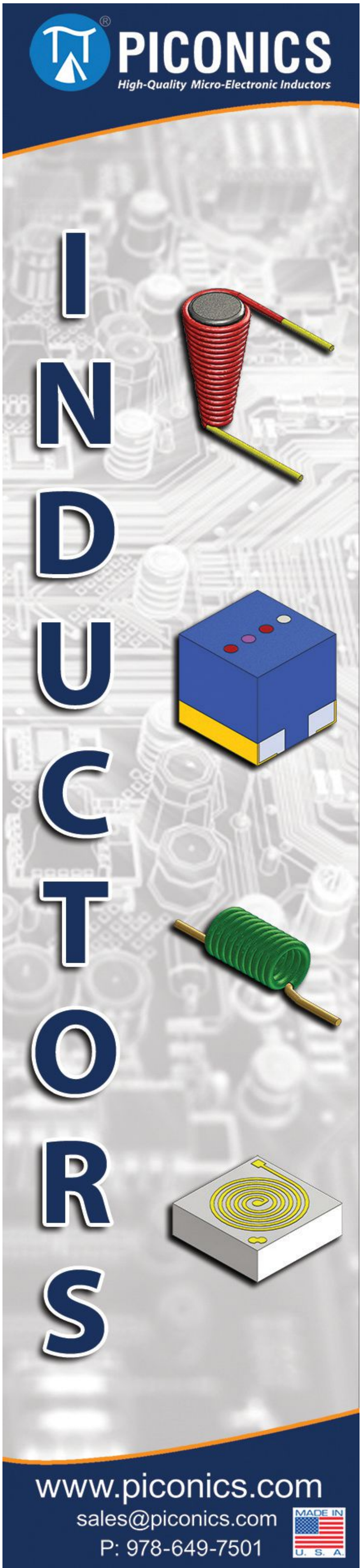

core platforms for interconnection to the Internet and other telco networks, as shown in Figure 3. However, when looking at the future of enabling 6G edge applications from an API platform perspective, very few independent software developers will write a latency-sensitive multi-access edge computing (MEC) application that uniquely leverages only one access network or results in vastly differing performance across users due to varying routing and hops across multiple access networks. Developers need consistency for the system to scale, or they fall back to common solutions. High performance edge applications need to run in localized neutral-host locations.

Application developer revenues are maximized when they cut across a fully converged set of wireline and wireless access networks by operating in neutral colocation data centers. The challenge for the industry is the need to invest in the data center infrastructure in advance to support future low latency mission-critical or real-time inferencing applications. Performance dictates the need to peer or exchange access traffic horizontally, east to west, not simply south to north, to different processing locations by each operator. The traffic routing problem is solved if we could put in a 6G-enabled wireless mesh at the higher frequencies and use all the tower infrastructure to create another layer of resiliency on top of the existing fiber network, not to replace but to augment with a deterministic latency bound across multiple access networks for a subset of the traffic. We can make it both timely and cost-effective to bring traffic uniquely to a multi-MNO MEC hub site (e.g., edge aggregation site) and process applications for all users that require low latency, such as workloads requiring an AI inferencing model or agent.

Edge computing, where data processing occurs close to the source of data generation, goes together with 6G. By reducing the distance that data needs to travel to be processed, edge computing lowers the end-to-end latency and enables faster decision-making. This will be important while using machine-to-machine applications for which real-time data processing is critical, such as autonomous vehicles, drones, electric vertical take-off and landing aircraft and real-time video and sensing to improve safety in smart cities.

The future need for orchestrating a service employing specific AI agents, after moving from training to inferencing, will be spread throughout the infrastructure, from hyperscale data centers to devices. We need the AI orchestrator to piece together what workloads to run in which location. If you are trying to talk to a device that is not a smartphone but another input device to "help solve this problem," is there a visual component? Is there an uplink challenge? How do I process this?

At American Tower, we are focused on leveraging our assets to answer those questions. We are working on a MW scale modular aggregation edge data center in Raleigh, N.C., with partners. We also seek to repurpose our older shelters and leverage them for local workload processing and data access. The data today is not available at local sites, so we need to add the local breakout and evolve to where the user plane function can deposit the traffic anywhere across the edge continuum with specific intent and purpose.

Despite the challenges that 6G will require, such as significant investment in infrastructure, including new antenna systems and the need for regulatory bodies to establish the allocation of frequencies to ensure network efficiency, the future is bright. 6G will change the landscape of communication, enabling faster, more reliable and more immersive connectivity than ever before. With advancements in AI, traditional and new radio band communications, sensing and edge computing, 6G will usher in an era of connected technologies that will enhance every aspect of our lives. 6G will open the door to greater digital and AI enterprise and consumer transformation in the coming decades ■

INVITED PAPER

Four Innovative Trends Reshaping the Microwave Radio Market

Emmy Johnson
Sky Light Research, Scottsdale, Ariz.

Microwave radios have long been a key component in transporting mobile backhaul traffic between towers and the central office. As wireless networks evolve, microwave radio development becomes a crucial enabler. Advancements in energy efficiency, traffic management and capacity thresholds are collectively moving the market forward to meet the requirements of advanced 5G and 6G networks.

ENERGY EFFICIENCY: A GOLD STANDARD

Energy efficiency is a key metric for mobile networks, as energy sources are only expected to be further strained. According to research by Morgan Stanley,[1] energy requirements for generative AI could grow by 70 percent each year. By 2027, the energy consumption of generative AI alone could match Spain's total energy usage in 2022. According to the Energy Information Administration's International Energy Outlook,[2] global energy consumption could increase by 34 percent between 2022 and 2050. It is statistics like these, as well as increasing energy costs, that make energy efficiency important in the minds of customers like mobile operators, enterprises and government agencies.

Microwave radios are making great strides in energy efficiency by integrating generative AI into their offerings. Although creating generative AI models is initially energy-intensive, it is hoped that the energy savings achieved over time will outweigh the energy required for their development. Generative AI models have the power to transform the operation and management of microwave radios by optimizing network performance, predicting maintenance needs, enhancing energy processes and improving signal processing capabilities. These technologies enable operators to optimize resource utilization, reduce operational costs and maintain high service quality. Deep sleep mode, in particular, represents a leap forward in energy-saving potential, aligning well with industry goals of greater efficiency and sustainability.

Deep sleep mode is a power-saving feature in microwave radios designed to reduce energy use during times of reduced network demand. This capability is particularly useful in multi-carrier configurations, like 2+0 or 4+0 configurations, where full capacity is not needed 24 hours a day. Using generative AI-powered traffic-aware algorithms, the system monitors traffic patterns specific to each link. By examining past trends and current conditions, it identifies the best op-

portunities for activating deep sleep mode while avoiding any risk of overloading the network. This approach ensures that inactive carriers are temporarily powered down only when it is operationally safe, delivering significant energy savings without degrading service quality. Compared to standard operational states or lighter power-saving methods, AI-powered deep sleep mode offers a more substantial reduction in energy consumption, making it a valuable tool for improving network efficiency.

Ericsson's MINI-LINK microwave radio is an interesting example of how deep sleep mode using AI can save the operator money on energy. In a case study of a medium-sized network with 5,000 2+0 links, Ericsson demonstrated that the combination of AI-powered deep sleep functionality and traffic-aware output power adjustments for multi-carrier links resulted in energy savings of 20 percent over five years, with negligible impact on user experience or service availability. This significant reduction in power consumption highlights the energy-saving potential of AI-enhanced deep sleep technology and its ability to contribute to more environmentally-friendly microwave networks. ***Figure 1*** shows Ericsson's energy savings using no deep sleep, fixed deep sleep and AI-powered deep sleep for the traffic-aware output power.

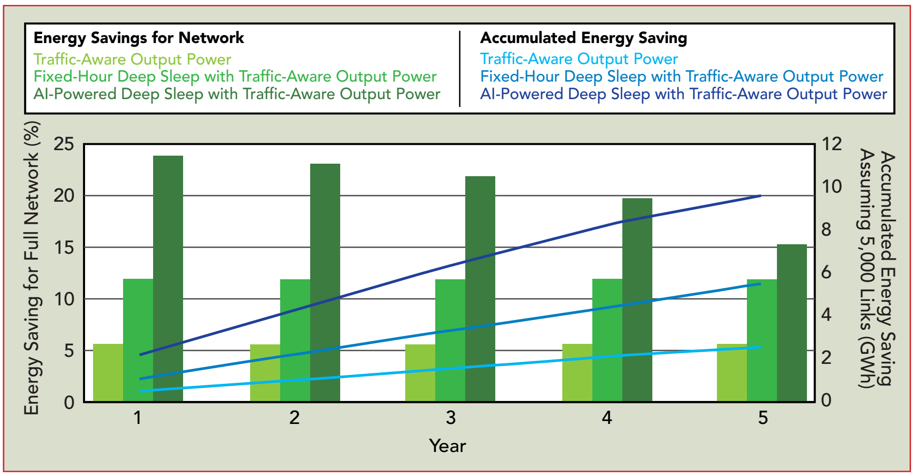

Fig. 1 **Ericsson energy savings for various network configurations. *Source:* Ericsson Microwave Outlook, 2022.**

YOU CANNOT IMPROVE IT IF YOU CANNOT MEASURE IT

Predictive maintenance is another area where AI has made a significant impact by providing hardware degradation alerts and high-temperature early warnings. This allows for proactive management of potential issues, preventing costly emergency repairs and enhancing overall network efficiency. Generative AI models can also forecast network traffic growth, enabling operators to proactively optimize resource allocation and energy usage, thereby maintaining smooth network operations while preparing for future demands. Often, a technique called automated root cause analysis (RCA) is employed to help monitor and improve signal management.

One of the key applications of automated RCA is the detection and mitigation of antenna misalignment issues. By collecting and analyzing performance data at frequent intervals (i.e., every 10 seconds), link quality is assessed with high precision. This enables the detection and diagnosis of signal degradation, distinguishing between causes such as radio interference, obstructions, rainfall or alignment shifts before outages occur. These systems can determine whether immediate action is necessary or if an issue is temporary. For example, during periods of heavy rainfall, the systems can identify the weather as the probable cause of a signal drop, allowing operators to monitor the situation rather than dispatching a maintenance team un-

Quantic™ PMI
PLANAR MONOLITHICS

Components & Modules to 70 GHz

- Modern hybrid MIC/MMIC design
- 4,500+ Hi-Rel Commercial, Off-the-shelf (COTS) Models
- Industry-leading customer and applications support
- Form, fit, function and custom package designs
- Hermetic sealing, military or aerospace screening

Quantic PMI designs and manufactures a full range of solutions for your most demanding RF and Microwave challenges.

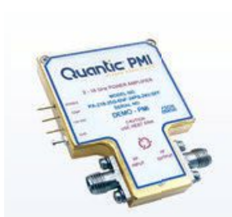

Amplifiers: Solid State Low Noise (LNAs) & High Power (SSPAs)

Attenuators: Digital & Analog Control, Fixed

Filters & Switched Filter Banks

Integrated Microwave Modules & Assemblies (IMAs)

Limiters: High Power (100 W CW, 1 kW peak)

Log Amplifiers: DLVAs, ERDLVAs, & SDLVAs

Phase Shifters & Bi-Phase Modulators

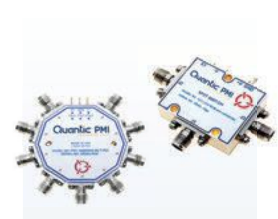

Switches: Solid State (SPST to SP128T)

Get a complete list of our components and module portfolio, available options, download product features and other technical data at **quanticpmi.com**

Or contact us at **1-877-752-6271** or **sales@quanticpmi.com**

SATELLITE 2025 CONFERENCE & EXHIBITION

Visit us at Booth #1421
Washington, DC, March 10-13
satshow.com

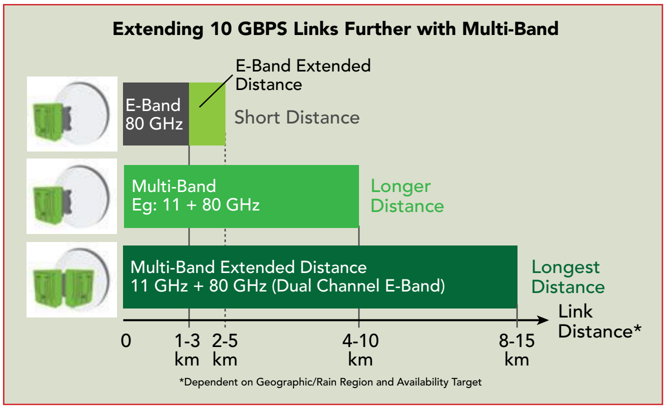

Fig. 2 **Link distance for Aviat 4800 options.** ***Source:*** **Aviat Networks.**

necessarily. This targeted approach to troubleshooting and maintenance has led to significant reductions in site visits. By minimizing site visits, network efficiency improves while operational costs and energy consumption decrease. Combined with energy-saving processes like deep sleep modes and AI-based management processes, operators can enhance energy efficiency, reduce costs and reduce their carbon footprint, all while maintaining high-quality service.

An excellent example of using AI to streamline network management is Ceragon's Insight Tool. In the last 24 months, Ceragon has reshaped its approach to network management with the integration of AI and machine learning. By leveraging AI, the platform provides comprehensive oversight of network performance, enabling operators to tackle complex challenges more effectively and use network resources more efficiently, saving them time and money. Key features of the platform include the ability to correlate alarms and incidents for faster troubleshooting, analyze link performance to detect irregularities and manage traffic predictively to anticipate capacity issues before they escalate. Additionally, the tool's preventative monitoring capabilities enable operators to mitigate potential outages, while remote maintenance features reduce operational expenditures and enhance network performance. By addressing these critical aspects, AI-powered platforms, like Ceragon's Insight Tool, are becoming integral to modern microwave networks. These tools help operators achieve greater efficiency and reliability in increasingly demanding environments.

THE BRASS RING: MAXIMIZING CAPACITY WITH LOW LATENCY

Besides using resources more efficiently, increased capacity is on top of mind for all operators. Advanced 5G and 6G networks use large amounts of data, which require large amounts of capacity. It is central for operators to be able to scale their existing resources to keep pace with customer demands. There are a few ways in which to increase capacity: increase the channel size, adopt higher modulation schemes (up to 16K-QAM), add another carrier or implement multi-band technology.

Multi-band technology is becoming a more common way in which operators are maximizing their links for both distance and capacity. Multi-band technology combines high capacity frequencies, like E-Band, with lower frequencies that offer higher availability and longer hop lengths, significantly boosting capacity. This approach leverages the strengths of both frequency bands to extend the reach and increase the capacity of traditional microwave links.

The Aviat Networks WTM 4800 family of products is a proven example of efficient multi-band technology. By leveraging E-Band's capacity, in parallel with one or more microwave channels, Aviat can extend the 10+ Gbps link to more than 10 km. Aviat's 4800 product family is compelling because it offers several options, including E-Band in a single box for vendor-agnostic multi-band, multi-band in a single box and extended-distance multi-band configurations. The extended-distance multi-band configuration is a unique option, featuring two separate boxes with four channels that share a


VULCAN
WIRELESS INC
Advanced Phased Arrays and High-Speed
Communications for Lunar and Earth Orbits.
• TSAB Encryption
• Space Flight Proven
• SDA Network Compatible
WWW.VULCANWIRELESS.COM

single antenna. One box contains two E-Band channels, while the other houses two microwave channels, all seamlessly integrated through the shared antenna. Other features include integrated L1-LA traffic aggregation, no requirement for an indoor unit and optimized low power consumption. By deploying radios that combine multiple frequency bands in a single unit, operators can enhance link capacity, reliability and distance without the need for additional antennas or equipment. ***Figure 2*** shows the link distances for these options from Aviat's 4800 product family.

Although Aviat has found success with multi-band configurations, particularly in rural areas of the U.S., Europe and the Middle East, have been using multi-band E-Band for a while. To make the best use of resources in multi-band configurations, ETSI has been working on new backhaul key performance indicators, known as backhaul traffic availability (BTA). BTA takes into account the operator's RAN traffic statistics to minimize over-engineering of the link, ensuring efficiency without compromising the end-user experience. Multi-band, along with BTA, is just another example of how layering innovative processes can take network efficiency to another level while significantly reducing backhaul costs.

D-BAND: ANOTHER OPTION FOR ULTRA-HIGH CAPACITY

By accessing higher frequencies, operators can transmit more capacity. Just like with multi-band, traditional microwave bands add more capacity by utilizing E-Band in the 80 GHz range. D-Band is yet another frequency band that provides even more capacity by using a wide range of spectrum in an even higher frequency range of 130 to 157 GHz.

Although D-Band technology is relatively new, advancements in the technology demonstrate the ability to push past traditional benchmarks of 20 Gbps. This can be done while preserving important metrics like power, latency and efficiency. Innovations like compact, high gain antennas help make these systems even more adaptable to urban small cell networks, while the wide channel bandwidths enable faster and more efficient data transmission, enhancing deployment flexibility.

There have only been a few trials with D-Band, Nokia's trial in France is one of the first live trials and the only trial using frequency-division duplexing (FDD). By using FDD, with simultaneous transmission and reception over a single channel, Nokia effectively doubles capacity compared to traditional time-division duplex (TDD) transmission while keeping latency low. Nokia reported that with FDD D-Band, they were able to achieve 10+10 Gbps capacity, meaning 10 Gbps each for uplink and downlink, using a single 2 GHz channel. Further, they were able to increase spectral efficiency by 100 percent by utilizing the full channel bandwidth without the need for separate frequencies.

Energy efficiency is also enhanced, with a 100 percent improvement over TDD systems due to the elimination of switching between transmission and reception modes. Additionally, hardware costs decreased by up to 50 percent due to a simplified design that requires fewer components, employs more streamlined deployment and follows a standardized approach for various applications. Innovations like this that access higher frequencies, along with other microwave technology advancements, solve technical capacity and latency barriers in wireless backhaul and fronthaul technologies, which enable efficient 5G Advanced and 6G networks.

Sky Light Research does not expect commercial D-Band shipments until after 2027, with significant shipments occurring no sooner than 2029. As of now, traditional microwave radios make up the bulk of the shipments, while E-Band radios are driving growth. ***Figure 3*** shows Sky Light's latest forecast for the trends of traditional microwave versus E-Band radios.

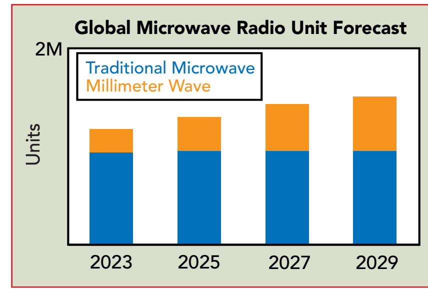

Fig. 3 **Microwave radio forecast and segmentation.** ***Source:*** **Sky Light Research.**

By investing in D-Band technology now, the industry is laying the groundwork for next-generation networks. Moreover, D-Band radios provide a practical solution for high capacity wireless links in places where fiber installation is challenging. This will offer a valuable complement to existing network infrastructure.

Microwave radios are steadily advancing to meet the growing demands of advanced mobile networks, focusing on improving energy efficiency, capacity and reliability. Innovations like AI-powered deep sleep modes, predictive maintenance, multi-band configurations and the emerging use of D-Band frequencies are reshaping how operators think about wireless backhaul. These developments not only cut costs and energy consumption but also enhance network performance, enabling operators to handle the massive data demands of 5G and lay the foundation for 6G. While traditional microwave radios remain a critical part of network infrastructure, technologies like E-Band and D-Band are gradually pushing the boundaries of what is possible in wireless backhaul, paving the way for more efficient and scalable networks. ■

References

1. www.morganstanley.com/ideas/sustainability-industry-trends-energy-transition-AI.
2. www.instituteforenergyresearch.org/international-issues/eia-expects-global-energy-consumption-to-increase-through-2050.

INVITED PAPER

Powering the Future: The Journey to a Handheld Microwave Ablation System

Eamon McErlean
Emblation®, Stirling, Scotland

Microwave ablation has emerged as a transformative technology in the medical field, particularly for the minimally invasive treatment of cancerous tumors. Traditional systems operating at 2.45 GHz have often been bulky, expensive and challenging to maneuver in clinical environments. Emblation® is addressing these challenges with the SwiftPro® device, the first commercially available FDA-cleared compact handheld microwave ablation system. At the heart of this solution is a highly integrated 8 GHz microwave source module, which is crucial for achieving the compact size, efficiency and performance required for a handheld device. This article explores the design and development challenges, with a special focus on the thermal management technology that makes compact microwave ablation possible.

Traditional microwave ablation systems rely on magnetron-based technology, known for its effectiveness but also its considerable drawbacks. The equipment is large, operates at high voltage and requires bulky cooling mechanisms, making it cumbersome and costly to operate. These limitations restrict the use of such systems to surgical operating environments, hindering the broader adoption of microwave ablation, especially in outpatient or resource-constrained settings.

Developing a handheld microwave ablation system presents a range of unique challenges. One of the primary hurdles is managing size and weight constraints. Unlike conventional systems, a handheld device must be both compact and lightweight, all while maintaining the performance standards required for effective ablation. Another critical consideration is power efficiency. Microwave ablation requires precise delivery of high frequency electromagnetic energy. In a handheld device, this requirement demands careful optimization of power consumption and advanced thermal management to ensure reliable operation without excessive heat generation. Integration of microwave components also poses significant challenges. Achieving miniaturization without compromising the performance or reliability of crucial components requires rethinking design approaches and engineering methods. Finally, user safety and ergonomics are essential factors. A handheld ablation device must be not only safe for the patient and user but also comfortable and easy to use for medical professionals during extended procedures, emphasizing the importance of ergonomic design and user-friendly controls.

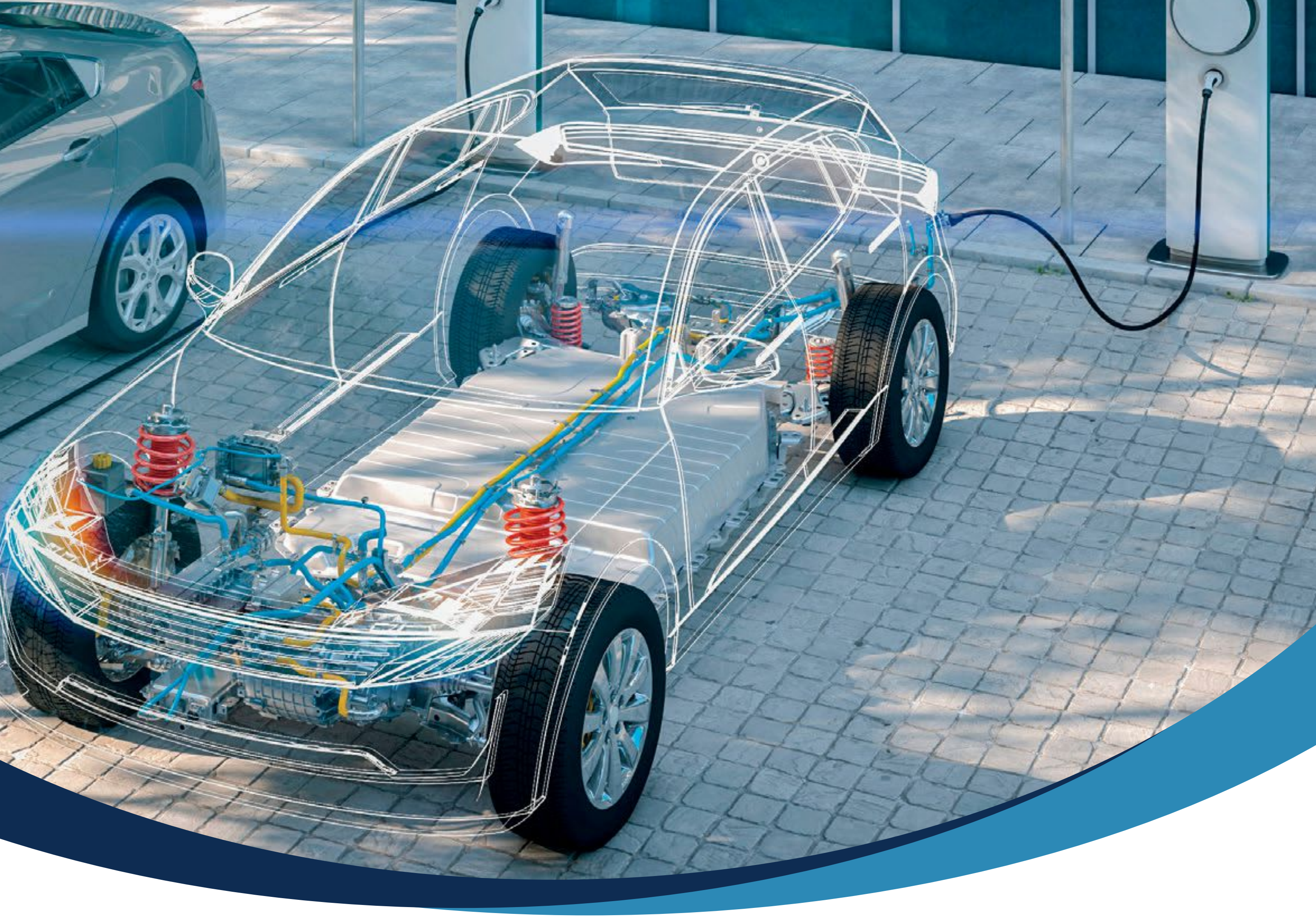

To overcome key design challenges that include performance, weight, power efficiency and thermal management, Emblation developed the highly integrated microwave source module shown in ***Figure 1***. The microwave source module, which is intentionally blurred, is mounted on a copper carrier. The printed circuit assembly is a six-layer, double-sided board combining microwave laminate/FR4 with embedded copper coins.

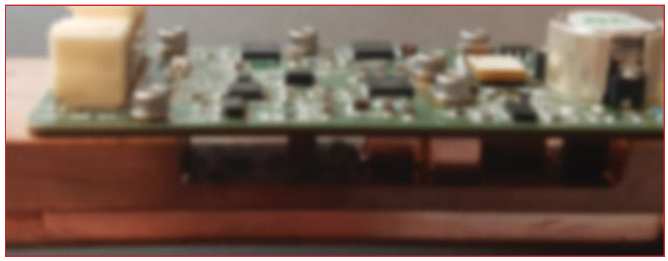

Fig. 1 SwiftPro microwave source module.

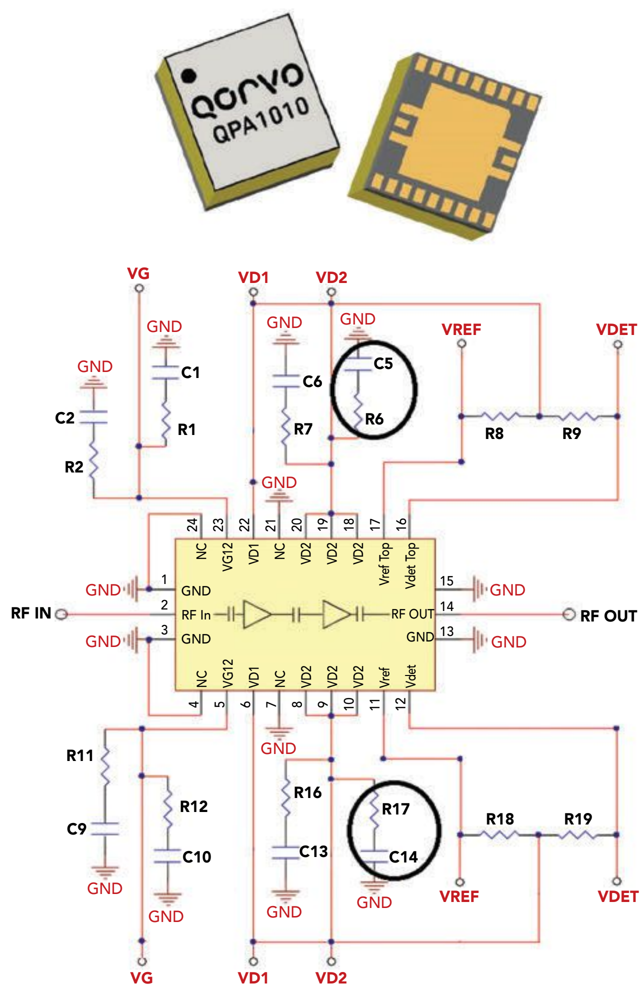

Note: Power Detector $V_{DELTA} = V_{REF} - V_{DET}$

Fig. 2 Qorvo QPA1010 application circuit and package.

At the heart of this module is the Qorvo QPA1010 MMIC amplifier, shown in ***Figure 2***. This device is an X-Band GaN-on-SiC amplifier operating from 7.9 to 11 GHz. The QPA1010 amplifier provides 15 W of saturated output power with 38 percent power-added efficiency and a large signal gain of 18 dB. This device is powered by a 24 V supply with IDQ = 600 mA and includes an integrated power detector in the 24-lead 4.5 × 5.0 × 1.72 mm air cavity laminate package. To achieve the desired linearity, R6, R17, C5 and C14 are required as extra bypassing components.

The QPA1010 incorporates multiple amplifier stages, bias circuits and control logic into a single MMIC chip. This integration significantly reduces the MMIC size, parasitic losses and overall size of the amplifier, which are all crucial factors when designing a portable device that operates at microwave frequencies. The QPA1010's compact form factor allows it to be easily integrated with other components of the ablation device, such as power management and control systems while maintaining optimal performance.

Ensuring that the handheld ablation device could supply 10 W of operating power to the antenna and meet the performance requirements while operating at 8 GHz required extensive simulation and modeling. Circuit-level modeling

Telonic Berkeley

1080 La Mirada Court
Vista, CA 92081

Phone
(760) 744-8350

Fax
(760) 744-8360

Web Address
www.telonicberkeley.com

email
info@telonicberkeley.com

TELONIC BERKELEY INC.

AS9100D AND ISO 9001:2015 CERTIFIED AND AN ITAR CONTROLLED COMPANY

A Pioneer of RF & Microwave Filters

…employing proven design elements (Lumped, Combline/Cavity, and Tubular) to produce high-quality Passband, Lowpass, Highpass, and Bandstop Microwave Filters… including Diplexers, Multiplexers, Filter Banks, Switches, Multipliers… also Rotary Attenuators

Telonic Berkeley **Fixed Filters** are known and used worldwide. Our impressive array of fixed filter types has evolved over the years in responding to the demanding needs of the electronic industry while offering performance parameters tailored specifically to each customer's unique requirements.

Telonic Berkeley Engineers are ready and anxious to provide innovative solutions for your RF multi-channel or **Multiplexer** needs. Our Diplexer, Triplexer or Quadraplexer designs in lumped element or combline/cavity designs may be the solution you are looking for.

Telonic Tubular Bandpass Filters are available in 2 to 12 sections. Three different and frequency sizes ranges allow for the selection of an optimal design for each requirement. Almost any type of input or output connection is available as a standard item.

Tunable Filters including Manually Tuned Bandpass Filters, Manually Tuned Bandstop Filters, Digitally Tuned Bandstop Filters, and Multi-Octave Digitally Tuned Filters up to 36 Gigahertz are available.

Telonic Berkeley offers a full range of **RF Cable Assemblies,** Flat Ribbon Cables, Grounding Cables, Wire Harnesses, Discrete Harnesses, and Power Cords

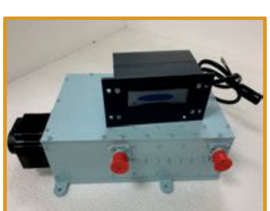

Network Managed Tunable RF Filters provide remote management, monitoring and diagnostic capabilities. High Power Tunable BSF and BPF are available

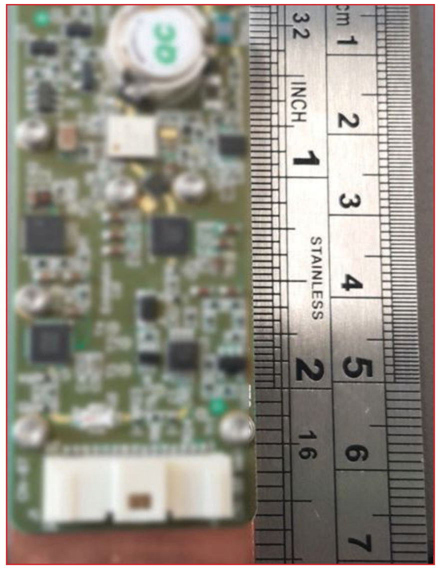

Fig. 3 Compact size of microwave source module circuit assembly.

techniques were used to optimize key performance metrics, including gain, output power, stability and efficiency. These simulations guided the integration of the QPA1010 amplifier with pre-amplifier gain stages to make sure that the complete amplifier met the performance specifications needed for effective ablation. This was particularly challenging given that the source module design had to meet a 60 mm × 25 mm footprint, as shown in ***Figure 3***, which has also been intentionally blurred. With the limited space, the design and integration used very short transmission lines between components, which prevented the use of tapers or bends to adjust for variations in the dimensions of the component connection pads. In addition, the compact design and cascaded high-gain stages were prone to feedback and oscillations, which were overcome through careful filtering of device supply inputs.

The high power density of the handheld microwave ablation system necessitated advanced cooling techniques. These include selective heat-sinking strategies for specific areas of concentrated heat and specialized thermal interfacing to maintain the amplifier within safe operating temperatures. A key component of the thermal management strategy was the use of copper coin technology, a common practice in high-power electronic devices that enhances heat dissipation. The copper coin serves as an efficient thermal bridge embedded directly into the printed circuit board beneath the component, providing an efficient path for heat transfer to the thermal mass heat sink. With its high thermal conductivity, the integrated copper coin is placed in direct contact with the component's base, where the most heat is generated, minimizing thermal resistance and allowing for rapid heat transfer. It is thermally connected to a compact thermal mass heat sink strategically positioned to dissipate the transferred heat from a number of specific circuit locations, maintaining a lightweight and compact design while ensuring efficient cooling.

Copper coin technology significantly enhances thermal performance by enabling rapid heat removal, maintaining optimal operating temperatures and helping maintain performance in concert with thermal compensation techniques. This efficient heat transfer also allows for a smaller heat sink, which helps keep the overall device size and weight to a minimum. Additionally, effective heat management ensures that the overall device remains cool to the touch, improving user comfort during extended procedures. This requirement was subsequently verified using FLIR measurements during prolonged use analysis testing, with results shown in ***Figure 4***.

Once the microwave design was finalized, it was integrated into the overall ablation device. This required coordination between the microwave design team and other teams working on power management, control electronics, firmware, user interface (UI), product design and me-

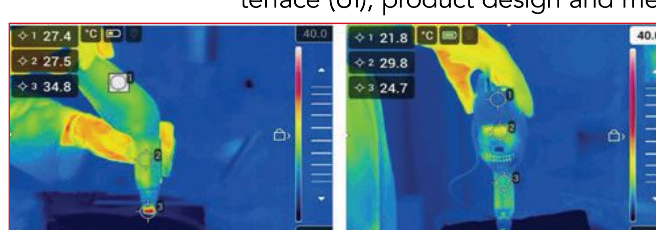

Fig. 4 Thermal camera images of the SwiftPro device during simulated prolonged usage.

chanical design. The amplifier's power requirements had to be managed to ensure efficient operation while minimizing battery drain. A custom power distribution unit (PDU) was designed to provide stable power to the amplifier, even under varying load conditions. This PDU also had to power the higher voltage microwave circuitry and all other electronics from a low-voltage 3.7 V lithium cell-based battery supply or via an optional main-derived DC power input. Integrating an efficient power management system was crucial for the device, balancing the need for high performance with the goal of minimizing battery consumption.

This power management effort was another important challenge for the design. Traditional microwave power amplifier designs often maintain a constant quiescent bias, resulting in continuous power consumption even when the device is idle. This inefficiency can significantly impact battery life in a portable device, limiting the practicality of handheld devices in clinical environments where mobility and extended operation are essential. To address this challenge, the SwiftPro device implements a power management strategy centered around dynamic bias control. This approach dynamically adjusts the amplifier's bias via firmware control to reduce power consumption during idle periods and between every energy treatment pause. Full bias is only engaged when active energy delivery is required at the point of treatment delivery.

The dynamic bias control mechanism of the ablation device allows the amplifier to rapidly ramp up bias during energy delivery and remove it when the device is not in use. This required coordination between the amplifier's control circuitry, the PDU and the overall system logic to ensure smooth transitions without affecting the quality or precision of the ablation process. By minimizing power draw during idle periods, the device can operate for extended durations, delivering hundreds of treatment applications on a single battery charge. This feature makes the device attractive for multiple procedures in outpatient or remote settings since it does not require frequent recharging.

The custom-designed PDU plays a vital role in supporting the dynamic bias control strategy. Engineered to provide stable and efficient power across varying load conditions, the PDU delivers precise voltage and current to the amplifier during both active and idle states. The PDU incorporates adaptive power delivery techniques, managed in firmware, continuously adjusting output based on the amplifier's current bias requirements to minimize wasted power and maximize overall energy efficiency. These adaptive power delivery techniques ensure that the amplifier receives the exact amount of power needed at any given moment, optimizing performance while conserving battery life.

In addition to managing power delivery, the PDU includes battery conservation features such as low-power "sleep" modes and rapid wake-up capabilities. These features enable the SwiftPro device to transition quickly between standby and active states, reducing power consumption during prolonged downtime without compromising the device's readiness. This intelligent power management system is governed by software and firmware algorithms that monitor the device's operational state, battery levels and usage patterns, making real-time adjustments to optimize power consumption. The integration of these algorithms with the UI provides healthcare professionals with real-time feedback on battery status and energy usage, allowing them to make informed decisions about device operation during procedures.

The UI was designed with the needs of medical professionals in mind, prioritizing ease of use and intuitive operation. The interface provides controls for adjusting ablation parameters of power level and time, allowing users to quickly adapt the device's settings to suit specific clinical requirements. Custom software and firmware were developed to ensure seamless communication between the UI and the amplifier's control logic. This UI was also specifically designed to maintain the ease of use and usability of the existing Swift® product from Emblation, coupled with the energy protocols that healthcare professionals

were already familiar with. This user-centric approach allows the ablation device to be easily integrated into clinical workflows, even for practitioners who may be new to microwave ablation technology.

Following the initial design and simulation phase, prototypes were developed and tested under various use conditions to validate performance and identify areas for improvement. These prototypes were subjected to stringent performance requirements under the 60601 medical device standards, including the IEC 60601-2-6 standard specific to microwave medical equipment. Managing the heat generated by the amplifier during operation was a primary challenge due to the compact design and significant heat output of the high-power microwave amplifier.

The regulatory journey is as rigorous as its technical development. As a medical device intended for direct clinical use, ablation devices must meet stringent regulatory standards in multiple markets. The SwiftPro device achieved FDA 510(k) clearance (K222388, K240518) in the U.S. and CE marking in Europe is currently pending.

Manufacturing the SwiftPro involved scaling up production while maintaining strict quality control standards. The in-house production process was designed to ensure consistency and reliability, with each device undergoing comprehensive testing before shipping. Key components, particularly the GaN-based amplifier, were sourced from leading providers of semiconductor solutions with established reputations in the industry. This careful selection of suppliers helped to ensure a reliable supply chain, reducing the risk of component shortages or inconsistencies that could impact the device's performance. The final SwiftPro device, along with its docking stand, is shown in ***Figure 5***.

A pilot program involving key opinion leaders and leading clinicians supported the market introduction. These early adopters provided valuable feedback on the device's performance, ergonomics and clinical utility, helping to refine the final product. The insights gained from these pilot programs were instrumental in optimizing the design and functionality, ensuring that the needs of healthcare professionals were met in real-world settings. A comprehensive training program was also developed to support clinicians in adopting the new technology, including detailed tutorials, in-person demonstrations and dedicated customer support.

Fig. 5 **SwiftPro microwave ablation device and docking stand.**

CONCLUSION

The successful delivery of the SwiftPro device to the market represents a significant milestone in the evolution of microwave ablation technology. The performance and compact, portable design open new possibilities for microwave ablation procedures outside of traditional surgical suites. The device and the technology can be used in outpatient clinics, remote locations and potentially even home-based care environments in the future. This expanded accessibility has the potential to greatly enhance patient care by providing more treatment options in a broader range of settings.

Beyond its current use in tissue ablation, there is future potential for expanding the technology's use in other medical applications such as dermatology and podiatry. These applications may include the treatment of benign and malignant skin conditions and a variety of other dermatological conditions. Future developments at Emblation may include software enhancements, expanded clinical applications and new treatment protocols to further increase the device's versatility and clinical value. ■

ACKNOWLEDGMENT

Emblation received funding under the 1906 Eureka Singapore UKRI Grant number 105977.

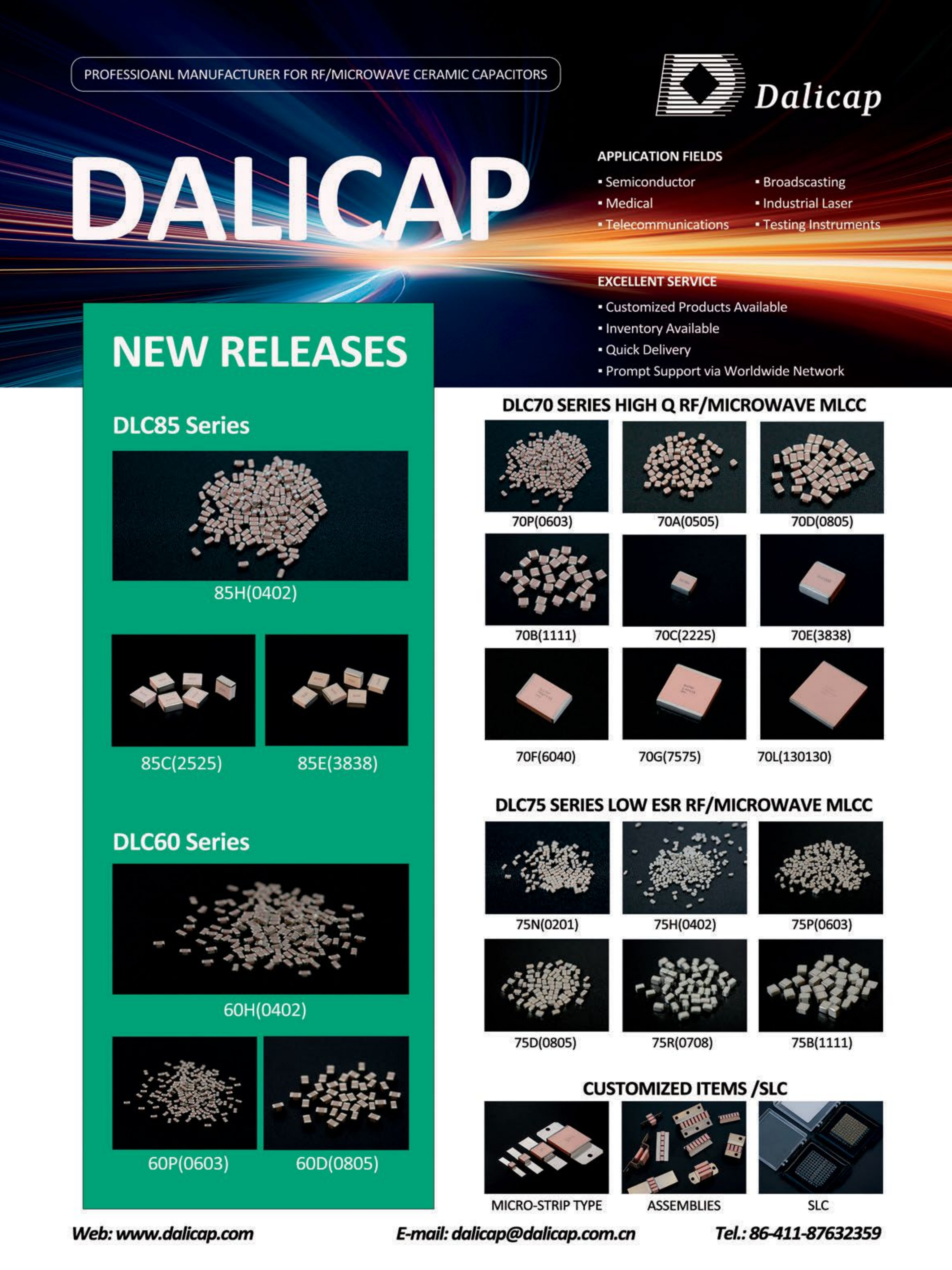
PROFESSIOANL MANUFACTURER FOR RF/MICROWAVE CERAMIC CAPACITORS
Dalicap
DALICAP
APPLICATION FIELDS
▪ Semiconductor
▪ Medical
▪ Telecommunications
▪ Broadcasting
▪ Industrial Laser
▪ Testing Instruments
EXCELLENT SERVICE
▪ Customized Products Available
▪ Inventory Available
▪ Quick Delivery
▪ Prompt Support via Worldwide Network
NEW RELEASES
DLC85 Series
85H(0402)
85C(2525)
85E(3838)
DLC60 Series
60H(0402)
60P(0603)
60D(0805)
DLC70 SERIES HIGH Q RF/MICROWAVE MLCC
70P(0603)
70A(0505)
70D(0805)
70B(1111)
70C(2225)
70E(3838)
70F(6040)
70G(7575)
70L(130130)
DLC75 SERIES LOW ESR RF/MICROWAVE MLCC
75N(0201)
75H(0402)
75P(0603)
75D(0805)
75R(0708)
75B(1111)
CUSTOMIZED ITEMS /SLC
MICRO-STRIP TYPE
ASSEMBLIES
SLC
Web: www.dalicap.com
E-mail: dalicap@dalicap.com.cn
Tel.: 86-411-87632359

INVITED PAPER

Antenna Communications in the Lunar Environment

Stuart Golden
Vulcan Wireless, Carlsbad, Calif.

Most satellite landers and orbiters today use either a dish or a single fixed antenna. This article will examine the benefits of using different antenna designs in the lunar environment. Specifically, the article will focus on a lunar orbit on the far side of the moon, where Vulcan Wireless has contributed to the development of advanced lunar communication devices for upcoming missions. Using a typical lunar orbit, the article examines the link performance for a particular operating scenario. The operational scenario that will be considered has three devices on the lunar surface, where all three devices are in a band and trying to exfiltrate sensor data back to Earth.

Landing and surviving on the moon require careful attention to both radio and antenna design. As an example, environmental conditions include extreme temperature changes ranging from -410°F (-246°C) to 250°F (121°C) on the lunar surface. Several upcoming missions will be utilizing both Vulcan Wireless's software-defined radio (SDR) and cryogenic antenna for S-Band. This article compares the performance of this system with a Vulcan Wireless phased array antenna that is currently in development and available for future deployments. The basic metric that will be utilized for link performance is the data exfiltration rate. This is the amount of data, typically sensor data, that the lander or rover can transmit back to Earth on an average Earth day. The article will describe ways to maximize this data.

Vulcan Wireless is producing multiple SDRs for lunar operations within NASA Commercial Lunar Payload Services (CLPS) programs. Shown in ***Figure 1*** are past and upcoming CLPS missions. Specifically, Vulcan Wireless has SDRs in Firefly's Blue Ghost Mission 1, Firefly's Blue Ghost Mission 2 and Firefly's Lunar Orbiter. These missions are depicted in Figure 1 as item numbers 3 and 4.

Note that some near-side lunar missions can communicate directly with the Earth without the use of a lunar orbiter. However, far-side missions require an orbiter for communication. To communicate to a far-side lunar lander/rover, a basic approach involves the use of a directional satellite dish on the orbiter. This article will examine the communication performance in this extreme lunar environment. The key communication performance metric that is used is the number of data bits that the lunar lander can exfiltrate per Earth day. A larger number of exfiltrated bits means more sensor data and more images can be captured and analyzed back on Earth. The communication performance in the presence of interference will be discussed. The article will show how Vulcan Wireless's phased array antenna can be used to combat interference and significantly increase the exfiltration rate.

For the communications protocol, a number of different communication waveform protocols can be used. The Vulcan SDR, shown in ***Figure 2***, supports many different Consultative Committee for Space

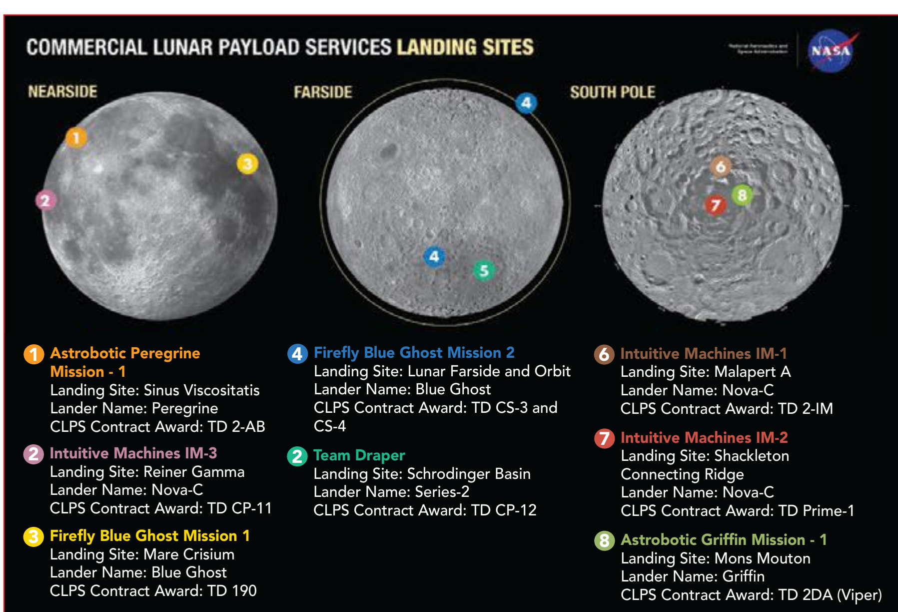

Fig. 1 **Lunar landers and lunar orbiters in the NASA CLPS program.**

Data Systems (CCSDS) protocols that are used in space and lunar applications. Specifically, it supports CCSDS telecommand (TC), CCSDS telemetry (TM), CCSDS proximity and CCSDS DVB-S2, which are critical for ensuring reliable and standardized data transmission. The SDR has been used for uplinks, downlinks and crosslinks. The SDR also has support for precision navigation and timing. Software configurations allow the radio to be used for both time transfer and ranging applications. The SDR exceeds expectations in radiation testing at the NASA Goddard facility and it is also available with military-grade top secret and below encryption.

The simulations use the antenna profile of the Vulcan Wireless cryogenic S-Band antenna shown in ***Figure 3***. NASA has approved this antenna to withstand the lunar night, which can reach -410°F (-246°C). The lunar surface is particularly challenging due to the temperature extremes accompanying the change between lunar day and lunar night. A lunar day and lunar night are equal to one Earth month, which is 30 Earth days.

SINGLE ANTENNA POINTING AT THE LUNAR LANDER

To understand data exfiltration on the moon, a lunar orbit derived from the expected ephemeris of upcoming launches is used as an example. The tracks are shown in ***Figure 4***. The upper image in Figure 4 shows the track for one Earth day and there are three distinct tracks. These are three passes that would occur during a 24-hour Earth day. The lower picture has many tracks, which correspond to all the passes within a 30-day Earth month. The yellow markings on both images in Figure 4 indicate the locations used in the simulation analysis.

Figure 4 identifies three hypothetical rover locations to be used in the simulations. The location of Rover 0 is at the proposed location for Lunar Surface Electromagnetics Experiment Night. The location of Rover 1 is at the South Pole at an upcoming planned lunar mission site and the Rover 2 location is on the near side in Mare Crisium.

Figure 5 shows the simulation results for Rover 0 pointed at a single orbiter with no other rovers transmitting. The top subplot shows the carrier-to-noise density over time, the middle subplot shows the data rate over time and the bottom subplot shows the total amount of exfiltration data over time. ***Figure 6*** shows the same data presentation for Rover 1 pointed at a single orbiter with no other rovers transmitting. ***Figure 7*** shows the data presentation for Rover 2 pointed at a single orbiter with no other rovers transmitting.

In this hypothetical comparison, the orbital satellite and the rovers

Fig. 2 **Vulcan Wireless SDR.**

Fig. 3 **Vulcan Wireless cryogenic antenna.**

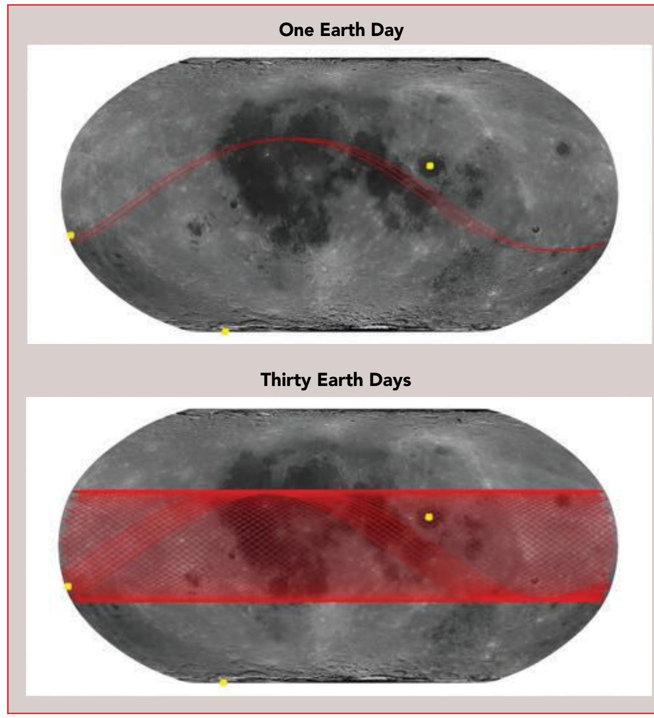

Fig. 4 **Lunar orbiter track and simulation analysis locations.**

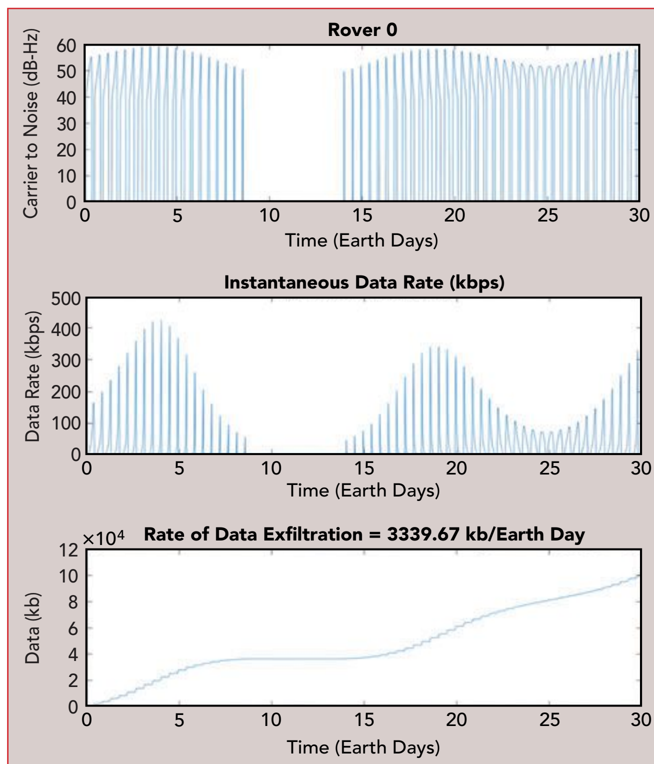

Fig. 5 **Single orbiter pointed at Rover 0, other rovers not transmitting.**

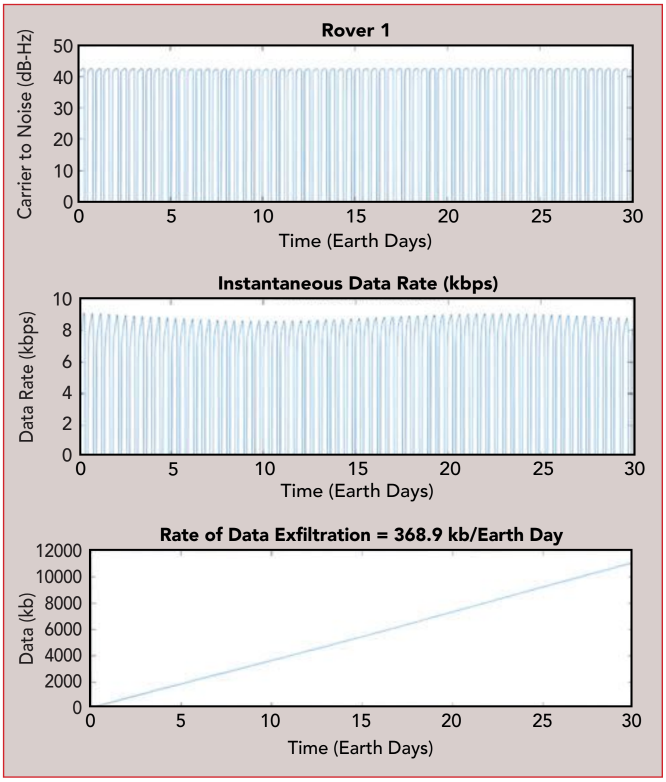

Fig. 6 Single orbiter pointed at Rover 1, other rovers not transmitting.

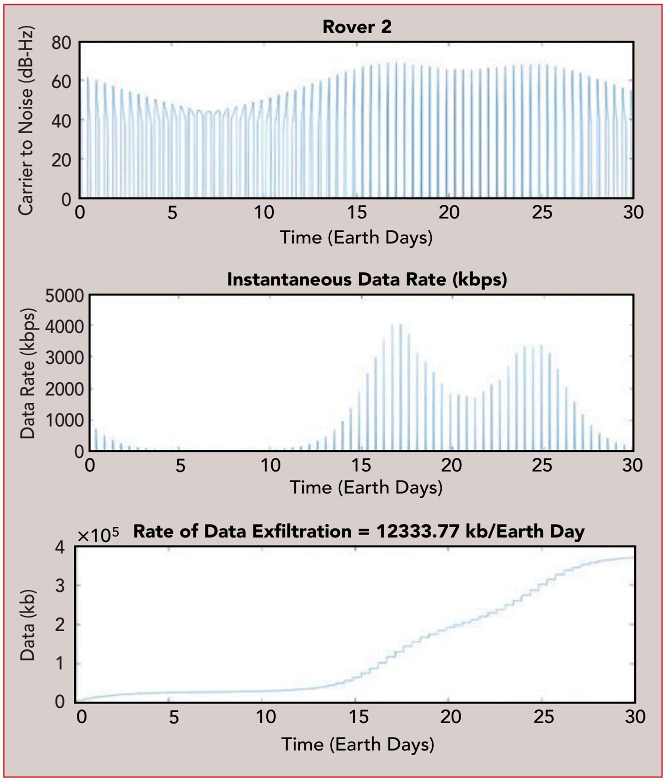

Fig. 7 Single orbiter pointed at Rover 2, other rovers not transmitting.

all have consistent and realistic link parameters, such as transmit power and antenna gain. They are kept constant across the data examples to make realistic comparisons. From the data plots, it can be observed that Rover 1 has the lowest exfiltration of the three. That is, Rover 1 can exfiltrate 0.37 Mb/day on average, while Rover 0 is able to exfiltrate almost 10x that, at 3.3 Mb/day and Rover 2 is able to exfiltrate the most, at 12.3 Mb/day.

As the data shows, the location of the lunar lander can have a significant effect on the amount of exfiltration data that can be captured. Note that for some rover locations, the amount of data per pass can change significantly, as in the case of Rover 0. But for some rover locations, a pass is very consistent. This is the case for Rover 1, located at the South Pole. The three hypothetical rover locations used in the simulations and the resulting average exfiltration rates shown in Figures 5 to 7 are summarized in ***Table 1***.

TABLE 1

ROVER LOCATION USED IN SIMULATIONS AND AVERAGE EXFILTRATION RATE PER EARTH DAY

Identifier	Lunar Location Site	Lunar Latitude (⁰)	Lunar Longitude (⁰)	Exfiltration Rate (Mb/day)
Rover 0	Far side: near Van de Graaff Crater	23.8 S	182.2 E	3.34
Rover 1	South Pole: Shackleton Connecting Ridge	89.5 S	137.3 W	0.369
Rover 2	Near side: Mare Crisium	17 N	59.1 E	12.334

SINGLE ANTENNA POINTING AT THE LUNAR LANDER WITH INTERFERENCE

To illustrate the effect of unintentional co-channel interference, this section considers the case when the orbiter is communicating with Rover 1, but Rover 0 is transmitting in the same band. That is, Rover 0 is causing interference with Rover 1 communicating to the orbiter. This may be the case when Rover 0 is deployed from a country that does not participate in widely accepted spectrum allocations and standards. For exam-

TABLE 2

DATA EXFILTRATION IN THE PRESENCE OF INTERFERENCE

Identifier	Exfiltration Rate (Mb/day)
Rover 0 interfering with Rover 1	0.18
Rover 1 without Rover 0 interfering	0.37
Rover 0 interfering with Rover 1 and the orbiter has a phased array antenna	5.90


MI-WAVE
Millimeter Wave Products Inc.
NEW!
COMPACT ULTRA WIDEBAND OMNI-DIRECTIONAL ANTENNAS
Available from 5.0-70 GHz
Standard Gain Horns
Available from 8.2 to 750 GHz
Trihedral Corner Reflector Antenna
Standard sizes from 1 to 8 inch configurations
Conical Horn Antennas
Available from 8.2 to 325 GHz
Cassegrain Reflector Antennas
Available from 5.0-110 GHz
Diameters from 10 to 48 Inches
Prime Focus Antennas
Available from 5.0-110 GHz
Diameters from 10 to 48 Inches
Linear to Circular Polarizers
Available from 8.5 – 220 GHz
RF Orthomode Transducers OMT
Available from 8.5 – 220 GHz
NEW!
GUI CONTROLLED FREQUENCY AGILE WIDEBAND SYNTHESIZER
APPLICATIONS
• Automated Test Equipment (ATE)
• Frequency Agile Radar Signal Generation
• Local Oscillators & System Clock Source
• Telecommunications/Satellite Communications
• Embedded Systems
• Secure Communications & Electronic Warfare
• Beamforming & MIMO R&D
• Spectroscopy
MI-WAVE SYNTHESIZER CONTROL INTERFACE
MI-WAVE
Millimeter Wave Products Inc.
INT REF
REF IN
REF OUT
RF OUT
LOCK
POWER
FEATURES
• Output Power +20 dBm Typical, Higher Output Power Available
• Digital Phase Shifter with 0.0002° resolution and Full 360° range
• Remote RF Control: Seamlessly operate RF signals via an intuitive GUI over Wi-Fi or Ethernet.
• Four Operating Modes: CW, Frequency Sweep, Frequency Hop, and External Trigger.
• Modulation: Supports external configuration for FSK modulation.
• CW Mode Filter: Customizable internal filter for precise and clean signal output.
• High Resolution: Achieve fine frequency adjustments with 0.01 Hz resolution.
• Ultra-Fast Switching: Less than 10 µs for rapid frequency transitions.
• Integrated Attenuators: Up to 70 dB attenuation for enhanced signal management.
• Low Phase Noise: Ensures outstanding signal clarity and quality.
• Reference Switching: Easily switch between internal and external references, including an integrated 10 MHz or 100 MHz option.
• Reference Compatibility: Supports a wide range of reference frequencies, from 10 MHz to 250 MHz.
• Temperature Monitoring: Built-in sensor for stable and consistent performance.
• Single Supply Operation: Efficiently runs on 8VDC to 15VDC power.
958 SERIES
GUI CONTROLLED WIDEBAND SYNTHESIZERS
0.1-8 GHz
0.1-16 GHz
0.1-32 GHz
0.1-67 GHz
V-Band (WR-15)
E-Band (WR-12)
W-Band (WR-10)
MIWV.COM
SATELLITE 2025 BOOTH #2623
2007 Gandy Blvd N Suite 1310
St. Petersburg, FL 33702
Tel: (727) 563-0034
Email: sales@miwv.com
MADE IN THE U.S.A. WITH PRIDE
CERTIFIED ISO 9001-2015 COMPANY
ANNIVERSARY 35 YEARS IN BUSINESS

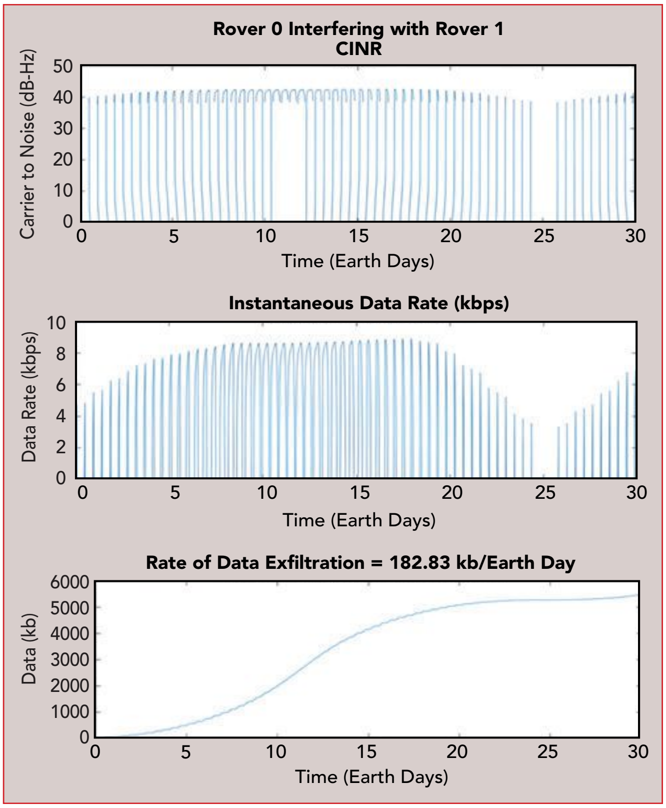

Fig. 8 **Rover 0 interfering with Rover 1 with the orbiter pointed to Rover 1.**

ple, in this scenario, the country may not have gotten approvals from the National Telecommunications and Information Administration (NTIA).

In this case, Rover 0 degrades Rover 1's performance. This is illustrated in ***Table 2***. The instantaneous data rate and carrier-to-noise density are shown in ***Figure 8***. Note that the interference from Rover 0 degrades the performance significantly on some passes and insignificantly on others. The overall performance reduces the exfiltration rate by over 50 percent of the non-interfering exfiltration rate. Specifically, without interference, Rover 0 was able to exfiltrate 0.37 Mb/day, but in the presence of interference, that result gets reduced to 0.18 Mb/day.

PHASED ARRAY ANTENNA POINTING AT THE LUNAR LANDER WITH INTERFERENCE

The other interesting result shown in Table 2 is the improvement in the data exfiltration rate when the orbiter has a phased array antenna, even when Rover 0 is interfering with Rover 1. For this application, Vulcan Wireless has developed the S-Band phased array shown in ***Figure 9***. The phased array antenna is a smart antenna that autonomously determines the direction of arrival of both the desired source and the interference. The performance curves for Rover 0 interfering with Rover 1 when the orbiter uses a phased array radar are shown in ***Figure 10***. Comparing the results of Figure 10 with the results of Figure 8, it is clear that the phased ar-

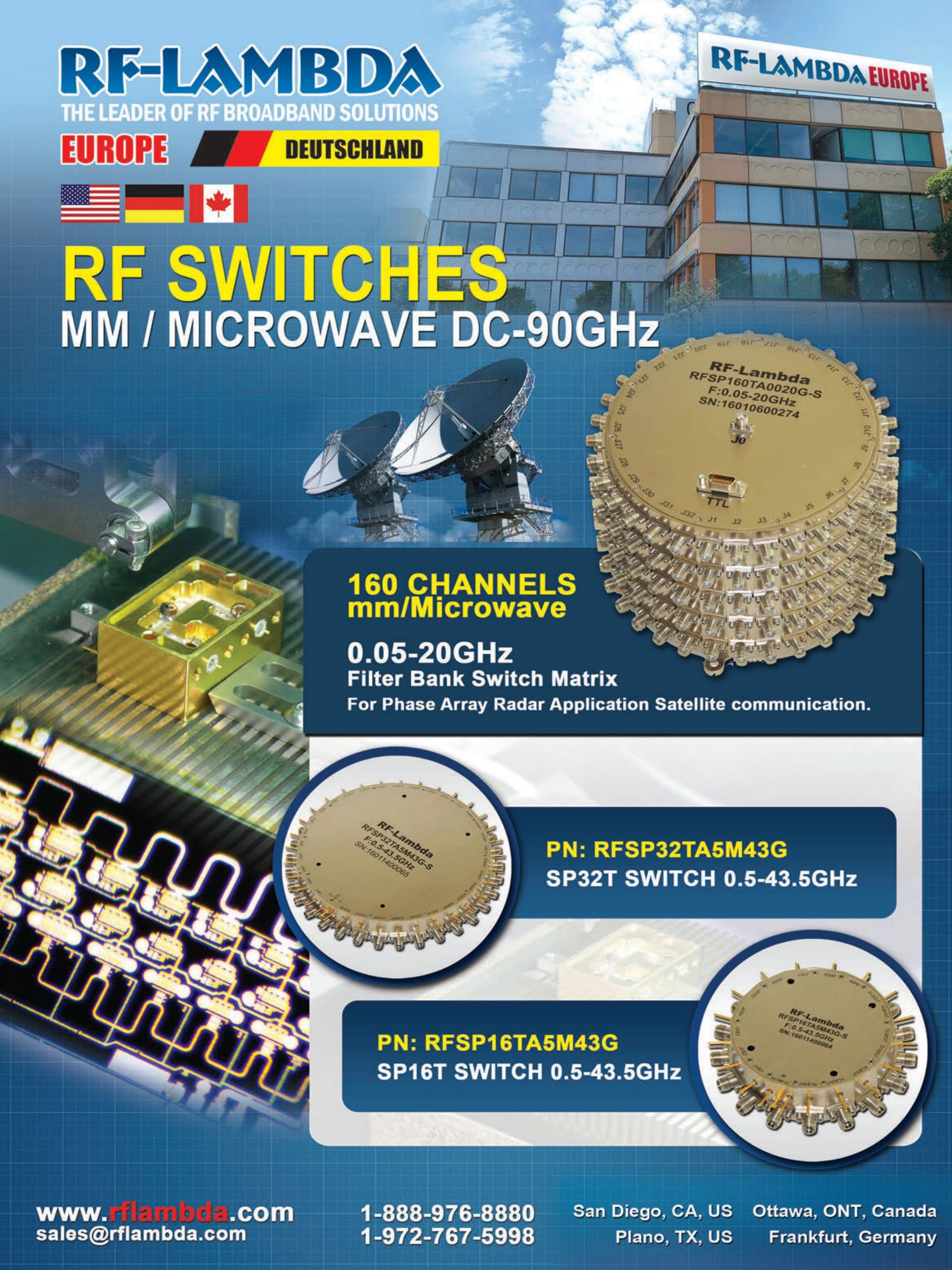

Fig. 9 **Vulcan Wireless S-Band phased array antenna.**

ray improves the performance by more than an order of magnitude over the single antenna case in the presence of interference. The hardware for the phased array SDR and smart antenna leverages the flight-proven technology of a previous generation of phased array antennas.

CONCLUSION

This article has discussed data exfiltration from the lunar surface back to Earth. It has looked at several cases to illustrate how the data exfiltration rate depends upon the location of the rover relative to the orbiter. A significant degradation in data exfiltration rate has been observed when a second rover is broadcasting its data to a secondary orbiter. However, introducing a phased array antenna on the orbiter increases the gain to the desired user and helps to mitigate the effects of the in-channel interferences. Even in the presence of interference, this architecture has been shown to increase the amount of data exfiltration by a lunar rover by more than an order of magnitude versus the best-case performance of a single antenna with no interference. ■

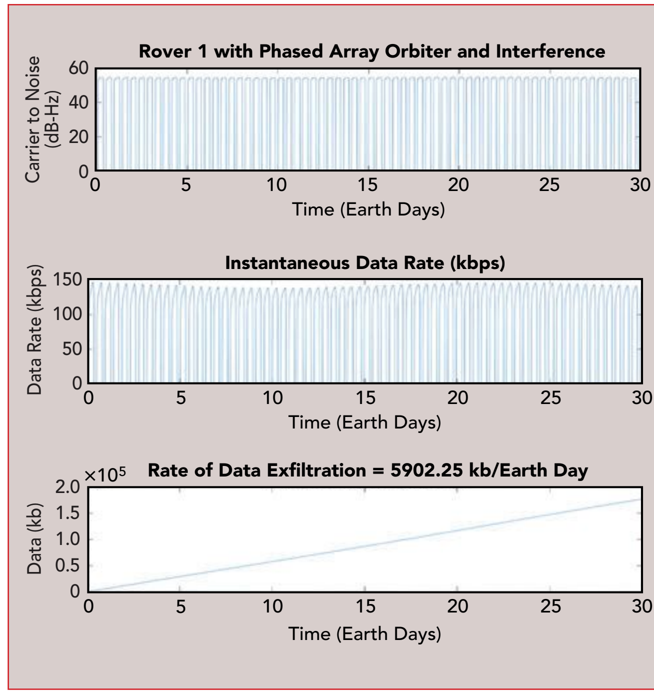

Fig. 10 **Rover 0 interfering with Rover 1 and orbiter using phased array antenna.**

Compact UWB Patch Antenna with Open-Loop Resonator for Dual-Band Rejection

Ibrahim Fortas
Electrical Systems Engineering, LIST Laboratory, University of M'hammed Bougara Boumerdes, Algeria

Mouloud Ayad
Department of Telecommunications University of Setif Setif, Algeria

Bachir Zoubiri
Division Telecom, Center for Development of Advanced Technologies, CDTA Algiers, Algeria

An innovative design for a compact ultra-wideband (UWB) patch antenna with improved frequency rejection features integrates a dual-ellipse structure in the patch geometry fed by a coplanar waveguide (CPW). The antenna is constructed on a low-profile FR-4 substrate measuring 18 × 19 × 1.5 mm. Four open-loop resonators are incorporated between the patch and the ground plane to provide rejection capabilities for two specific undesired frequency bands: WLAN (5.2 to 5.8 GHz) and X-Band satellite downlink (7 to 8 GHz). The prototype exhibits promising UWB performance and dual-band rejection using metamaterials, providing valuable insights into compact UWB antenna design for applications in wireless communication.

In the field of wireless communications, the use of UWB technology seeks to achieve high data rates at limited distances. UWB technology is defined by its capacity to function across an extensive frequency spectrum, typically 3.1 to 10.6 GHz, by Federal Communications Commission regulations established in 2002.[1] This expansive frequency range includes numerous narrow bands, such as WiMAX (3.3 to 3.7 GHz), 5G sub-6 GHz (3.4 to 3.8 GHz), WLAN (5.15 to 5.75 GHz) and others, causing significant interference.

A band-notch refers to a specific frequency range within the broader frequency spectrum that is intentionally suppressed or attenuated. Band notching is commonly employed in antenna design to reject or minimize interference.[2] Several techniques are used, e.g., slots,[3,4] defected ground structures (DGSs),[5,6] electromagnetic band gaps (EBGs),[7,8] resonators[9,10] and metamaterials.[11,12]

These techniques are employed to reject certain frequency bands, although some exhibit suboptimal rejection performance. While certain techniques are complex, i.e., they can only be realized by specialized technologies, others fall short of achieving a compact design. Researchers have used metamaterial structures, based on their unique electromagnetic properties, particularly negative permittivity and negative permeability, to achieve enhanced performance as band-reject filters.[13] This technique employs precise control over the metamaterial's response to electromagnetic waves; however, the process of designing a compact UWB antenna employing metamaterial structures that effectively reject unwanted bands is challenging.

This article describes an UWB patch design featuring a compact dual elliptical shape fed by CPW. Four open-loop resonators are used to reject radiation across two separate frequency bands: WLAN (5.2 to 5.8) GHz and the satellite downlink band (7 to 8 GHz). Rejection is significantly increased by integrating metamaterials between the patch and ground plane.

METAMATERIAL UNIT CELL DESIGN

Figure 1 illustrates the open-loop resonator metamaterial unit cell printed on a 1.5 mm thick FR-4

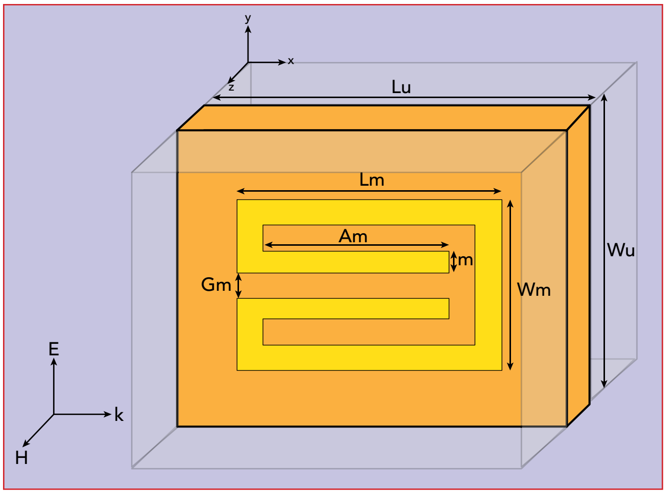

Fig. 1 **3D metamaterial unit cell.**

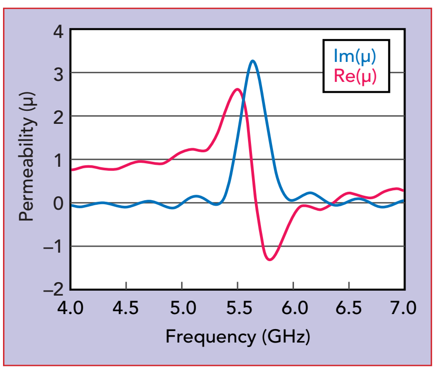

Fig. 2 **Real and imaginary parts of retrieved permeability.**

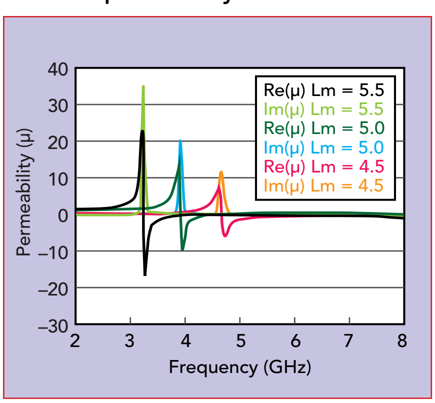

Fig. 3 **Permeability for different values of Lm.**

epoxy substrate with a relative permittivity, ε_r, of 4.3 and a loss tangent of tan, δ, of 0.025. A plane electromagnetic wave incident in the x-direction approaches the unit cell, with the magnetic field oriented along the z-axis and the electric field along the y-axis. Perfect electrical conductors serve as boundary walls along the y-axis (at the x/z-oriented sides). This configuration facilitates the design of rings that resonate near the desired frequency and enables metamaterial characterization through the calculation of S-parameters and the retrieval of effective electromagnetic characteristics ε_{eff} and μ_{eff}.

To further investigate the impact of metamaterials, a standard parameter retrieval technique is used to calculate the effective magnetic permeability.[14,15] Real and imaginary components of the magnetic permeability are acquired with CST Studio software (see ***Figure 2***). It is evident that the planar representation of the metamaterial structure exhibits a frequency range characterized by negative permeability in a specific band. This evaluation is an estimation. Nevertheless, simulation and permeability retrieval do provide a reasonable indication of the presence of metamaterial properties, even at the individual cell level. This not only facilitates resonator design but also offers an alternative justification for the results obtained.

Figure 3 shows the retrieval of the metamaterial's permeability, including both its real and imaginary parts, for various unit cell lengths, Lm. The results indicate a direct influence of unit cell length on the frequency at which the band effect manifests. This reveals an inversely proportional relationship between the unit cell's length and the frequency of observed bands in the metamaterials. This enhances the understanding of the design parameters' impact, particularly regarding negative permeability.

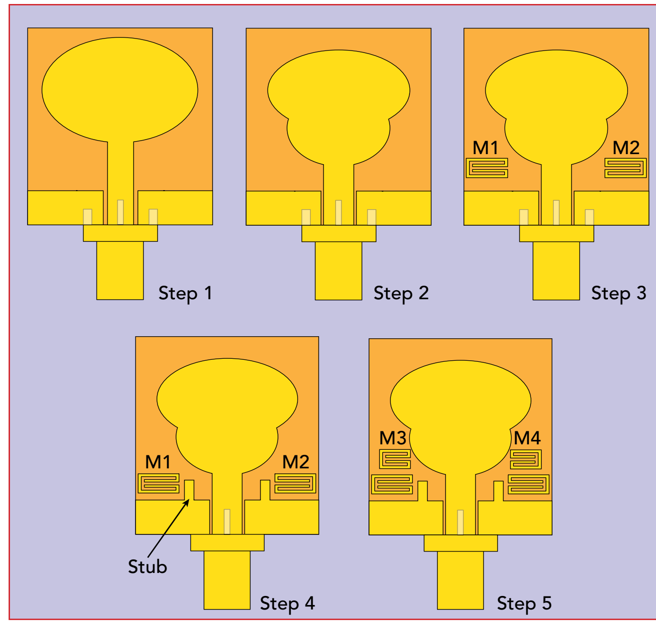

Fig. 4 **Antenna design evolution.**

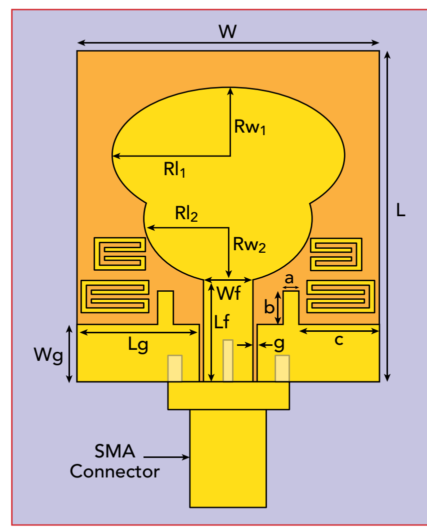

Fig. 5 **Antenna geometry.**

ANTENNA DESIGN

The design process (see ***Figure 4***) begins with the creation of an initial elliptical patch antenna in CST Studio. Then, a double-ellipse configuration fed by coplanar waveguide with an impedance of 50 Ω is used to achieve UWB performance. Finally, four metamaterial open-loop resonators are integrated into the design to effectively reject two unwanted frequency bands while further improving antenna performance.

The antenna is printed on a low-profile FR-4 substrate with ε_r of 4.3 and δ of 0.025. ***Figure 5*** shows the final design's structural layout and key components. **Table 1** lists the dimensions of key parameters.

This UWB patch antenna represents an innovative departure from the conventional single ellipse design[16] (see Figure 4, Step 1). Instead, it uses a dual-intersecting ellipse configuration (see Figure 4, Step 2) to improve UWB characteristics. The impedance bandwidth with the dual-ellipse structure shown in **Figure 6a** is greater than that of the reference single ellipse design, effectively covering the UWB spectrum from 3 to 10.5 GHz.

TABLE 1

ANTENNA PARAMETERS

Parameter	Value (mm)	Parameter	Value (mm)	Parameter	Value (mm)
L	19	Rw_1	2	Lm (M1, M2)	4.15
W	18	Rl_2	2.5	Am (M1, M2)	3.25
Lf	6.38	Rw_2	2	Lm (M3, M4)	3
Wf	3	A	1	Am (M3, M4)	2.1
Lg	7.3	B	2.08	Wm	2
Wg	3.5	C	4.8	Gm	0.3
Rl_1	3.5	G	0.2	M	0.2
Lu	5	Wu	5		

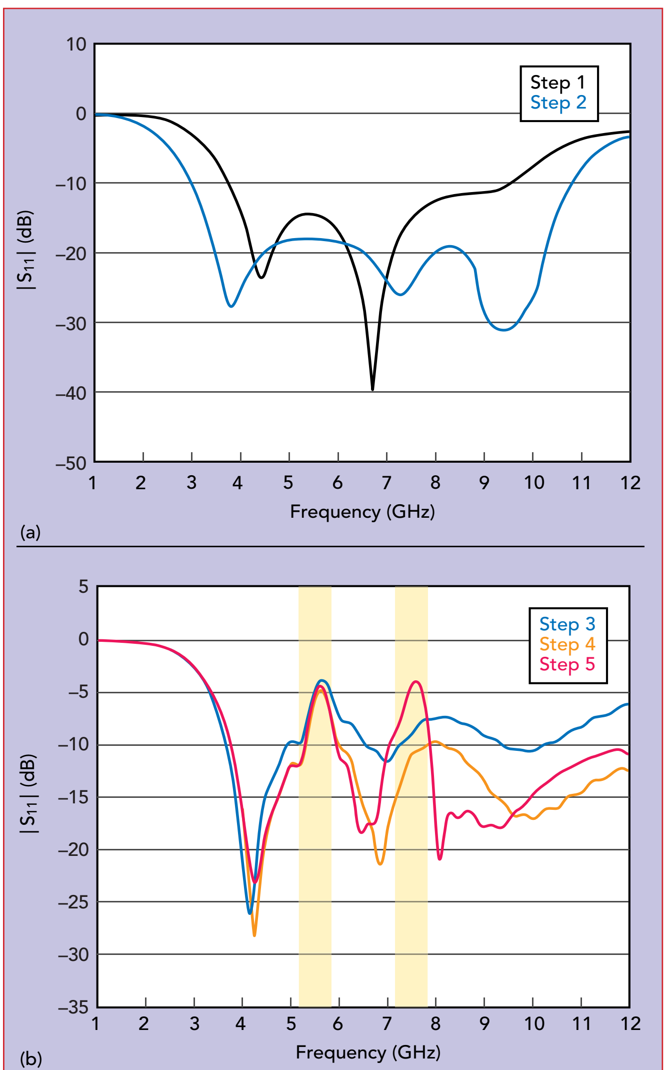

Fig. 6 Refection coefficient for design Steps 1, 2 (a) and Steps 3 through 5 (b).

In this design, metamaterials are used to reject unwanted bands. Two metamaterial unit cells, M1 and M2, are positioned above the ground (see Figure 4, Step 3). **Equation 1** determines the center frequency of the band-notch for a given effective dielectric constant and **Equation 2** determines ε_{eff}:

$$F_n = \frac{C}{L_m\sqrt{\varepsilon_{eff}}} \quad (1)$$

$$\varepsilon_{eff} = \frac{1+\varepsilon_r}{2} \quad (2)$$

Where:

Lm is the length of the resonator

C is the speed of light

ε_r is the dielectric constant of the substrate.

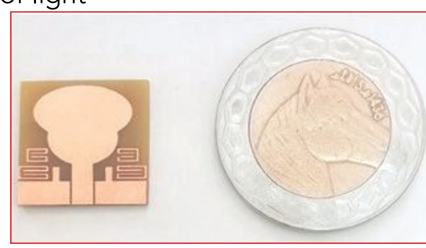

Fig. 7 Prototype UWB antenna.

Figure 6b shows -4 dB $|S_{11}|$ at the center frequency (f_{n1}) of the first unwanted band (5.2 to 5.8 GHz); however, the integration of metamaterials in Step 3 introduces a noticeable degradation in antenna matching, particularly above 7 GHz. To address this effectively, two rectangular stubs are added

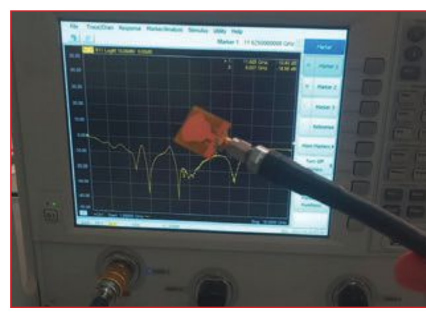

Fig. 8 Measurement setup.

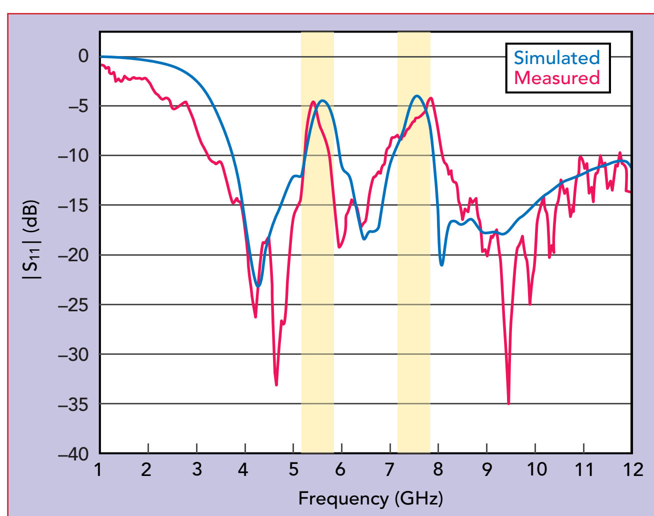

Fig. 9 Simulated and measured antenna reflection coefficients.

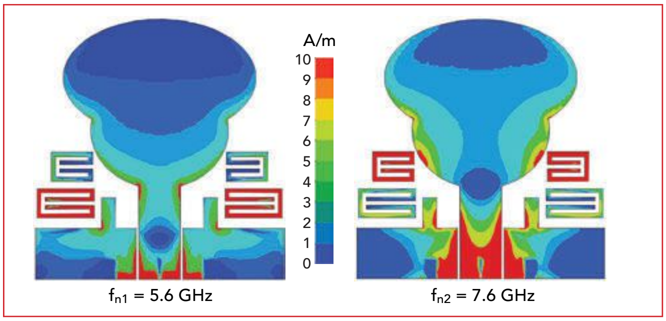

Fig. 10 Simulated antenna current distributions at the notch center frequencies.

(see Figure 4, Step 4) and $|S_{11}|$ is reduced to under -10 dB.

Finally, in Step 5, two additional unit cells, M3 and M4, are integrated. This results in significant rejection over the second targeted band (7.2 to 7.8 GHz). $|S_{11}|$ reaches approximately -4 dB at the center frequency of f_{n2} = 7.6 GHz.

PROTOTYPE FABRICATION AND MEASUREMENT RESULTS

An antenna prototype, shown in ***Figure 7***, is fabricated to verify the simulations experimentally. Measurements of $|S_{11}|$ are made using a Keysight N5224A vector network analyzer, as shown in ***Figure 8***. ***Figure 9*** compares simulated and measured results, showing a close correspondence.

To provide a more comprehensive illustration of the characteristics associated with the dual band-notch features, ***Figure 10*** shows simulated current distributions at frequencies f_{n1} and f_{n2}. It reveals a concentration of current around metamaterial unit cells M1 and M2 within the WLAN band. Within the satellite data link band, current clusters around metamaterials M3 and M4.

Radiation patterns are measured in both the E-plane (YZ-plane) and H-plane (XZ-plane) at 4.3, 6.6 and 9 GHz, with the results shown in ***Figure 11***. The results show bidirectional characteristics in the E-plane and omnidirectional characteristics in the H-plane for all frequencies of interest. Minimal changes at high frequencies are attributed to substrate power loss.

Figure 12 shows the measured and simulated peak gain, demonstrating close agreement. Gain remains stable across the entire UWB range, reaching a maximum of 3.7 dBi at 10.3 GHz. This is accompanied by a significant decrease at f_{n1} (-3.8 dBi) and f_{n2} (-3.7 dBi). It validates the effectiveness of the metamaterials technique for rejecting radiation within the two undesired frequency bands.

A comprehensive comparison of this with other related works is shown in ***Table 2***, highlighting distinctive aspects such as dimensions, frequency range, rejected bands, employed techniques, complexity and design technology. This design is compact and features a simple rejection technique based on metamaterials. The use of a single-faced CPW configuration not only simplifies its construction but also enhances

practicality and ease of integration into diverse antenna systems.

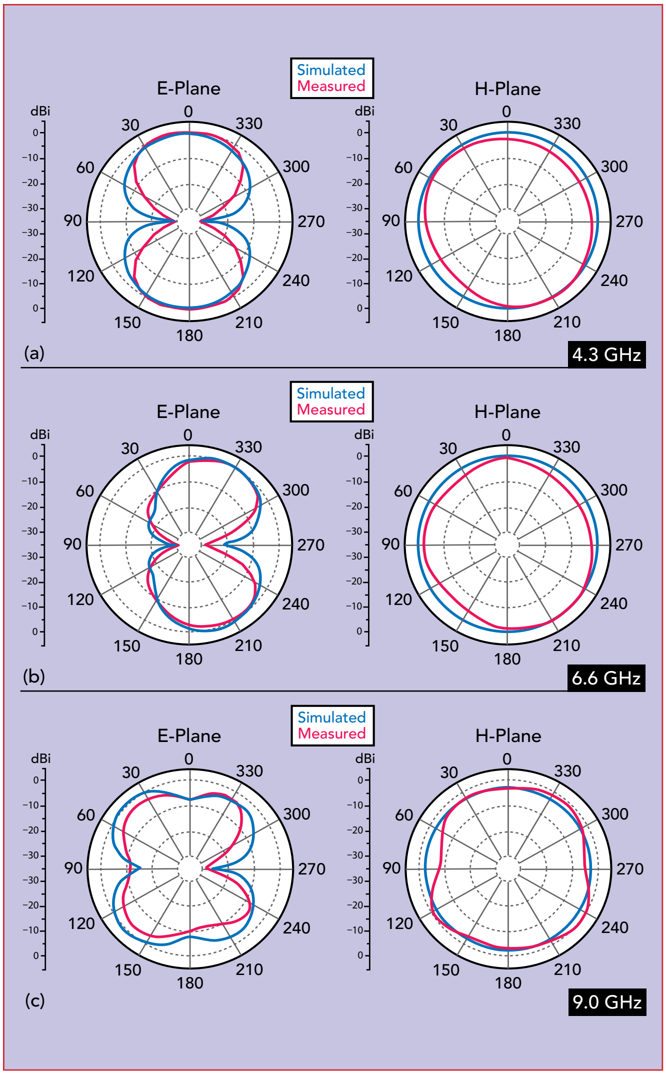

Fig. 11 Simulated and measured antenna radiation patterns at 4.3 (a), 6.6 (b) and 9 (c) GHz.

CONCLUSION

A novel approach to the design of a compact UWB patch antenna with improved rejection capabilities integrates a dual-ellipse structure in the patch geometry fed by CPW. It also employs four open-loop resonators to selectively target undesirable frequency bands, specifically WLAN (5.2 to 5.8 GHz) and the satellite downlink band (7 to 8 GHz). Experimental results closely align with the simulation, verifying the effectiveness of the open-loop resonators in enhancing rejection. The final design, incorporating metamaterials, demonstrates UWB performance with dual-band rejection. The use of metamaterials to reject radiation in undesirable frequency bands provides insight into the development of compact UWB antennas for applications in wireless communication systems. ■

References

1. "First Report and Order, Revision of Part 15 of the Commission's Rules Regarding Ultra-Wideband Transmission Systems," *Federal Communications Commission*, 2002.
2. K. L. Wong, Y. W. Chi, C. M. Su and F. S. Chang, "Band-Notched Ultra-Wideband Circular-Disk Monopole Antenna with an Arc-

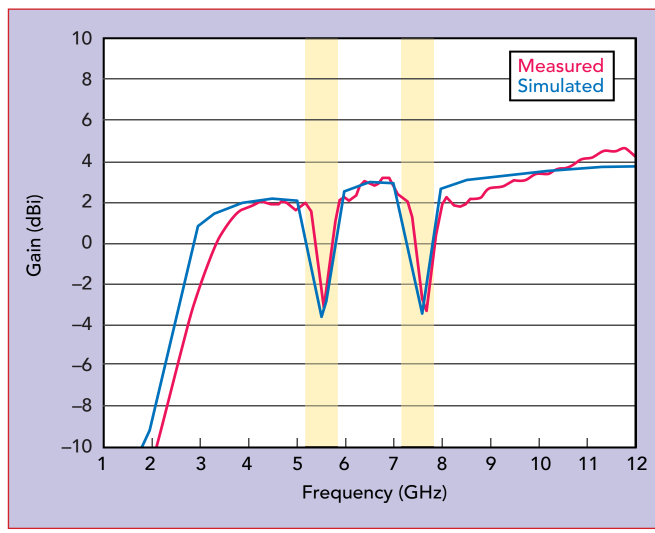

Fig. 12 Simulated and measured antenna peak gain.

TABLE 2
COMPARISON WITH OTHER WORK

Reference	Dimensions (mm)	Frequency Range (GHz)	Rejected Bands (GHz)	Rejection Technique	Complexity	Design Technology
17	28 x 18 x 0.8	3.5 to 12	5.1 to 6.0 7.83 to 8.47	Slots	Low	Microstrip
18	24.6 x 38.1 x 1.5	3 to 7.5	3.3 to 3.7 5.15 to 5.825	Slots and Resonators	High	Microstrip
19	42 x 50 x 1.6	2 to 11	3.3 to 3.8 5.15 to 5.825 7.1 to 7.9	EBG	High	Microstrip
8	20 x 26 x 1.52	3.1 to 11.8	3.4 to 3.9 5.15 to 5.82 7.25 to 7.75	EBG and Resonators	High	CPW
20	40 x 30 x 0.81	2.85 to 11.52	3.39 to 3.82 5.13 to 5.40 5.71 to 5.91	Metamaterials	Low	Microstrip
This Work	18 x 19 x 1.5	3 to 12	5.2 to 5.8 7 to 8	Open-Loop Resonator (Metamaterials)	Low	CPW

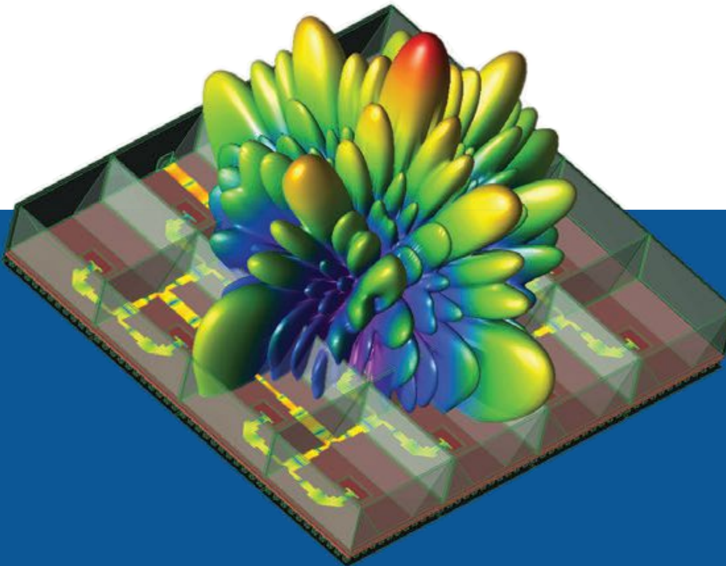

Shaped Slot," *Microwave and Optical Technology Letters*, Vol. 45, No. 3, May 2005, pp. 188–191.

3. D. K. Naji, "Miniature Slotted Semi-Circular Dual-Band Antenna for WiMAX and WLAN Applications," *Journal of Electromagnetic Engineering and Science*, Vol. 20, No. 2, April 2020, pp. 115–124.
4. S. Modak, T. Khan and R. H. Laskar, "Penta-Notched UWB Monopole Antenna Using EBG Structures and Fork-Shaped Slots," *Radio Science*, Vol. 55, No. 9, September 2020, pp. 1–11.
5. A. Sarma, K. Sarmah, S. Goswami, K. K. Sarma and S. Baruah, "DGS Based Planer UWB Antenna with Band Rejection Features," *International Conference on Wireless Communications, Signal Processing and Networking*, March 2017.
6. A. Dharmarajan, P. Kumar and T. J. Afullo, "A Human Face Shaped Ultra Wideband Microstrip Patch Antenna with Enhanced Bandwidth," *IEEE International Multidisciplinary Information Technology and Engineering Conference*, November 2019.
7. L. Peng and C. -L. Ruan, "UWB Band-Notched Monopole Antenna Design Using Electromagnetic-Bandgap Structures," *IEEE Transactions on Microwave Theory and Techniques*, Vol. 59, No. 4, April 2011, pp. 1074–1081.
8. A. Abbas, N. Hussain, J. Lee, S. G. Park and N. Kim, "Triple Rectangular Notch UWB Antenna Using EBG and SRR," *IEEE Access*, Vol. 9, December 2020, pp. 2508–2515.
9. T. Arshed and F. A. Tahir, "A Miniaturized Triple Band-Notched UWB Antenna," *Microwave and Optical Technology Letters*, Vol. 59, No. 10, July 2017, pp. 2581–2586.
10. G. Gao, L. He, B. Hu and X. Cong, "Novel Dual Band-Notched UWB Antenna with T-Shaped Slot and CSRR Structure," *Microwave and Optical Technology Letters*, Vol. 57, No. 7, July 2015, pp. 1584–1590.
11. A. Ali and Z. Hu, "Metamaterial Resonator Based Wave Propagation Notch for Ultrawideband Filter Applications," *IEEE Antennas and Wireless Propagation Letters*, Vol. 7, March 2008, pp. 210–212.
12. D. K. Ntaikos, N. K. Bourgis and T. V. Yioultsis, "Metamaterial-Based Electrically Small Multiband Planar Monopole Antennas," *IEEE Antennas and Wireless Propagation Letters*, Vol. 10, September 2011, pp. 963–966.
13. C. Milias, R. B. Andersen, P. I. Lazaridis, Z. D. Zaharis, B. Muhammad, J. T. Kristensen, A. Mihovska and D. D. Hermansen, "Metamaterial-Inspired Antennas: A Review of the State of the Art and Future Design Challenges," *IEEE Access*, Vol. 9, June 2021, pp. 89846–89865.
14. X. Chen, T. M. Grzegorczyk, B. I. Wu, J. Pacheco Jr. and J. A. Kong, "Robust Method to Retrieve the Constitutive Effective Parameters of Metamaterials," *Physical Review E*, Vol. 70, No. 1, July 2004.
15. J. Li, J. -B. Zhao, J. -J. Liang, L. -L. Zhong and J. -S. Hong, "Metamaterial-Based Planar Compact MIMO Antenna with Low Mutual Coupling," *Microwave Journal*, Vol. 61, No. 5, May 2018, pp. 116–126.
16. S. N. Mishra, D. Konhar, D. Mishra and R. K. Mishra, "On the Possibility of Linear Polarization in Elliptical Microstrip Patch Antenna," *Microwave and Optical Technology Letters*, Vol. 61, No. 4, April 2019, pp. 1048–1051.
17. W. -A. Li, Z. -H. Tu, Q. -X. Chu and X. -H. Wu, "Differential Stepped-Slot UWB Antenna with Common-Mode Suppression and Dual Sharp-Selectivity Notched Bands," *IEEE Antennas Wireless Propagation Letters*, Vol. 15, October 2016, pp. 1120–1123.
18. G. Gao, L. He, B. Hu and X. Cong, "Novel Dual Band-Notched UWB Antenna with T-Shaped Slot and CSRR Structure," *Microwave and Optical Technology Letters*, Vol. 57, No. 7, July 2015, pp. 1584–1590.
19. N. Jaglan, B. Kanaujia, S. D. Gupta and S. Srivastava, "Triple Band Notched UWB Antenna Design Using Electromagnetic Band Gap Structures," *Progress In Electromagnetics Research C*, Vol. 66, July 2016, pp. 139–147.
20. M. J. Jeong, N. Hussain, H. U. Bong, J. W. Park, K. S. Shin, S. W. Lee, S. Y. Rhee and N. Kim, "Ultrawideband Microstrip Patch Antenna with Quadruple Band Notch Characteristic Using Negative Permittivity Unit Cells," *Microwave and Optical Technology Letters*, Vol. 62, No. 2, February 2020, pp. 816–824.

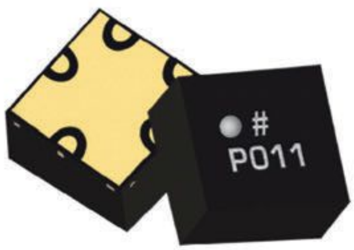

Miniaturized Power Dividers and Packaging for New Space Applications

Marki Microwave
Morgan Hill, Calif.

COMPACT AND RELIABLE INNOVATIONS FOR MODERN SPACE SYSTEMS

Modern satellite systems demand compact, high performance components to meet increasingly stringent operational and environmental challenges. As satellites incorporate phased array antennas or other high channel count systems, component size and weight become more relevant. The advent of lumped-element Wilkinson power dividers and chip scale packaging (CSP) offers groundbreaking advancements, enabling efficient and reliable technologies critical for space applications.

MINIATURIZATION REVOLUTION: LUMPED-ELEMENT WILKINSON POWER DIVIDERS

Wilkinson power dividers are the preferred splitter/combiner technology for phased array systems due to their exceptional performance. These splitter/combiners ensure minimal insertion loss and excellent impedance matching, which are critical for maintaining signal integrity across multiple channels. Additionally, their inherent design provides high isolation between output ports, preventing signal interference and enhancing overall system efficiency. Wilkinson dividers also feature excellent amplitude and phase balance, ensuring uniform signal distribution across antenna elements and enabling improved beamforming and resolution for phased arrays.

While Wilkinson power dividers are typically designed using quarter-wave transformers, Marki Microwave's new MMIC power dividers use a lumped-element approach, replacing traditional, bulky quarter-wave structures and reducing component size by a factor of 10. This compact solution is crucial for densely packed systems where space is at a premium. For LEO satellite constellations, where size and weight must be reduced as much as possible, these compact power dividers seamlessly integrate into high performance architectures. However, achieving such integration demands more than just miniaturized die designs; a compact packaged solution is needed to ensure efficient assembly and reliability in constrained spaces. ***Figure 1 (a)*** shows Marki Microwave's lumped-element transmission line approach and ***Figure 1 (b)*** shows how this method is incorporated into a four-way Wilkinson splitter design.

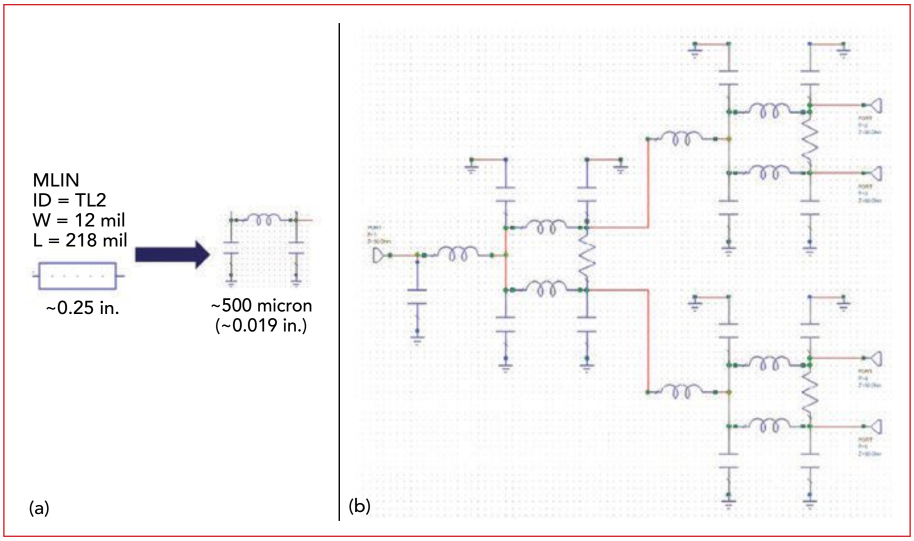

Fig. 1 **(a) Quasi lumped-element transmission line. (b) ADS four-way Wilkinson splitter with Quasi transmission lines.**

Fig. 2 **CSP product offering and physical scale.**

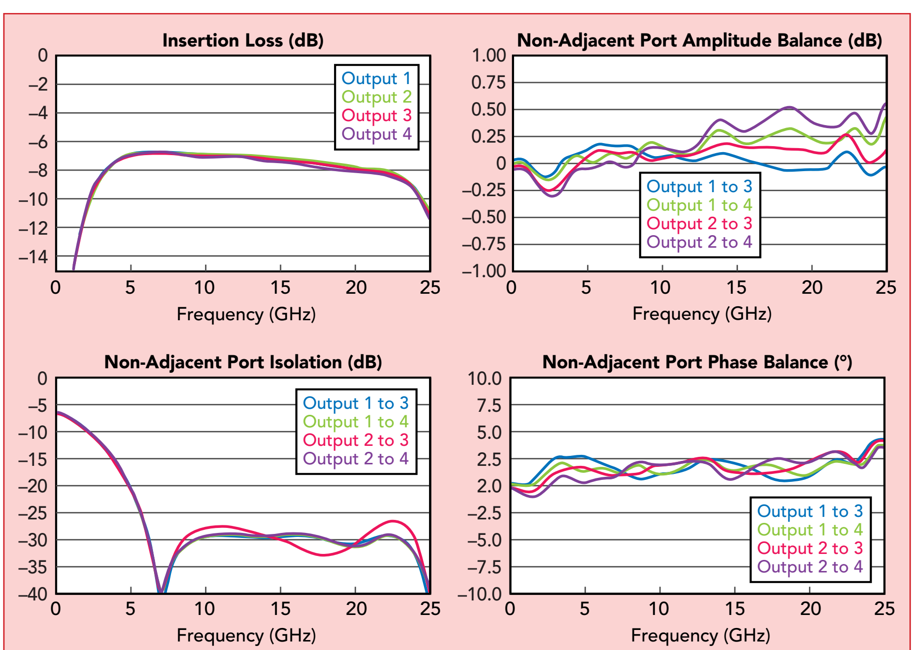

Fig. 3 **MPD4-0422CSP2 electrical performance.**

CHIP SCALE PACKAGING: A GAME-CHANGER IN PACKAGING TECHNOLOGY

Marki Microwave's patented CSP eliminates performance limitations associated with traditional wire bonding techniques. CSP uses hot-via technology, eliminating bond wire parasitic effects and achieving die-level performance in a dramatically smaller footprint.

CSP technology offers:

- **Significant Miniaturization:** Reducing component size by up to 75 percent compared to legacy QFN packages.
- **High Frequency Performance:** Supporting operations up to 85 GHz, making them suitable for advanced systems.
- **Streamlined Integration:** Compatibility with automated manufacturing processes simplifies system assembly.

Figure 2 shows Marki Microwave's CSP offering by product category, along with comparative package sizes.

CSP LUMPED-ELEMENT WILKINSON DIVIDER PERFORMANCE

Marki Microwave's new family of CSP Wilkinson power dividers include both two-way and four-way splitter designs with frequency coverage up to 70 GHz. ***Figure 3*** shows performance curves from Marki Microwave's new MPD4-0422CSP2, a 4 to 22 GHz four-way Wilkinson power divider.

The MPD4-0422CSP2 features:

- **Insertion Loss:** Approximately 1 dB excess insertion loss above the theoretical 6 dB loss for a four-way splitter.
- **Amplitude and Phase Balance:** Less than 0.5 dB and 3 degrees, respectively, across the operational bandwidth.
- **Isolation**: 30 dB typical isolation between output ports.
- **Size:** Available in Marki Microwave's 2.5 mm CSP2 chip scale package.

These performance results and metrics highlight the capability of Marki Microwave's CSP Wilkinson dividers. These characteristics enable them to meet the rigorous performance demands of phased array applications while minimizing size and weight for new space applications.

RIGOROUS SPACE QUALIFICATION FOR RELIABILITY

LEO satellite constellations have significantly transformed the space industry by emphasizing cost reduction and rapid deployment. Unlike traditional geosynchronous satellites with decade-long missions, LEO systems have shorter lifespans, requiring cost-effective solutions without compromising reliability. This shift has driven the adoption of upscreened commercial off-the-shelf (COTS) components. By adapting and qualifying these components for space use, manufacturers achieve substantial cost savings and faster development cycles.

Upscreening ensures that COTS components meet the performance and durability requirements for LEO satellites, which must operate in dynamic and harsh orbital conditions. The approach involves rigorous testing to validate components against thermal cycling, radiation exposure and mechanical stress requirements. For phased array systems in LEO satellites, upscreened components provide a reliable yet economical option to achieve optimal signal distribution and system efficiency.

CSP components such as Marki Microwave's new Wilkinson splitters can undergo extensive qualification, verifying performance under extreme thermal and structural conditions. These tests confirm their resilience and operational reliability for critical space missions. The majority of Marki's components, from bare die, surface-mount and connectorized devices to waveguides, can be upscreened and qualified for space applications. Marki Microwave follows MIL-PRF-38534, MIL-PRF-35835, MIL-PRF-27 and NASA EEE-INST-002 standards. These standards serve as guidelines to screen and qualify commercial components to standard military levels or the highest level of reliability for space. Space qualification protocols ensure that CSP components meet the reliability thresholds for extreme environments.

Key testing phases include:

- **Comprehensive Screening:** Encompasses visual inspection, electrical validation and thermal cycling.
- **Robust Qualification Testing:** Covers life tests, mechanical shock resistance and environmental stress analysis.

Marki Microwave partners with customers to tailor testing and qualification processes to specific mission needs, balancing cost, reliability and timelines for optimal outcomes.

VENDORVIEW

Marki Microwave
Morgan Hill, Calif.
markimicrowave.com

Multichannel Rubidium Frequency Calibrator/Analyzer

Pendulum Instruments Inc.
Redwood City, Calif.

Pendulum's new CNT-104R is the latest addition to its high performance, multichannel frequency and time-interval calibration analyzer family. This compact benchtop unit combines an ultra-stable 10 MHz Rubidium frequency reference with a four-channel advanced frequency analyzer, allowing users to verify and calibrate up to four oscillators/clocks in parallel on four input channels simultaneously. The unit is shown in ***Figure 1***.

The unit can also be equipped with an optional multiband GNSS receiver that disciplines the built-in Rubidium clock. This eliminates any small intrinsic drift due to aging and provides exceptional accuracy for both portable and laboratory test applications. The GNSS control not only enables continuous disciplining of the Rubidium time base, but it allows the user to reset any accumulated aging when operated in previously GNSS-denied environments.

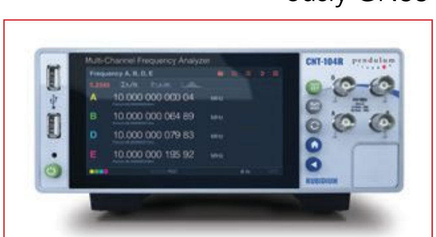

Fig. 1 **CNT-104R frequency calibrator/analyzer.**

The GNSS receiver provides an uncertainty of 10 ns rms to UTC. This enables the calibration of one to three external sync signals with unprecedented accuracy. The internal phase/time reference functionality allows users to view drift over time and frequency distribution, including traditional numeric and statistical parameters, on the large color graphic display.

Featuring a time resolution of less than 7 ps, 12 to 13 digits/sec frequency resolution and variable gate time setting from 50 nsec to 1000 sec, the analyzer is purpose-built and optimized for demanding metrology applications. All four input channels support gap-free, zero-deadtime counting, providing back-to-back measurements without losing any cycle, even over extended measurement periods. The standard frequency range for each channel is up to 400 MHz. However, input channel C can support microwave frequencies up to 24 GHz via different software upgrade options.

The CNT-104R is also a high performance modulation domain analyzer for the advanced user. The analyzer has a high speed design and sample rates of up to 20 million measurements per second for four parallel input signals. This allows very fast frequency variations or phase/time changes to be captured in real-time.

The unit is offered in its standard configuration with one 10 MHz reference output with frequency stability of 1×10^{-12} over a 24-hour average when the optional integrated GNSS receiver controls the Rubidium oscillator. Additional, highly stable 10 MHz outputs are achieved when the unit is used in conjunction with Pendulum's FDA-301A

Fig. 2 **Four simultaneous signals on CNT-104R display.**

frequency distribution amplifier. This amplifier multiplies the number of outputs by a factor of 4, 8 or 12 over copper or 6, 12, or 18 via fiber interfaces, depending on the output module configuration.

The four-channel CNT-104R design enables four parallel frequency measurements. This means that the CNT-104R can replace four frequency counters in a test system, decreasing the effective cost per counter. It can also provide an ultra-stable 10 MHz reference frequency to the test stand. This makes the CNT-104R the equivalent of five separate instruments in a single box, reducing space requirements and capital investment. You can choose between Ethernet or WLAN as a communication interface to a variety of devices, including PCs, laptops, tablets or the test system controller. The bus speed, with block measurements occurring at up to 170k measurements per second, reduces test time in ATE test systems compared to existing solutions.

A large, color touch screen, along with an intuitive menu structure, allows simple navigation and setup of instrument test parameters. The unit is equipped standard with a Gbit Ethernet interface, offering complete flexibility for remote control and test result data transfer. Users can also operate the unit using a wireless mouse and a connected USB dongle. A built-in web server allows the unit to be accessed and controlled from your lab bench or almost anywhere in the world via a PC or mobile device using the integrated web interface. This enables wired Gigabit Ethernet or wireless Wi-Fi connectivity to provide flexible remote control capability.

Notable features of the CNT-104R are the menu-oriented settings in the graphic display. Intelligent AUTO SET configures the best settings for each measurement. Thanks to the guided instruction on most setting pages, the non-expert can easily make correct settings. Valuable signal information, given in multiparameter displays, removes the need for other instruments like DVMs and scopes for quick signal verification. Measured results are presented in numerical and graphical formats. Graphical presentation of results like distribution, trends etc., gives a better understanding of the nature of jitter. It also provides a much better view of changes versus time (e.g., drift). A toggle function allows test data to be viewed in numerical, statistical, distribution and timeline modes. It is quite easy to capture and toggle between views of the same data set. ***Figure 2*** shows a typical display of four simultaneous signals. This display makes it easy to see why the CNT-104R can be considered as four instruments in one.

Pendulum's frequency counters/analyzers are reputable and well-known as industry-leading time and frequency measurement instruments. For over 60 years, Pendulum Instruments has served the aerospace and defense, telecom, metrology and R&D industries worldwide. Contact us to learn how the CNT-104R can be configured according to your specific needs and/or budget demands.

Pendulum Instruments Inc.
Redwood City, Calif.
www.pendulum-instruments.com

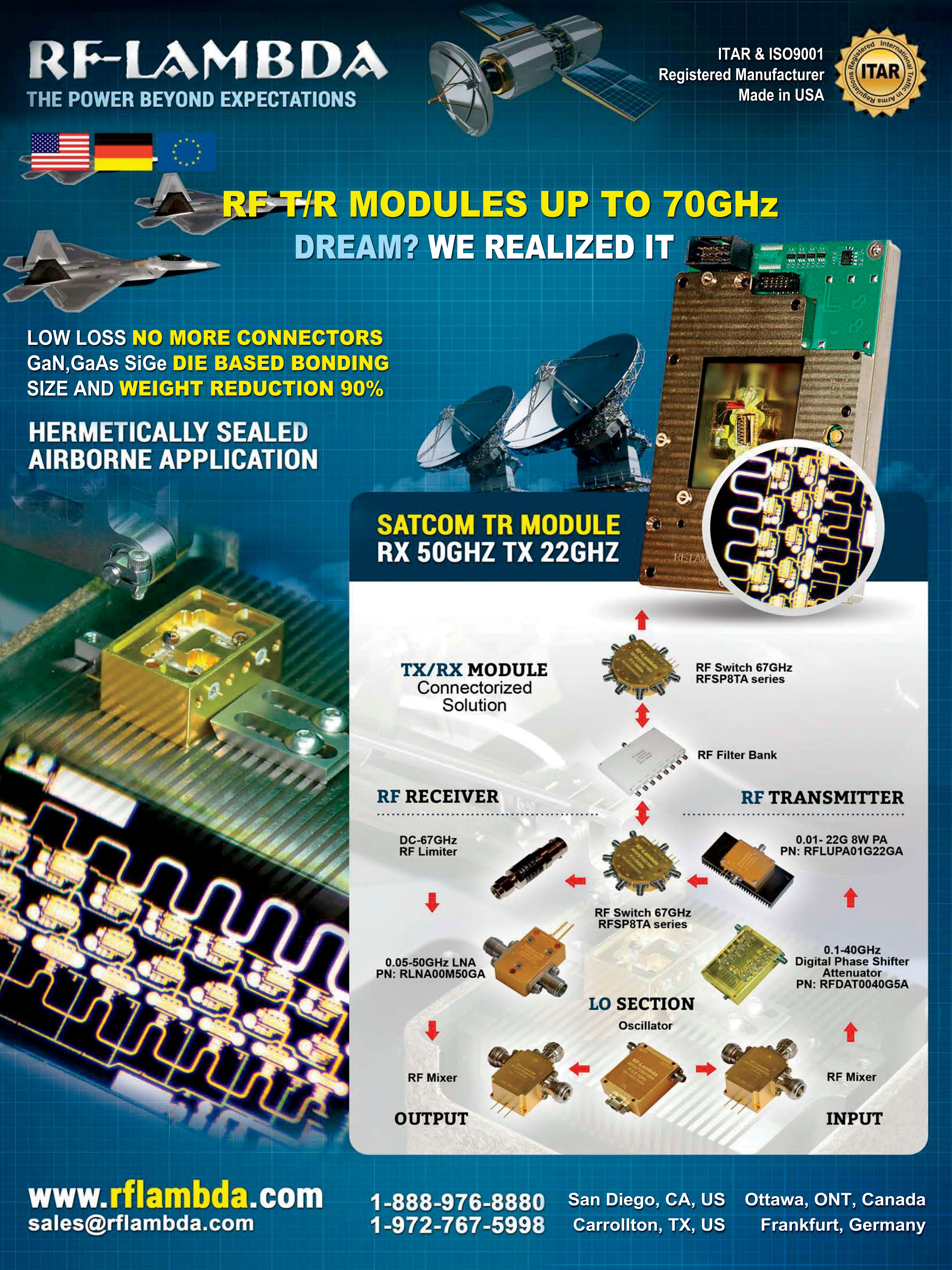

RF-LAMBDA
THE POWER BEYOND EXPECTATIONS
ITAR & ISO9001
Registered Manufacturer
Made in USA
ITAR
Registered International Traffic in Arms Regulations
RF T/R MODULES UP TO 70GHz
DREAM? WE REALIZED IT
LOW LOSS NO MORE CONNECTORS
GaN,GaAs SiGe DIE BASED BONDING
SIZE AND WEIGHT REDUCTION 90%
HERMETICALLY SEALED
AIRBORNE APPLICATION
SATCOM TR MODULE
RX 50GHZ TX 22GHZ
TX/RX MODULE
Connectorized
Solution
RF Switch 67GHz
RFSP8TA series
RF Filter Bank
RF RECEIVER
RF TRANSMITTER
DC-67GHz
RF Limiter
0.01- 22G 8W PA
PN: RFLUPA01G22GA
RF Switch 67GHz
RFSP8TA series
0.05-50GHz LNA
PN: RLNA00M50GA
0.1-40GHz
Digital Phase Shifter
Attenuator
PN: RFDAT0040G5A
LO SECTION
Oscillator
RF Mixer
RF Mixer
OUTPUT
INPUT
www.rflambda.com
sales@rflambda.com
1-888-976-8880
1-972-767-5998
San Diego, CA, US
Carrollton, TX, US
Ottawa, ONT, Canada
Frankfurt, Germany

Photonic Microwave Oscillator Offers Ultra-Low Phase Noise

QuSine
Potsdam, Germany

QuSine, a spin-off from the Heinz Nixdorf Institute at the University of Paderborn, Germany, introduces the QuSine PureWave Photonic Microwave Oscillator (PMO) product family. Designed to redefine precision in RF signal generation, the PureWave PMO series offers excellent phase noise performance, critical for today's advanced applications in telecommunications, radar systems, quantum computing, aerospace and beyond. With specifications that surpass conventional electronic signal generators, the QuSine PureWave PMO, with an example shown in ***Figure 1***, sets new benchmarks for signal clarity, stability and precision across a broad frequency range.

The QuSine PureWave PMO offers performance metrics designed to address the most demanding requirements in RF and microwave applications:

- **Phase noise**: At 10 GHz, the PureWave PMO achieves a measured value of -154 dBc/Hz at a 100 kHz offset.
- **Jitter**: The oscillator boasts a jitter of just 6.3 femtoseconds over a 1 kHz to 100 MHz frequency range for excellent timing precision.
- **Frequency range**: The product family covers a range from 3 to 60 GHz, with 250 MHz intervals, offering flexibility for a variety of applications.
- **Output power range**: The output power range is selectable from -20 to +13 dBm.
- **Operating temperature range**: Optimized for laboratory and high-precision environments, the PureWave functions best in the temperature range of 18°C to 23°C.

Fig. 1 **PureWave Photonic Microwave Oscillator.**

This combination of specifications makes the QuSine PureWave PMO a best-in-class solution for high performance RF signal generation where phase noise and signal stability are paramount requirements.

The PureWave PMO leverages a photonic-based architecture for signal generation. In a conventional RF signal generator, a microwave oscillator phase locks to a low noise electronic reference oscillator, typically an oven-controlled quartz oscillator. By phase-locking, the microwave oscillator inherits the phase noise characteristic of the low frequency electronic reference. Optical oscillators such as mode-locked lasers or optical frequency combs generate optical pulse trains, which offer significantly better phase noise than any electronic oscillator technology. In QuSine's PMO, the microwave oscillator phase locks to an optical reference oscillator, inheriting the superior phase stability of the optical oscillator. This new concept ensures outstanding phase noise and jitter.

The oscillator phase noise is much better than most conventional RF signal generators. With its exceptional jitter performance, the QuSine PureWave PMO series ensures that even demanding applications like high speed data converters and precise timing systems can rely on its stability and performance.

By offering different frequencies, the QuSine PureWave PMO family addresses various applications. These include next-generation telecommunications technolo-

MiCable

SSMP 40GHz Female Right Angle

C25F Series MILLIMETER WAVE CABLE ASSEMBLY

Ideal for connection and jumper requiring extremely limited installation space and high reliability

NEW

3mm Min. Bend Radius

Excellent Phase Stability vs. Temp.

Excellent Mechanical/Temp. Stability

High Freq. Low Loss Low VSWR

Small Size for High Density Arrangement

VSWR

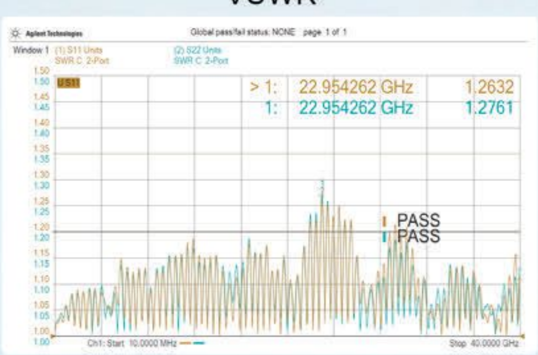

Cable Diameter	1.42mm
Frequency	DC~40GHz
Cable Attenuation	7.69dB/m@40GHz
VSWR	<1.40@40GHz
Shielding Effectiveness	<-90dB
Phase Stability vs. Flex.	<±4°@40GHz
Phase Stability vs. Temp.	<200ppm@-15°C~+35°C <400ppm@-40°C~+70°C
Amplitude Stability vs. Flex.	<±0.1dB/m@40GHz

More Information-
Scan the QR Code

MIcable Inc.

www.micable.cn sales@micable.cn +86-591-87382856

TABLE 1

PUREWAVE PMO FAMILY PERFORMANCE

Part Number	Frequency (GHz)	Phase Noise (dBc/Hz at 100 KHz offset)
QSPMO03G	3	-154
QSPMO06G	6	-154
QSPMO08G	8	-154
QSPMO10G	10	-154
QSPMO20G	20	-148
QSPMO30G	30	-144
QSPMO40G	40	-142
QSPMO50G	50	-140
QSPMO60G	60	-138

gies to precise laboratory measurements and aerospace communication systems. ***Table 1*** shows the phase noise for different frequency options available from the PureWave PMO family.

Users can select from the available frequency ranges for their specific requirements. The oscillator output power, ranging from -20 to +13 dBm, can be chosen to customize signal strength for particular application needs. The adaptability of the PureWave PMO family ensures that it can meet the exacting demands of any project, whether it be in a research environment or an industrial setting.

SETTING A NEW STANDARD FOR PHASE NOISE

Achieving ultra-low phase noise is the cornerstone of the PureWave PMO design. The product's phase noise at 10 GHz is over 10 dB better than the best laboratory-grade RF signal generators, allowing for highly accurate and trustworthy measurements. ***Figure 2*** shows phase noise comparisons at 10 GHz for QuSine products versus an industry benchmark.

Phase noise is a critical factor in many applications that prioritize signal purity. In radar systems, low phase noise improves range and resolution by enhancing the radar's ability to distinguish between nearby objects and reducing clutter. Using Doppler measurements to distinguish slow-moving targets from the environment is easier with superior phase noise performance. In wireless communications, low phase noise generally improves the receiver's signal to noise ratio and error vector magnitude, reduces reciprocal mixing with interferers and improves signal integrity in multi-carrier modulation schemes. Broadband digital-to-analog converter digital-to-analog converter and analog-to-digital converter precision degrades with clock jitter, so reducing clock jitter can improve the effective resolution of these devices.

APPLICATIONS

The QuSine PureWave PMO addresses a wide range of applications that require high-precision signal generation:

- **Radar systems**: The phase noise and jitter performance improve signal resolution and target detection capabilities in radar applications.

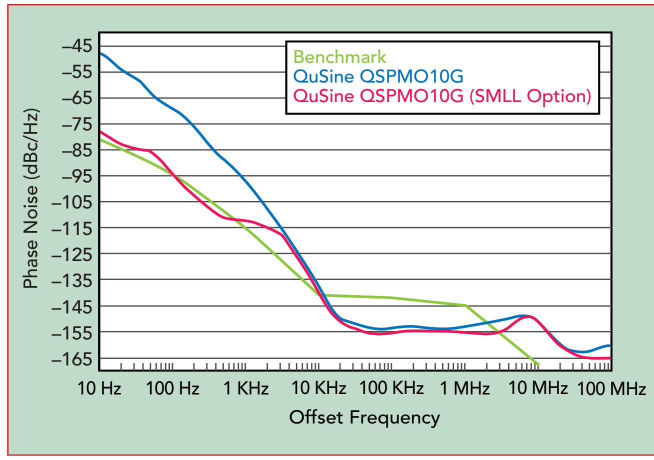

Fig. 2 **10 GHz phase noise performance comparisons.**

- **Telecommunications**: The broad frequency range and stable signal generation enhance the performance of next-generation communication systems, ensuring high-quality, low-error data transmission.
- **Quantum computing**: Quantum systems require precise timing and low noise environments to operate effectively. The jitter and phase noise performance aids in controlling qubits and maintaining system coherence.
- **Aerospace and satellite communication**: The wide frequency range and robust output power ensure stable and reliable data links, even in challenging environments, for high frequency communication systems in aerospace applications.
- **Test and measurement**: The PureWave PMO offers the precision and flexibility needed for accurate testing and measurements in RF and microwave technology research and development.

CONCLUSION

The QuSine PureWave PMO is a high performance addition to the RF signal generator market. With its ultra-low phase noise, minimal jitter and wide range of frequency options, the PureWave PMO series offers high precision and flexibility for various applications. By leveraging photonic technology, QuSine has been able to push the boundaries of what is possible in microwave signal generation, making the PureWave family the best-in-class choice for advanced research, telecommunications, radar, quantum computing and more.

For engineers, researchers and developers looking for a high performance, reliable signal generator, the QuSine PureWave PMO provides the ultimate solution. As technologies continue to evolve and demand even greater precision, the PureWave series allows users to stay ahead of the curve. It offers the low noise, high frequency performance needed to drive innovation in a wide range of industries.

QuSine
Potsdam, Germany
qusine.com

Multichannel Ultra-Broadband Software-Defined Radio

Nxbeam has expanded its product portfolio with the introduction of a multi-channel ultra-broadband software-defined radio (SDR) based on the RFSoC-DFE platform, which provides a fully hardened subsystem, including DDC, DUC, FIR, Resampler, FFT, Mixer and DPD and CFR. This product features four receivers and four transmitters, providing versatile functionality tailored to various use cases in communication and radar applications. For communication applications, the transmitters and receivers can be configured for QAM or DVB-S2X modulations, with adjustable output frequencies reaching up to C-Band, based on customer requirements. The ultra-wideband transmitter supports symbol rates of 500 Msps per channel and a raw data rate of up to 4 Gbps per channel. The SDR includes built-in digital predistortion technology to ensure high linearity. For radar applications, the transmitter can generate linear chirp waveforms with bandwidths up to 1 GHz, while the receiver functions as both a radar receiver and a data acquisition system. The integrated FPGA offers robust radar signal processing capabilities, making the system suitable for demanding radar applications.

The SDR is packaged in a compact CubeSat form factor. It supports high speed LVDS data transmission and 10G-BaseR SFP optical Ethernet connectivity. With low DC power consumption, the system provides an optimal size, weight and power solution for customers seeking high performance, energy-efficient systems.

Nxbeam was founded in 2018 with the mission to deliver the next generation of wireless communication infrastructure products to power the future of information communication technology. With a focus on compound semiconductor solutions using GaN and InP technologies, Nxbeam develops both standard and custom products that support customers in the satellite and 5G communication markets.

VENDORVIEW

Nxbeam Inc.
Los Alamitos, Calif.
www.nxbeam.com

ADSY1100 Video

Check out Analog Devices ADSY1100-series: A 4 Tx/Rx, 3UVPX Tuner+Digitizer+Processor SOM, impressively contained within a single 1 in. pitch chassis.

Analog Devices
www.analog.com/en/resources/media-center/videos/6355240460112.html

Automated Valet Parking Simulation

Watch Anritsu's brief video to learn about the test solutions that improve Type-2 AVP reliability.

Anritsu
https://bit.ly/3sVsv9k

Vector Network Analyzer Measurement of S-Parameters in a Pulsed RF System

Copper Mountain Technologies' Senior Design Engineer Brian Walker demonstrates how to make pulsed S-parameter measurements with an external pulse and a Cobalt VNA.

Copper Mountain Technologies
www.youtube.com/watch?v=pT2iTTbFPPY

MACOM Reaches 75 Years

MACOM kicked off 2025 as a milestone year, their 75th anniversary. Some 2024 company highlights include: the acquisition ENGIN-IC, the selection to a lead advanced GaN-on-SiC semiconductor technology development project by CHIPS and joining PHLX Semiconductor Sector Index.

MACOM
www.macom.com

GaAs Switches Are a High Performance Alternative to SOI for Test & Measurement Instrumentation

In this application note, Mini-Circuits' discuss why GaAs switches are re-emerging as an attractive option in test and measurement due to technology advances, and the key metrics that make choosing a GaAs RF switch an easy decision.

Mini-Circuits
blog.minicircuits.com

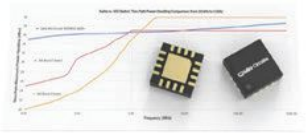

Cybersecurity Matters — Boost IoT Confidence with Qorvo Matter Technology

Stay ahead in IoT security with Qorvo's IoT Dev Kit for the QPG6200L. Explore energy-efficient solutions, advanced security features and insights to meet evolving standards and drive success.

Qorvo
https://bit.ly/3PLZIMJ

NEW PRODUCTS

FOR MORE NEW PRODUCTS, VISIT WWW.MWJOURNAL.COM/BUYERSGUIDE
FEATURING VENDORVIEW STOREFRONTS

DEVICES/ COMPONENTS/MODULES

V-Band Bandstop Filter

VENDORVIEW

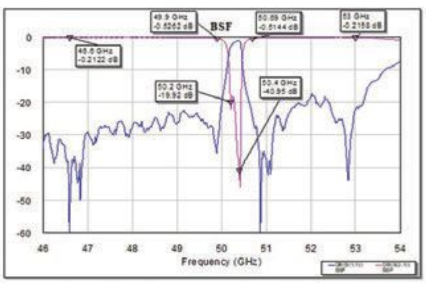

Exceed Microwave's BSF-W-00208 is a WR19 bandstop filter that provides >15 dB rejection across a very narrow bandwidth of 50.2 to 50.4 GHz. The filter passes 46 to 49.9 GHz and 50.69 to 53 GHz. Both sides of the passband have low insertion loss of 0.2 dB typical with 0.6 dB at the band edges and a minimum 15 dB return loss.
Exceed Microwave
www.exceedmicrowave.com

Surface-Mount Failsafe Electromechanical Relay Switches

VENDORVIEW

Fairview Microwave has announced its latest offering: the Quartz Series of surface-mount failsafe electromechanical relay switches. These precision switches come in a pioneering, micro-sized package and offer an extensive frequency bandwidth from DC up to an impressive 26 GHz. The Quartz Series also stands out for its robust power handling, capable of managing up to 40 W average power during hot switching.
Fairview Microwave
www.fairviewmicrowave.com

Directional Coupler

VENDORVIEW

KRYTAR, Inc. announced a new directional coupler operating in the wideband frequency range of 0.5 to 26.5 GHz (L- through K-Bands) offering nominal coupling of 30 dB. The new coupler offers solutions for emerging designs and test and measurement applications, including wireless communications, radar and satellite communications. This new directional coupler, Model 152630, offers superior performance ratings, including nominal coupling (with respect to output) of 30 dB, ±1.8 dB. Frequency sensitivity is ±1.8 dB.
KRYTAR Inc.
www.krytar.com

0.3-50 GHz Ultra-Wideband 2-Way Power Divider/Combiner

VENDORVIEW

MIcable 0.3 to 50 GHz ultra-wideband 2-way power divider/combiner can accept and divide a 0.3 to 50 GHz signal into two output signals with equal amplitude unbalance (±0.5 dB maximum) and phase unbalance (±7 degrees maximum). Due to extremely wide bandwidth, excellent VSWR (1.6:1 maximum), insertion loss (5.8 dB maximum) and isolation (16 dB minimum). It can be widely applied in 5G, test & measurement, instruments and other wideband applications.
MIcable
www.micable.cn

MMIC Attenuators

VENDORVIEW

Mini-Circuits' BAT-series GaAs MMIC attenuators provide fixed attenuation with low loss from DC to 60 GHz. They handle 2 W power while fitting tiny six-lead QFN-style surface-mount packages measuring just 0.059 × 0.059 in. (1.50 × 1.50 mm). Ideal for electronic warfare, radar and satellite communications applications, these passive 50 Ω devices exhibit 20 dB typical input return loss over the full bandwidth. They are available in a wide range of fixed attenuation values, including 0, 5, 15 and 30 dB.
Mini-Circuits
www.minicircuits.com

Reflective Switch

VENDORVIEW

Quantic PMI Model P6T-2G18G-55-R-512-SFF-ROHS is a high speed, single pole, six throw, reflective switch capable of switching within 15 ns. The frequency range is 2 to 18 GHz and has over 55 dB of isolation. This model was designed to produce extremely low transients of 15 mV peak to peak and a video transient spectral content of -65 dBm maximum. Package size is 1.0 × 1.4 × 0.3 in. with SMA female connectors. RoHs compliant and COTS availability.
Quantic PMI
www.quanticpmi.com

Super Wideband, Double-Balanced, Passive Mixer

VENDORVIEW

ED2's ED2-0024 is a super wideband, double-balanced, passive mixer in an advanced 2.5 × 2.5 mm glass SMT BGA package. The ED2-0024 mixer can be used as an up-converter or down-converter for LO and RF frequencies from 20 to 65 GHz and covers IF bandwidths from DC to 20 GHz. The mixer provides excellent LO to RF and LO to IF isolation and is ideal for use in wideband mmWave systems for communications, defense and test and measurement applications.
RFMW/ED2
www.rfmw.com

mmWave Block Converter

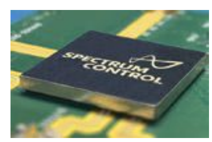

Spectrum Control introduced a new standard product to its RF+ System in Package (SiP) platform. The SCRS-00-1001 RF+ SiP down-converts wideband mmWave signals between 18 to 40 GHz into standard 2 to 18 GHz bands for direct sampling and processing. This first standard SiP expands Spectrum Control's RF+ SiP platform that delivers unrivaled miniaturization of integrated microwave assemblies (IMAs) and was designed, tuned and tested inside the company's new RF+ Digital development pipeline, which reduces the typical IMA productization timeline by 75 percent.
Spectrum Control
www.spectrumcontrol.com

CABLES & CONNECTORS

Micro RF Connector

Hirose has developed a micro RF connector that features a low profile of only 1.2 mm when mated. Offering design flexibility, the space-saving K.FL2 Series connector is available in two versions: an RF cable mating type and an FPC-to-board mating type. Both versions support high density mounting to further save valuable PCB real estate. Compatible with pick-and-place mounting, the K.FL2 Series connector is commonly used in consumer applications, including laptop computers, smartphones, tablets, VR/AR glasses, routers and more.
Hirose
www.hirose.com

NewProducts

Multicoax Cable Assemblies

Withave's high speed and high-density multicoax cable assemblies (WMX Series) provide a wide range of multiple coax connectors and flexible cable assemblies with a choice of 20, 40, 50, 67 and 110 GHz configurations based on precision array design and superior high frequency cabling solutions. The WMX series is an excellent signal integrity solution for benchtop and automated test equipment to meet increasing demands of the semiconductor and optical test industries.

withwave co., ltd
www.with-wave.com

AMPLIFIERS

Rack-Mount Broadband GaN High Power Amplifiers

Cernex's line of GaN rack-mount amplifiers are high power, efficient and can be customized to your project's needs. The model CBP-G30404040R-01 has a large band from 30 to 40 GHz, a high 40 dB gain and an output of 40 dBm. It is packaged in a 4U rack mount with a cooling apparatus included and runs on standard AC power so it will always be ready to strengthen your RF signal whenever needed.

Cernex Inc.
www.cernex.com

Pulse Solid-State Amplifier

Exodus AMP2103P-LC, dual-mode (CW and pulse) amplifier is ideal for automotive pulse/r EMC-testing and commercial applications. Pulse widths to 560 μs, duty cycle to 10 percent, 60 dB gain and outstanding pulse fidelity. Monitoring parameters for forward/reflected power in watts and dBm, VSWR, voltage, current and temperature, with unprecedented reliability and ruggedness in a compact 7U chassis.

Exodus Advanced Communications
www.exoduscomm.com

SOURCES

Ultra-Low Noise Crystal-Controlled Sources and Custom Module

Q-Tech Corporation announced the introduction of the AXTAL GHz Series of high performance/ultra-low noise/high frequency crystal oscillators and modules to the U.S. market. Developed and manufactured by Q-Tech's recently acquired European affiliate, AXTAL, these ultra-low phase noise (close-in and noise floor) crystal-controlled sources offer competitive packaging and performance advantages in a range of applications (military, aviation and space). Benefits include higher resolution and accuracy for radar systems, better quality and more transmittable information in communication systems and higher accuracy and a lower measurement limit in RF measurement systems.

Q-Tech Corporation
www.q-tech.com

ANTENNAS

Slotted Array Antenna

With half-power beam widths of 2 degrees in the H-plane and 16 degrees in the E-plane, model SAW-3533532716-28-L2-WR is a slot array antenna that operates from 34.75 to 35.25 GHz. Nominal gain is 27 dBi and minimum return loss is 13 dB. Dimensions are 11.8 × 3.9 × 0.9 in.

Eravant
www.eravant.com

Low Frequency Waveguide Standard Gain Horns

Pasternack announced the launch of its new low frequency waveguide standard gain horns. They are available in WR-510, WR-650 and WR-770 sizes with 10 and 15 dBi gain options. Their features suit them well for test and measurement applications, allowing users to characterize antennas and wireless systems with precision. Supporting frequencies as low as 320 MHz, the new horns provide an economical option for customers who do not require TAA compliance.

Pasternack
www.pasternack.com

TEST & MEASUREMENT

4-Channel Rubidium Frequency Calibrator/Analyzer

Pendulum Instruments announced the new CNT-104R Multi-channel Rubidium Frequency Calibrator/Analyzer. The CNT-104R expands Pendulum's Multi-channel Frequency Analyzer family and is the third instrument in the series available in the color touchscreen, benchtop form factor. Parallel and independent time and frequency measurements leveraging gap-free technology inherited from the pioneering and award winning four-channel CNT-104S MFA, simplifies the verification of period, time interval error, pulse width, rise/fall time, slew rate, totalize and voltage parameters.

Pendulum Instruments
www.pendulum-instruments.com

Power Sensors

The new R&S NRPxE power sensors from Rohde & Schwarz offer unmatched performance and versatility. They feature an impressive dynamic range of 80 dB, a video bandwidth of 100 kHz and the ability to perform up to 1000 measurements per second. With frequency ranges from 10 MHz to 8 or 18 GHz, the power sensors cater to various measurement needs. Their compact design and ruggedized housing ensure easy handling and reliable operation in demanding environments.

Rohde & Schwarz
www.rohde-schwarz.com

Review by: Reena Dahle

Bookend

EW 103: Tactical Battlefield Communications Electronic Warfare

By: David L. Adamy

The approach David Adamy uses in "EW103 Tactical Battlefield Communications Electronic Warfare" is to simplify the practical aspects of electronic warfare (EW) for the reader. This book, which is part of a series, is a great resource for professionals who are new to the EW field. It starts with a solid introduction to communication signals, receiver and antenna architecture. Other chapters address performance parameters and provide a description of emitter and jammer signals. As a bonus, the book comes with a CD filled with formulas for propagation losses, J-to-S ratio and more. The book also includes a useful slide rule with valuable conversions, including free space attenuation and gain reduction.

ISBN: 9781596933873
Pages: 370
To order this book, contact:
Artech House (2008)
us.artechhouse.com

Advertising**Index**

Sales Representatives

Microwave Journal

Eastern and Central Time Zones
Carl Sheffres
Group Director
(New England, New York, Eastern Canada)
Tel: (781) 619-1949
csheffres@mwjournal.com

Michael Hallman
Associate Publisher
(NJ, Mid-Atlantic, Southeast, Midwest, TX)
Tel: (301) 371-8830
Cell: (781) 363-0338
mhallman@mwjournal.com

Pacific and Mountain Time Zones
Brian Landy
Western Reg. Sales Mgr.
(CA, AZ, OR, WA, ID, NV, UT, NM, CO, WY, MT, ND, SD, NE & Western Canada)
Tel: (831) 426-4143
Cell: (831) 713-9085
blandy@mwjournal.com

International Sales
Carl Sheffres
Tel: (781) 619-1949
csheffres@mwjournal.com

Germany, Austria, and Switzerland (German-speaking)
Victoria and Norbert Hufmann
victoria@hufmann.info
norbert@hufmann.info

France
Gaston Traboulsi
Tel: +44 207 596 8742
gtraboulsi@horizonhouse.com

Korea
Jaeho Chinn
JES MEDIA, INC.
Tel: +82 2 481-3411
corres1@jesmedia.com

China
Shanghai
Linda Li
ACT International
Tel: +86 136 7154 0807
lindal@actintl.com.hk

Wuhan
Phoebe Yin
ACT International
Tel: +86 134 7707 0600
phoebey@actintl.com.hk

Shenzhen
Annie Liu
ACT International
Tel: +135 9024 6961
anniel@actintl.com.hk

Beijing
Cecily Bian
ACT International
Tel: +86 135 5262 1310
cecilyb@actintl.com.hk

Hong Kong
Floyd Chun
ACT International
Tel: +852 28386298
floydc@actintl.com.hk

Taiwan, Singapore
Simon Lee
ACT International
Tel: +852 2838 6298
simonlee@actintl.com.hk

Japan
Katsuhiro Ishii
Ace Media Service Inc.
Tel: +81 3 5691 3335
amskatsu@dream.com

Submitting ad material?
Visit: www.adshuttle.com/mwj
(866) 774-5784
outside the U.S. call
+1-414-566-6940

Ed Kiessling
(781) 619-1963
ekiessling@mwjournal.com

Corporate Headquarters: 685 Canton Street, Norwood, MA 02062 • Tel: (781) 769-9750

FABS and LABS

ATEK MIDAS: ASIC & MMIC Expertise, Creativity and Passion

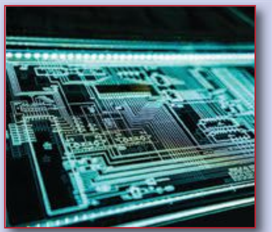

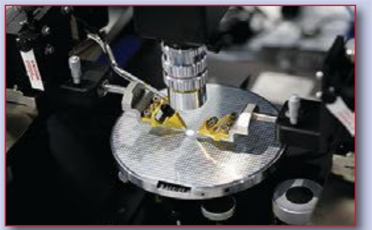

ATEK MIDAS, officially known as ATEK Mikrodalga A.S., was founded in 2017 in Istanbul, Türkiye, by Kagan Kaya, Ercan Altuntas and Altug Oz. The three co-founders brought extensive expertise in high speed mixed-signal, RF and microwave IC engineering with backgrounds at technology companies, most notably Hittite Microwave. Their mission is to partner with their customers to provide focused ASIC design and development services, delivering IP blocks, engineering prototypes and turn-key production solutions complemented by an MMIC standard product line for applications up to 80 GHz.

To realize this mission, the company has adopted a fabless model using leading wafer foundries for a variety of semiconductor technologies. These technologies include SiGe BiCMOS, RF CMOS, SOI CMOS, GaAs pHEMT and HBT and GaN. The ATEK vision is bold; they endeavor to cover all electronic circuits and the elements in between, from the antenna or fiber-optic cable end to the digital circuitry. With access to these processes and this vision, the product and IP portfolio are extensive. ATEK offers standard and custom switches, attenuators, LNAs, PAs, driver amplifiers, mixers, phase shifters, filters, equalizers and passives. Key standard product offerings include novel, compact tunable and fixed MMIC filters as well as switchable filter bank MMICs operating from less than 1 MHz through 40 GHz in QFN packages.

ATEK also offers a broad range of design to production services, collaborating with customers on the product concept, specification development and manufacture of prototypes to full production assuring supply chain resilience. These services encompass IC technology and process selection, schematic-level design and simulations, verified schematic layout, DRC, LVS, parasitic extraction, ESD analysis, 3D EM and post-layout simulations. Specific digital design tools include RTL synthesis and place and route up to 100k gates. Leveraging their portfolio of functional analog, digital, optical, power management, timing and RF/microwave core IP blocks results in novel product solutions as well as addressing customer-specific obsolescence/EOL risks.

ATEK works with several IC packaging companies offering plastic QFN, air cavity QFN and multi-chip module laminate package assemblies. Their 250 m^2 design and test facility has measurement capability through 44 GHz, including environmental testing from -55°C to +125°C. They can characterize SMT packaged products as well as probe wafer/die products.

With this portfolio of standard and custom ASIC and MMIC products and the range of services, it is not surprising that ATEK will work with customers on design and productization services for custom RF and microwave modules. They use these custom IC design capabilities and COTS parts to provide performance-driven SWAP-C-optimized modules in the DC to 50 GHz frequency range. Along with the technology and building block functions described earlier, ATEK has produced a wide range of custom transceivers, converters and synthesizers, along with modules for frequency agile and frequency hopping systems in a variety of satellite communication, telecommunication, test and measurement, aerospace and defense applications.

ATEK uses seasoned technical manufacturing representatives worldwide to promote its products and services to a wide customer base. Recently, it partnered with ViNo Waves LLC to manage its North American sales channel. ViNo Wave's primary mission is to provide sales, marketing and technical support management to ATEK MIDAS's network of manufacturer's representatives and distributors.

From its beginnings less than a decade ago, ATEK is leveraging its expertise, creativity and passion to fulfill its mission of creating a company capable of designing and manufacturing a full range of advanced analog and mixed-signal ASICs, RFICs and MMICs for a diverse range of industries.

atekmidas.com

REVIEW BOARD MWJ APPROVED

Compact IPD Bandpass Filter Design

Qi Zhang, Yazi Cao, Mingzhao Xu and Gaofeng Wang
Hangzhou Dianzi University, Hangzhou, China

A compact high out-of-band rejection bandpass filter (BPF) is fabricated using Si-based integrated passive devices (IPD) technology. It is designed with a modified topology for 5G applications. It contains two cascading modified π-sections and can generate four transmission zeros (TZs) near the passband, which greatly improves frequency selectivity. It is just 1.3 × 0.8 × 0.3 mm in size and achieves an insertion loss of less than 1.2 dB with a return loss of better than 18 dB in the passband and an upper stopband suppression level greater than 20 dB up to 16 GHz.

With advancements in wireless communication systems, BPFs have attracted a great deal of attention. BPFs with low insertion loss and high out-of-band rejection have received much research focus.[1-5] In general, these filters are mainly made using three fabrication processes: IPD,[4-6] low-temperature co-fired ceramic (LTCC)[1,2,7] and substrate-integrated waveguide (SIW).[3,8,9]

To improve out-of-band rejection, controllable TZs[1,8] and different coupling mechanisms[2,7,9] have been introduced in LTCC and SIW filters. However, these filters are usually large, which is not suitable for 5G miniaturized communication systems applications. For IPD filters,[4-6] the chip size can be greatly reduced in comparison. Lyu et al.[10] reported on a BPF with a center frequency of 3 GHz, an insertion loss of 1.2 dB and an upper stopband attenuation of more than 44 dB up to 30 GHz (> $10f_0$). Its size, however, is 2.16 × 0.90 mm, which is still too large for the chip miniaturization. Sitaraman et al.,[11] designed a BPF with a layout area of less than 1 mm^2; however, with only two TZs in the upper stopband, it is not suitable for high-selectivity applications.

In this article, a novel compact high out-of-band rejection 5G BPF is introduced. It uses Si IPD technology and a topology consisting of two modified π-sections. This topology generates four TZs near the passband, achieving very high out-of-band rejection. It measures 1.3 × 0.8 × 0.3 mm with upper stopband suppression greater than 20 dB up to 16 GHz.

BPF DESIGN AND ANALYSIS

The two modified π-sections are analyzed first. The first section consists of a TZ resonator in the main branch with a TZ resonator and a grounded capacitor in the shunt branches. This topology is shown in ***Figure 1a***. Its simulated transmission coefficient, shown in ***Figure 1b***, shows two TZs near the passband and a TZ at DC. The TZ in the upper band is generated by the TZ resonator in the main branch, while the TZ in the lower band is generated by the TZ resonator in the shunt branch.

Its ABCD matrix is given by ***Equation 1***:

$$\begin{pmatrix} A & B \\ C & D \end{pmatrix} = \begin{pmatrix} 1 & 0 \\ Y_1 & 1 \end{pmatrix} \begin{pmatrix} 1 & Z_1 \\ 0 & 1 \end{pmatrix} \begin{pmatrix} 1 & 0 \\ Y_2 & 1 \end{pmatrix} = \begin{pmatrix} 1 + Z_1 Y_2 & Z_1 \\ Y_1 + Y_1 Y_2 Z_1 + Y_2 & Y_1 Z_1 + 1 \end{pmatrix} \tag{1}$$

Where the Y_1, Z_1 and Y_2 variables are given by ***Equations 2-4***:

$$Y_1 = \frac{-\omega^2 C_4 L_3 + 1}{j\omega L_3} \tag{2}$$

$$Z_1 = \frac{1 - \omega^2 L_1 C_2}{j\omega(-\omega^2 L_1 C_1 C_2 + C_1 + C_2)} \tag{3}$$

$$Y_2 = j\omega C_5 \tag{4}$$

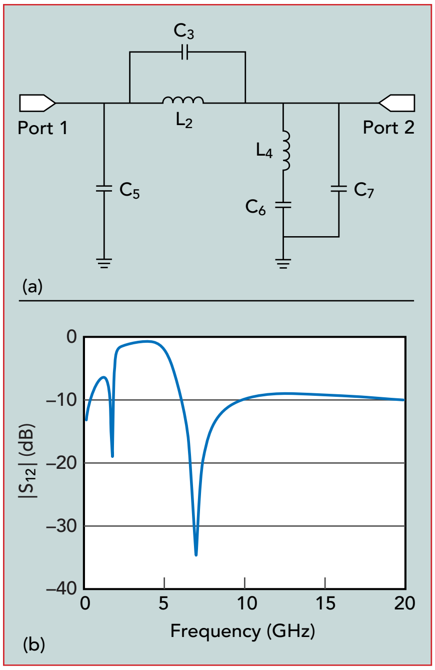

▲ **Fig. 1 First modified p-section: topology (a) and simulated $|S_{12}|$ (b).**

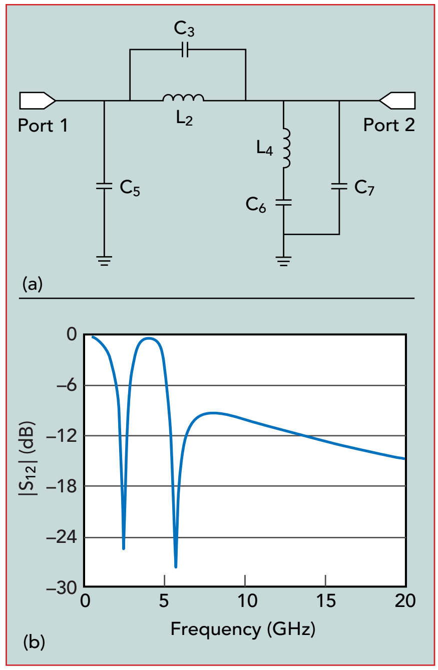

▲ **Fig. 2 Second modified p-section: topology (a) and simulated $|S_{12}|$ (b).**

Where ω is the transmission frequency of the filter. S-parameters can be derived from the ABCD matrix in ***Equation 5***:

$$S_{12} = \frac{2(AD - BC)}{A + \frac{B}{Z_0} + CZ_0 + D} \tag{5}$$

When $S_{12} = 0$, the values of ω can be determined by ***Equations 6-8***:

$$\omega_1 = 0 \tag{6}$$

$$\omega_2 = \sqrt{\frac{C_1 + C_2}{L_1 C_1 C_2}} \tag{7}$$

$$\omega_3 = \sqrt{\frac{C_1 + C_3}{L_1 L_3 C_1 C_2}} \tag{8}$$

It is assumed that C_1 = 1.22 pF, C_2 = 4.0 pF, C_4 = 3.31 pF, C_5 = 0.34 pF, L_1 = 0.51 nH and L_3 = 1.72 nH in the first modified π-section. The three TZs are at DC, 2.10 GHz and 7.28 GHz, respectively.

The second modified π-section consists of a TZ resonator in the main branch with a TZ resonator and a capacitor in the shunt branches, as shown in ***Figure 2a***. Its simulated transmission coefficient, shown in ***Figure 2b***, has two TZs generated near the passband. The second modified π-section achieves a bandpass performance. The TZ in the upper band is generated by the TZ resonator in the main branch, while the TZ in the lower band is generated by the TZ resonator in the shunt branch.

The ABCD matrix of its two-port network can be obtained from ***Equation 9*** to analyze the second modified π-section as follows:

$$\begin{pmatrix} A & B \\ C & D \end{pmatrix} = \begin{pmatrix} 1 & 0 \\ Y_3 & 1 \end{pmatrix} \begin{pmatrix} 1 & Z_2 \\ 0 & 1 \end{pmatrix} \begin{pmatrix} 1 & 0 \\ Y_4 & 1 \end{pmatrix} = \begin{pmatrix} 1 + Z_2 Y_4 & Z_2 \\ Y_3 + Y_3 Y_4 Z_2 & Y_3 Z_2 \end{pmatrix} \tag{9}$$

Where the Y_3, Z_2 and Y_4 variables are defined in ***Equations 10 – 12***:

$$Y_3 = j\omega C_5 \tag{10}$$

$$Z_2 = \frac{jwL_2}{1 - \omega^2 C_3 L_2} \tag{11}$$

$$Y4 = \frac{j\omega(C_7 - \omega^2 C_6 C_7 L_4)}{1 - \omega^2 C_7 L_4 - \omega^2 C_6 L_4} \tag{12}$$

Where ω is the transmission frequency of the filter. When $S_{12} = 0$, the values of ω are defined in ***Equation 13*** and ***Equation 14***:

$$\omega_1 = \sqrt{\frac{1}{L_2 C_3}} \tag{13}$$

$$\omega_2 = \sqrt{\frac{1}{L_4(C_6 + C_7)}} \tag{14}$$

It is assumed that C_5 = 0.01 pF, C_6 = 0.69 pF, C_7 = 0.53 pF, L_2 = 3.15 nH and L_4 = 1.14 nH in the second modified π-section. The two TZs are at 2.44 and 5.66 GHz, respectively.

The BPF topology with high out-of-band rejection shown in ***Figure 3a*** comprises the two modified π-sections. By cascading them, four TZs are generated near the passband, as shown in ***Figure 3b***. It achieves an insertion loss of less than 1.2 dB and an upper stopband suppression level greater than 20 dB up to 16 GHz.

FABRICATION AND MEASUREMENT

The BPF is fabricated using Si-based IPD technology. The Si substrate has a thickness of 250 microns, a relative dielectric constant, ε_r, of 11.69 and a loss tangent, tanδ, of 0.003. It includes three copper metal layers (M1, M2 and M3) with thicknesses of 2, 6 and 8 microns, respectively. In this design, the inductors are in the M3 layer. The metal-insulator-metal capacitors are in the M1 and M2 layers, separated

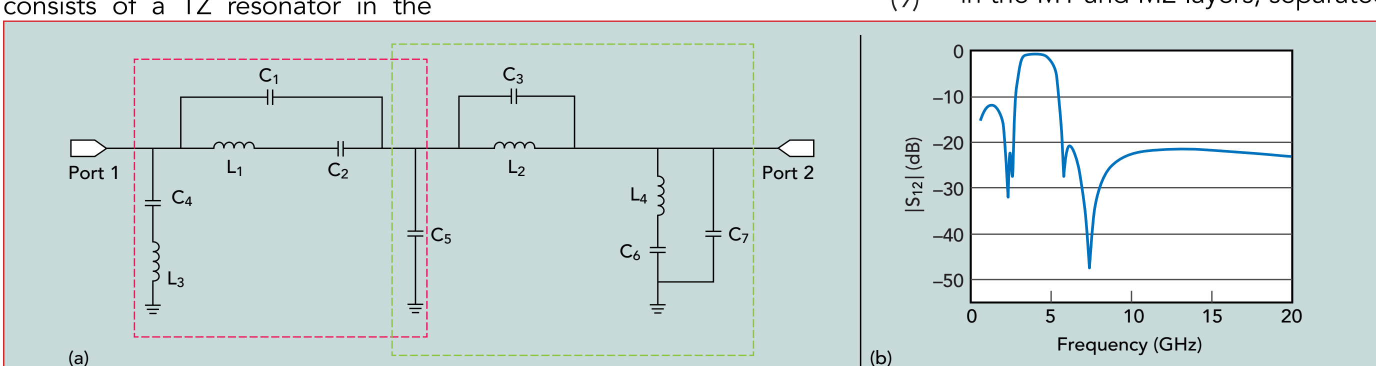

▲ **Fig. 3 BPF topology (a) and simulated $|S_{12}|$ (b).**

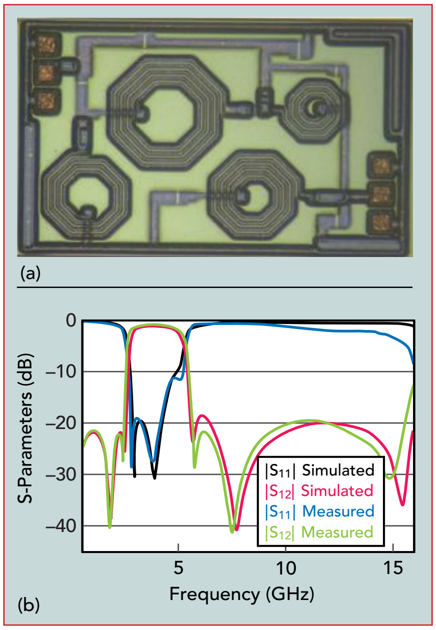

Fig. 4 BPF micrograph (a) and simulated and measured S-parameters (b).

by a dielectric layer with ε_r = 7.46 and tanδ = 0.002.

The BPF is simulated and its graphic design system layout is generated with the EM simulator UltraEM from Faraday Dynamics. A micrograph of the filter is shown in ***Figure 4a*** with a chip size of 1.3 × 0.8 × 0.3 mm. It is measured on-chip using a Keysight N5244A PNA-X vector network analyzer and Cascade summit-11000 probe station.

Simulated and measured S-parameters are shown in ***Figure 4b***. Compared with the circuit simulated results, both the EM simulation and measurement show an extra TZ in the upper stopband, which is caused by parasitic effects that are neglected in the circuit simulation. The measured BPF achieves an insertion loss of less than 1.2 dB and a return loss greater than 18 dB across the operating band. The upper stopband suppression level is greater than 20 dB up to 16 GHz. Measurements are in close agreement with the simulation.

This performance is compared in ***Table 1*** with several previously reported BPFs based on different technologies. For LTCC and SIW technologies,[1-3] the BPFs all occupy larger areas and have narrower stopbands. The GaAs IPD BPF[4] has a higher insertion loss. This design offers a good balance between high performance and chip size, which is attractive for 5G communication systems.

TABLE 1

COMPARISON WITH OTHER WORK

Reference	f_0 (GHz)	Insertion Loss (dB)	Size (mm²)	Number of TZs	Upper Stopband (dB)	Process
1	3.5	1.35	6.1 x 6.8	5	20/2.2 f_0	LTCC
2	3.1	1.9	8.55 x 6.7	4	20/3.1 f_0	LTCC
3	6.08	0.56	5.7 x 3.4	4	20/3.4 f_0	SIW
4	3	1.77	1.63 x 0.62	3	20/34.6 f_0	GaAs IPD
This work	3.75	1.2	1.3 x 0.8	4	20/4.3 f_0	Si-based IPD

CONCLUSION

A compact Si-based IPD high out-of-band rejection BPF uses two modified π-section BPF topologies. By cascading the two sections, four TZs are generated near the passband, improving frequency selectivity and out-of-band rejection. Simulated and measured results are in good agreement. With high out-of-band performance, it is a good candidate for 5G communication systems applications. ■

ACKNOWLEDGMENTS

This work was supported by the National Natural Science Foundation of China under Grants 92373202 and 62141409, the National Key Research and Development Program of China under Grant 2019YFB2205003 and the Zhejiang Provincial Key Research & Development Project under Grant 2021C01041.

References

1 W. Zhao, Y. Wu, Y. Yang and W. Wang, "LTCC Bandpass Filter Chips with Controllable TZs and Bandwidths Using Stepped-Impedance Stubs," *IEEE Transactions on Circuits and Systems II: Express Briefs*, Vol. 69, No. 4, April 2022, pp. 2071–2075.

2. W. Feng, X. Gao, W. Che, W. Yang and Q. Xue, "LTCC Wideband Bandpass Filters with High Performance Using Coupled Lines with Open/Shorted Stubs," *IEEE Transactions on Components, Packaging and Manufacturing Technology*, Vol. 7, No. 4, April 2017, pp. 602–609.

3. H. Tian and Y. Dong, "Wideband Low-Loss Filter with Compact Size and Wide Stopband Based on Folded Planar Waveguide," *IEEE Microwave and Wireless Technology Letters*, Vol. 33, No. 6, February 2023, pp. 651–654.

4. Y. Jiang, L. Feng, H. Zhu, W. Feng, H. Chen, Y. Shi, W. Che and Q. Xue, "Bandpass Filter with Ultra-Wide Upper Stopband on GaAs IPD Technology," *IEEE Transactions on Circuits and Systems II: Express Briefs*, Vol. 69, No. 2, February 2022, pp. 389–393.

5. W. Chen, Y. Wu, Y. Yang and W. Wang, "IPD-Based Miniaturized Wideband Bandpass Filter with Frequency-Dependent Complex Source and Load," *IEEE Transactions on Plasma Science*, Vol. 49, No. 3, March 2021, pp. 1115–1120.

6. D. -M. Kim, B. -W. Min and J. -M. Yook, "Compact mmWave Bandpass Filters Using Silicon Integrated Passive Device Technology," *IEEE Microwave and Wireless Components Letters*, Vol. 29, No. 10, October 2019, pp. 638–640.

7. X. Y. Zhang, X. Dai, H. -L. Kao, B. -H. Wei, Z. Y. Cai and Q. Xue, "Compact LTCC Bandpass Filter With Wide Stopband Using Discriminating Coupling," *IEEE Transactions on Components, Packaging and Manufacturing Technology*, Vol. 4, No. 4, April 2014, pp. 656–663.

8. G. Lin and Y. Dong, "A Compact, Hybrid SIW Filter with Controllable TZs and High Selectivity," *IEEE Transactions on Circuits and Systems II: Express Briefs*, Vol. 69, No. 4, April 2022, pp. 2051-2055.

9. Y. Zheng and Y. Dong, "Miniaturized Hybrid Filter Using Stripline and LC-Loaded SIW Resonators," *IEEE Transactions on Circuits and Systems II: Express Briefs*, Vol. 69, No. 9, September 2022, pp. 3719–3723, 2022.

10 Y. -P. Lyu, Y. -J. Zhou, L. Zhu and C. -H. Cheng, "Compact and High-Order On-Chip Wideband Bandpass Filters on Multimode Resonator in Integrated Passive Device Technology," *IEEE Electron Device Letters*, Vol. 43, No. 2, February 2022, pp.196–199.

11. S. Sitaraman, V. Sukumaran, M. R. Pulugurtha, Z. Wu, Y. Suzuki, Y. Kim, V. Sundaram, J. Kim and R. R. Tummala, "Miniaturized Bandpass Filters as Ultrathin 3-D IPDs and Embedded Thinfilms in 3-D Glass Modules," *IEEE Transactions on Components, Packaging and Manufacturing Technology*, Vol. 7, No. 9, September 2017, pp. 1410–1418.

eXclusive Digital Content >>>

Net Power Measurement Method Considering Mismatch Correction

Haoyu Lin and Pan Huang
National Institute of Metrology, Beijing, China

This article describes a net power measurement methodology based on a three-port directional coupler that demonstrates high relative and absolute accuracy while being unaffected by the mismatch. The measurement method and the evaluation of uncertainty are both simple and convenient. It is demonstrated to be useful for E-field probe calibration, which makes the method applicable to radio metrology.

Net power measurement is common in the field of RF metrology.[1-3] Xie et al.[4] described a method that calculates the net power delivered into a transverse electromagnetic (TEM) cell using a dual-directional coupler. The port orientation of this dual-directional coupler is shown in ***Figure 1*** for an E-field probe calibration application.

Two power sensors are used to measure forward and reverse power and the net power is calculated using ***Equation 1***:

$$P_{net} = C_3 P_3 - C_4 P_4 \quad (1)$$

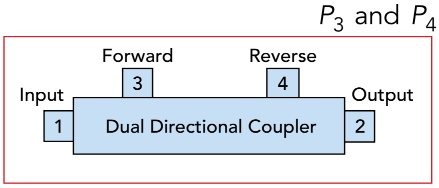

Fig. 1 Dual-directional coupler block diagram.

P_3 and P_4 are the readings of the power sensors for the two arms. C_3 and C_4 are the forward and reverse coupling coefficients of the coupler. The C_3 coefficient is calculated in ***Equation 2*** and the C_4 coefficient in ***Equation 3***:

$$C_3 = \left| \frac{S_{21}}{S_{31}} \right|^2 \quad (2)$$

$$C_4 = \left| \frac{1}{S_{42}} \right|^2 \quad (3)$$

Although Equation 1 is straightforward and commonly used, it is only an approximation. Due to the inevitable impact of impedance mismatch, if a precision measurement is required, the mismatch correction should be performed. Kanda and Orr[5] derived the exact net power (P_{exact}) as shown in ***Equation 4***:

$$P_{exact} = P_3 |g|^2 - P_4 |\Gamma_2|^2 |h|^2 \quad (4)$$

Where the parameters are defined in ***Equations 5*** to ***12***:

$$g = \frac{F_1 B_1 + A_1 E_1}{D_1 A_1 - F_1 C_1} \quad (5)$$

$$h = \frac{B_1 F_1 + A_1 E_1}{B_1 D_1 - E_1 C_1} \quad (6)$$

$$A_1 = S_{31}(1 - S_{44}\Gamma_4) + S_{34} S_{41} \Gamma_4 \quad (7)$$

$$B_1 = S_{41}(1 - S_{33}\Gamma_3) + S_{34} S_{31} \Gamma_3 \quad (8)$$

$$C_1 = (S_{31} S_{42} - S_{32} S_{41}) \Gamma_2 \quad (9)$$

$$D_1 = S_{31}(1 - S_{22}\Gamma_2) + S_{32} S_{12} \Gamma_2 \quad (10)$$

$$E_1 = S_{12}(1 - S_{33}\Gamma_3) + S_{31} S_{32} \Gamma_3 \quad (11)$$

$$F_1 = (S_{31} S_{42} - S_{34} S_{12}) \Gamma_4 \quad (12)$$

Γ_2, Γ_3 and Γ_4 are the reflection coefficients (RCs) of the load and power sensors

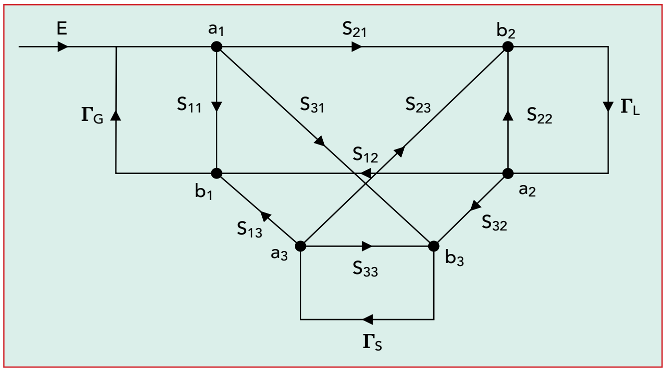

Fig. 2 Three-port directional coupler signal flow graph.

connected to Ports 2, 3 and 4, respectively, while the S-parameters are those of the directional coupler. Because these calculations are more complicated than the approximation using Equations 1 through 3, they add difficulty to the determination of net power.

Song and Meng[6] compared two methods for measuring net power. One is based on a dual-directional coupler and scalar coupling coefficients, VSWR and directivity. The other is a transfer method, which can be traced back to a power standard system. The principles for the selection of the two methods are also discussed in the article.

To guarantee measurement accuracy, all methods based on a dual-directional coupler require the coupler to be ideal or quasi-ideal with high directivity. Otherwise, according to the IEEE 1309-2013 standard,[7] when a transmitting antenna having a VSWR of 1.5:1 is connected to Port 2 and the coupler has a directivity of 25 dB, the uncertainty in the net power due to finite directivity is +0.19/-0.22 dB. This is considerable and may become the main component of uncertainty in the net power measurement.

However, a three-port directional coupler can be used for net power measurement with mismatch correction performed. In this article, a net power measurement that provides high accuracy is described. This method is based on a three-port directional coupler with the effects of mismatch removed. Measurements validate the technique and the final uncertainty is evaluated.

METHOD

The signal flow graph for a three-port directional coupler with a power sensor on its coupled arm and a load connected to its output is shown in **Figure 2**. E is the RMS amplitude of the signal generator (SG) output. Γ_G, Γ_S and Γ_L represent the RCs of the SG, the power sensor and the load, respectively. S-parameters are those of the directional coupler. ***Equation 13*** and ***Equation 14***[8] are derived from Figure 2 using microwave network theory.

$$b_2 = b_3\left[\frac{S_{21}}{S_{31}} + \Gamma_S\left(S_{23} - \frac{S_{21}S_{33}}{S_{31}}\right)\right] + a_2\left(S_{22} - \frac{S_{21}S_{32}}{S_{31}}\right) \quad (13)$$

$$a_2 = b_2\Gamma_L \quad (14)$$

Eliminating a_2 yields ***Equation 15***:

$$b_2 = b_3\left[\frac{S_{21}}{S_{31}} + \Gamma_S\left(S_{23} - \frac{S_{21}S_{33}}{S_{31}}\right)\right]\frac{1}{1 - \Gamma_L\left(S_{22} - \frac{S_{21}S_{32}}{S_{31}}\right)} \quad (15)$$

The net power received by the load is P_{net}, and its expression is given by ***Equation 16***:

$$P_{net} = \frac{|b_2|^2}{Z_0} - \frac{|a_2|^2}{Z_0} \quad (16)$$

In this expression, Z_0 is the characteristic impedance of the transmission line. Inserting Equations 14 and 15 into Equation 16 yields ***Equation 17***:

$$P_{net} = \frac{|b_3|^2}{Z_0}\left|\frac{S_{21}}{S_{31}} + \Gamma_S\left(S_{23} - \frac{S_{21}S_{33}}{S_{31}}\right)\right|^2 \frac{1 - |\Gamma_L|^2}{\left|1 - \Gamma_L\left(S_{22} - \frac{S_{21}S_{32}}{S_{31}}\right)\right|^2} \quad (17)$$

The power received by the power sensor is P_s, as expressed in ***Equation 18***, with a_3 defined in ***Equation 19***:

$$P_s = \frac{|b_3|^2}{Z_0} - \frac{|a_3|^2}{Z_0} \quad (18)$$

$$a_3 = b_3\Gamma_s \quad (19)$$

Inserting Equations 18 and 19 into Equation 17 and eliminating a_3 and b_3 yields ***Equation 20***, which is the final expression of the net power received by the load, considering the mismatch correction.

$$P_{net} = \frac{P_s}{1 - |\Gamma_s|^2}\left|\frac{S_{21}}{S_{31}} + \Gamma_s\left(S_{23} - \frac{S_{21}S_{33}}{S_{31}}\right)\right|^2 \frac{1 - |\Gamma_L|^2}{\left|1 - \Gamma_L\left(S_{22} - \frac{S_{21}S_{32}}{S_{31}}\right)\right|^2} \quad (20)$$

The right side of Equation 20 can be divided into three parts. The first part is $\frac{P_s}{1 - |\Gamma_s|^2}$, which is the correction to the forward coupled power output at Port 3, considering the mismatch of the power sensor. If the mismatch is not considered, $\Gamma_s = 0$ and this part becomes P_s.

The second part is $\left|\frac{S_{21}}{S_{31}} + \Gamma_S\left(S_{23} - \frac{S_{21}S_{33}}{S_{31}}\right)\right|^2$. This is the correction to the ratio of the insertion loss to the coupling coefficient of the coupler. If the mismatch of the power sensor is not considered, $\Gamma_s = 0$ and this part becomes $\left|\frac{S_{21}}{S_{31}}\right|^2$.

The third part is the correction to reflection occurring at the interface of the coupler and the load. If the mismatch of the load is not considered, $\Gamma_L = 0$ and this part equals 1. If all mismatches are not considered, the net power expression becomes ***Equation 21***, which is a commonly used approximate expression of the net power measured using a three-port directional coupler.

$$P_{net} = P_s\left|\frac{S_{21}}{S_{31}}\right|^2 \quad (21)$$

All effects on the net power calculation caused by mismatches are considered in the net power expression of Equation 20. It is a comprehensive and exact expression for the net power measurement of a three-port directional coupler.

MEASUREMENTS

Two experiments are presented. The purpose of Experiment (A) is to validate this proposed method by comparing net power measurement results using different methods with the reference net power. Experiment (B) applies the proposed method for E-field probe calibration

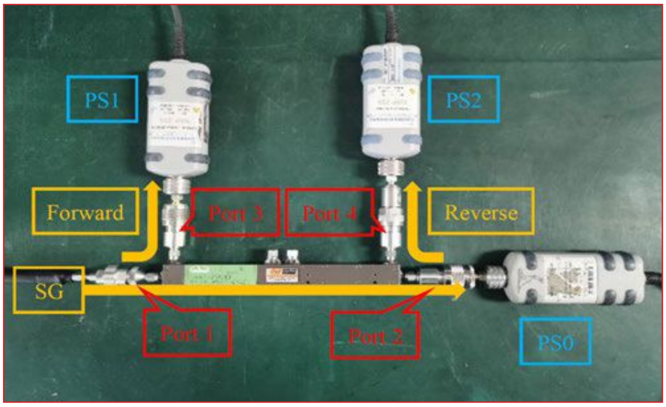

Fig. 3 **Experiment (A) configuration.**

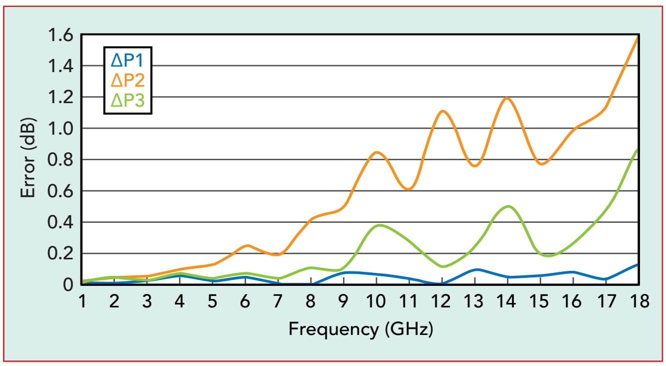

Fig. 4 **Measurement errors of net power calculated using different methods.**

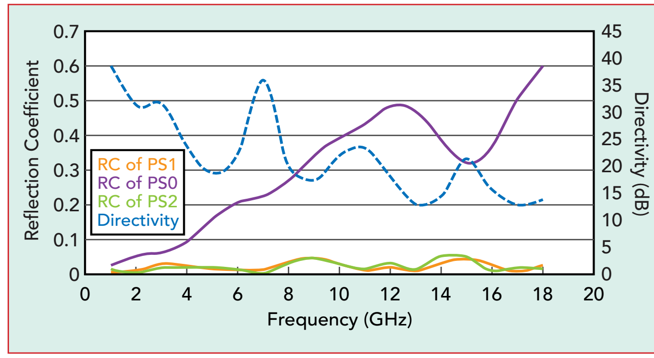

Fig. 5 **Power sensor RCs and coupler directivity.**

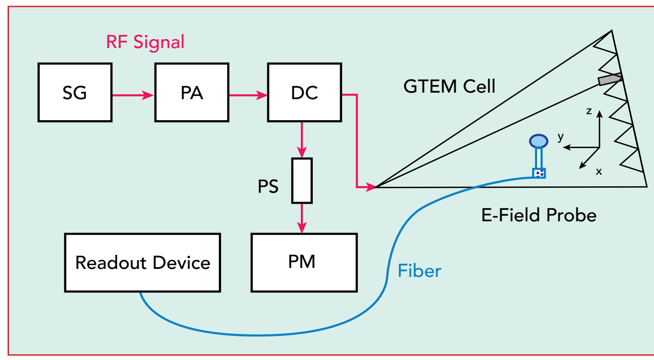

Fig. 6 **Experiment (B) block diagram.**

and compares the calibration results with different net power measurement methods.

Experiment (A): Net Power Measurement Based on a Dual-Directional Coupler

A dual-directional coupler with a nominal coupling coefficient of 20 dB is used, as shown in ***Figure 3***. Port 1 is connected to the SG, which can provide a maximum of 30 dBm output with the high-power option. A power sensor (PS0) is connected to Port 2 as a load to directly obtain the net power (P_{net0}) absorbed by the load. This is treated as the reference net power. Ports 3 and Port 4 are connected to two other power sensors, PS1 and PS2, to measure forward and reverse power, respectively.

To validate the proposed method, net power is calculated using Equations 20, 21 and 1, respectively. For Equations 20 and 21, the coupler is treated as a three-port directional coupler, which means that PS2 is used only as a load connected to Port 4 and its reading is not used. In this condition, the reading of PS1 is the P_S appearing in Equations 20 and 21 and the reading of PS0 is the reference net power (P_{net0}). ΔP_1, ΔP_2 and ΔP_3 are the measurement errors of the net powers calculated using Equations 20, 21 and 1. The calculations for these measurement errors are shown in ***Equations 22*** to ***24***.

$$\Delta P_1 = \left| P_{net(20)} - P_{net0} \right| \tag{22}$$

$$\Delta P_2 = \left| P_{net(21)} - P_{net0} \right| \tag{23}$$

$$\Delta P_1 = \left| P_{net(1)} - P_{net0} \right| \tag{24}$$

Where $P_{net(20)}$, $P_{net(21)}$ and $P_{net(1)}$ are net powers calculated using Equations 20, 21 and 1, respectively.

The frequency range is from 1 to 18 GHz with 1 GHz frequency steps and all the power sensors are calibrated against a traceable standard. All the RCs and S-parameters are individually measured using a vector network analyzer. P_{net0} is kept at a constant value of 19 dBm by manually adjusting the SG output power at each frequency with a resolution of 0.01 dBm. In this way, the effect on ΔP_1, ΔP_2 and ΔP_3 caused by drift and stability of P_{net0} is less than 0.01 dBm. The results are shown in ***Figure 4***.

The following conclusions are drawn, validating the proposed net power measurement method:

Relative Accuracy: ΔP_1 is smaller than ΔP_2 and ΔP_3 at all the frequency points and the maximum differences appear at 18 GHz, where ΔP_1 is 1.46 dB and 0.73 dB smaller than ΔP_2 and ΔP_3, respectively. Therefore, the method to calculate net power based on Equation 20 is more accurate than the methods based on Equations 1 and 21.

Absolute Accuracy: The maximum value of ΔP_1 is 0.13 dB at 18 GHz, where the RC of the load is extremely large, having a value of 0.60, as shown in ***Figure 5***. At other frequency points, ΔP_1 is always smaller than 0.1 dB. Therefore, the absolute accuracy of the proposed method is high enough for the measurements of net power using couplers.

Effect of Mismatch: Because the mismatch is not considered in Equations 1 and 21, the net power calculated using the two equations is affected by the mismatch. From Figure 4, ΔP_2 and ΔP_3 tend to increase in a sinusoidal fashion with frequency, which is in accordance with the variation of the RC of PS0, in general.

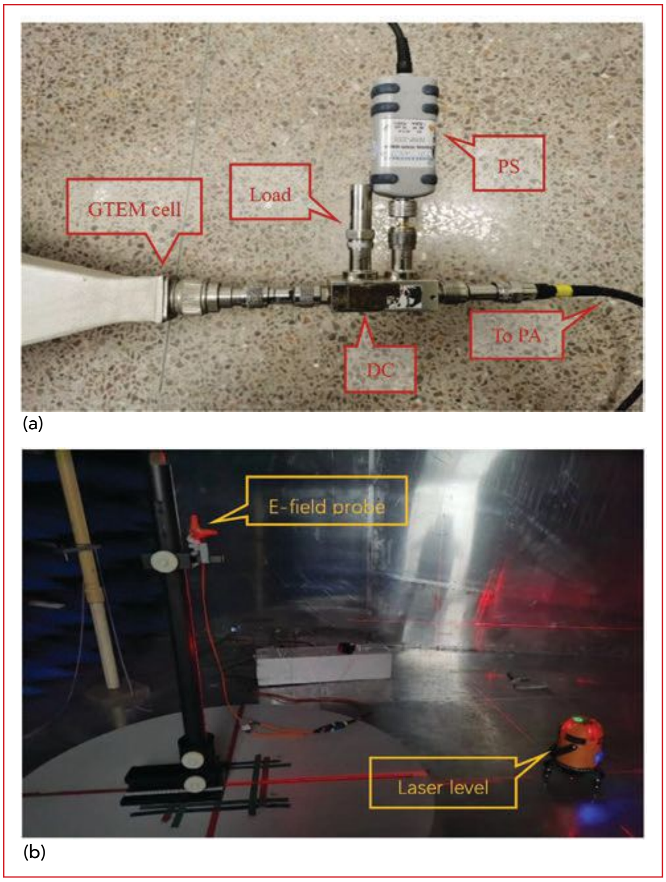

Fig. 7 Input port of the GTEM cell (a) and arrangement in the GTEM cell (b).

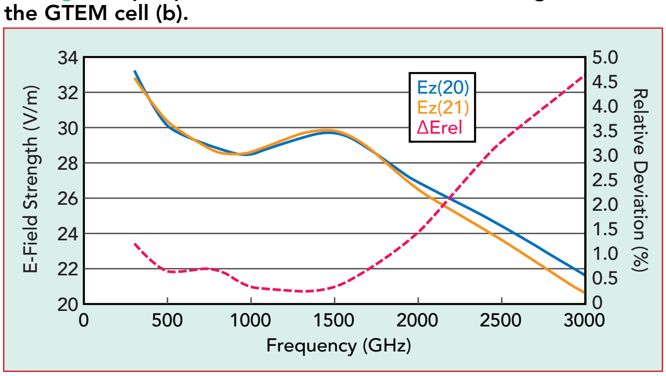

Fig. 8 Measured E-field strength and the relative deviation.

However, ΔP_1 does not exhibit this tendency; its variation is flatter than that of ΔP_2 and ΔP_3. Therefore, the effect of mismatch is removed using the proposed method.

Experiment (B): Net Power Calculation and E-Field Probe Calibration

The TEM cell, Gigahertz TEM (GTEM) cell and standard gain horn antenna are the E-field generators commonly used in E-field probe calibration. The E-field strength generated is associated with the net power fed into them; one net power corresponds to one standard E-field strength. A schematic diagram of this experiment is shown in ***Figure 6***. The system comprises an SG, power amplifier (PA), directional coupler, PS, power meter, E-field probe and a readout device. The RF signal emitted by the SG is amplified by the PA and fed into the GTEM cell through the directional coupler. The electric field occupies the test volume of the GTEM cell.

In this setup, a dual-directional coupler is used as a three-port directional coupler with the reverse coupling port connected to a matched load, as shown in ***Figure 7a***. The three-dimensional E-field probe is placed at the test point and the three sensors are aligned with the three components of the E-field, respectively, using a laser level. This setup is shown in ***Figure 7b***. However, only the reading of the z-axis of the E-field probe is used because it is parallel with the primary component of the E-field. The power meter, together with the PS, records the forward power fed into the GTEM cell.

The SG output power is first adjusted to a proper level and the readings of the PS and the E-field strength in the z-axis, $E_{z(20)}$, at each frequency point are recorded. The net power (P_{net}) is then calculated using the recorded reading of the PS based on Equation 20. Finally, the SG output power is adjusted again to make the net power calculated using Equation 21 equal to P_{net} at each frequency point and the E-field strength of the z-axis, $E_{z(21)}$, is recorded. ΔE_{rel} is the deviation of $E_{(21)}$ relative to $E_{(20)}$. This is shown in ***Equation 25***:

$$\Delta E_{rel} = \frac{E_{Z(21)} - E_{Z(20)}}{E_{Z(20)}} \quad (25)$$

The frequency range is from 300 MHz to 3 GHz. ***Figure 8*** shows that although the net power fed into the GTEM cell, calculated using Equations 20 and 21 individually, is the same, the generated E-field strengths are different and the maximum relative deviation is 4.63 percent at 3 GHz. This means that if the net power is calculated using Equation 21, the error in the standard E-field strength caused by the net power calculation error can reach 4.63 percent, which is considerable compared with a normal expanded uncertainty of 10 percent of the E-field probe calibration. Using the proposed method to calculate net power is, therefore, meaningful for E-field probe calibration, which can reduce the error in the generated standard E-field strength.

UNCERTAINTY

Net power measurement uncertainty is an important component in RF metrology, so it should be taken into consideration and appropriately evaluated. In Equation 20, there are many parameters and most of them are complex numbers. Therefore, using the method described by GUM[9] to evaluate the uncertainty makes the process very complicated and time-consuming.

To facilitate the uncertainty evaluation process, a Monte Carlo method is used based on the NIST Uncertainty Machine.[10] The input and out quantities are modeled as random variables with the mean and standard deviation equal to the corresponding estimate and standard uncertainty. Their probability distributions are used to characterize measurement uncertainty.[11]

The absolute and relative standard measurement uncertainty (u and u_{rel}) of P_{net} calculated using Equation 20 in Experiment (A) is evaluated. The values and standard

TABLE 1

UNCERTAINTY EVALUATION AT ALL FREQUENCY POINTS

Frequency (GHz)	Mean (W)	Std (W)	u_{rel} (%)
1	0.0799	0.0010	1.20
2	0.0802	0.0010	1.20
3	0.0800	0.0010	1.20
4	0.0806	0.0010	1.20
5	0.0798	0.0010	1.22
6	0.0803	0.0010	1.22
7	0.0796	0.0010	1.23
8	0.0790	0.0010	1.25
9	0.0824	0.0011	1.30
10	0.0771	0.0011	1.36
11	0.0818	0.0011	1.36
12	0.0797	0.0011	1.37
13	0.0843	0.0012	1.38
14	0.0806	0.0011	1.32
15	0.0806	0.0010	1.27
16	0.0823	0.0010	1.34
17	0.0770	0.0013	1.85
18	0.0772	0.0016	2.25

uncertainties of all the S-parameters are from the calibration certificates. The readings of PS1 are from the experiment and the uncertainty is from the calibration certificate.

The uncertainty evaluation results at all the frequency points are shown in ***Table 1***. Where the mean uncertainty is the common estimate of the actual value of P_{net} and the standard deviation is the common evaluation of u. The minimum value of u_{rel} is 1.20 percent at 1 GHz and the maximum value is 2.25 percent at 18 GHz. Comparing Figure 5 and Table 1, u_{rel} is strongly related to the RC of PS0 and when the RC is lower than 0.3 (VSWR lower than 1.86), u_{rel} is less than 1.3 percent. Therefore, for most of the loads commonly used in RF metrology, the uncertainty is small enough.

CONCLUSION

A net power measurement method based on a three-port directional coupler has been proposed. The associated experiments and uncertainty evaluation have been performed to validate this method. The results show that the relative and absolute accuracy of the method are both high and not affected by the mismatch.

It is also proven that this method is meaningful for E-field probe calibration, which can reduce the error in the standard E-field strength. Besides having high accuracy, the net power calculation and the uncertainty evaluation are both simple and convenient. Therefore, the proposed method has application in the field of radio metrology represented by E-field probe calibration. ■

ACKNOWLEDGMENT

This work is supported by Quality and Technology Foundation Capacity Building (ANL2306).

References

1. Y. -P. Hong, J. -I. Park, T. -W. Kang, J. -G. Lee and N. -W. Kang, "Ka-Band Electric-Field Probe Calibration System with Rotating and Linear Motion," *IEEE Transactions on Instrumentation and Measurement*, Vol. 70, January 2021.
2. M. Ali, M. Perenzoni and D. Stoppa, "A Methodology to Measure Input Power and Effective Area for Characterization of Direct THz Detectors," *IEEE Transactions on Instrumentation and Measurement*, Vol. 65, No. 5, May 2016, pp. 1225–1231.
3. F. Musolino, "Measurement of IC-Conducted Emissions by Employing a Backward-Wave Directional Coupler," *IEEE Transactions on Instrumentation and Measurement*, Vol. 59, No. 7, July 2010, pp. 1983–1985.
4. X. Liu, M. Xie, D. B. Li and J. Y. Li, "A Method to Calculate the Net Power Delivered into a TEM Cell Using a Directional Coupler in a Probe Calibration," *Applied Mechanics and Materials.*
5. M. Kanda and R. D. Orr, "A Radio-Frequency Power Delivery System: Procedures for Error Analysis and Self-Calibration," Technical Note (NIST TN) – 1083, *U.S. National Institute of Standards and Technology*, Gaithersburg, Md., 1985.
6. D. Li, Z. Song and D. Meng, "Comparison of Two Measurement Methods on Net Power Delivery with Dual Directional Couplers," *IEEE Conference Antenna Measurements & Applications*, December 2017.
7. "IEEE Standard for Calibration of Electromagnetic Field Sensors and Probes (Excluding Antennas) from 9 kHz to 40 GHz," IEEE Standard 1309, *IEEE*, November 2013.
8. D. Gentle, "Mismatch Corrections for the Extrapolation Range," *National Physical Laboratory*, Technical Report, Teddington, Middlesex, U.K., 2006, Unpublished.
9. "Evaluation of Measurement Data – Guide to the Expression of Uncertainty in Measurement (GUM)," JCGM 100:2008, *Joint Committee for Guides in Metrology*, September 2008.
10. The National Institute of Standards and Technology (NIST), Web: https://uncertainty.nist.gov/.
11. T. Lafarge and A. Possolo, "NIST Uncertainty Machine — User's Manual," *National Institute of Standards and Technology*, Gaithersburg, Md., November 2020.